TECHNICAL INFORMATION SERIES

AFOSR DOCUMENT 1494
R62SD32

HIGH ALTITUDE SHOCK WAVE STRUCTURE

I. THEORETICAL - S.M.SCALA AND L.TALBOT
II. EXPERIMENTAL - B.B.CARY

SPACE SCIENCES LABORATORY
GENERAL ELECTRIC
MISSILE AND SPACE DIVISION

Subject: Errata for AFOSR Document 1494, Part II
(Also General Electric TIS R62SD32)

To: Distribution List

On p II - 23 the top line should read:

In regard to the determination of S_1, figures 5, 7, and 8 show that 2.2 was slightly better than 2.0 or 2.5.

On p II - 23, the expression for K_{d_1} should read:

$$(N_2 - N_2): K_{d_1} = 2.2 10^{22} T^{-1.7} \times \exp - \left(\frac{113{,}260}{T}\right) \pm 25\% \ \frac{cc}{mole\text{-}sec}$$

The values of the vibrational relaxation time given in Table I p II - 36 were not reduced in the same fashion as Blackman's data. When the data was reduced by the identical method shorter times were obtained which agree quite well with his data. The following changes should be made in Table I:

For run No. 2 the shock velocity should be 2.96 mm/μsec.

The new relaxation times for 1 atmosphere of pressure in shock fixed coordinates in μsec are respectively for run Nos. 1 through 5: 2.6, 12.1, 4.3, 2.7, and .2.

The inferred efficiencies of Ne and A in exciting N_2 vibrationally remain unchanged. All the N_2 - Ne interferograms showed two curvatures in the relaxation zone inferring a slow vibrational relaxation prior to dissociation.

Presentations & Publications
Space Sciences Laboratory

SPACE SCIENCES LABORATORY

HIGH ALTITUDE SHOCK WAVE STRUCTURE[1]

Part I. Shock Wave Structure with Rotational and Vibrational Relaxation

S. M. Scala[2]

and

L. Talbot[3]

Part II. A Shock Tube Study of the Thermal Dissociation of Nitrogen

B. B. Cary[4]

[1]This report is based on work performed under the auspices of the Air Force Office of Scientific Research, of the Office of Aerospace Research under Contract No. AF 49(638)-931.

[2]Manager, High Altitude Aerodynamics.

[3]Associate Professor of Aeronautical Sciences, University of California, Berkeley, California

[4]Specialist Physicist

R62SD32 - Class I
October, 1962

MISSILE AND SPACE VEHICLE DEPARTMENT

GENERAL ELECTRIC

GENERAL INTRODUCTION

During high altitude flight at hypersonic speeds, the shock wave which forms upstream of an entry vehicle will have a finite thickness which can be an appreciable portion of the shock detachment distance, depending on the geometry of the vehicle, the flight speed and the free stream density. Further, due to the low ambient gas density, and the consequent lower number of intermolecular collisions, there is insufficient time for the gas to reach a new state of thermochemical equilibrium during the residence of the particles, and hence the gas flow in the immediate vicinity of the vehicle is a non-equilibrium viscous flow.

In Earth's low altitude flight regime (below 150,000 ft.), in first approximation, one can uncouple the fluid dynamic processes from the chemical kinetics. Here, one first merely solves the well-known algebraic relationships for the conservation of mass, momentum and energy (Rankine-Hugoniot equations) and then proceeds to calculate the rate of change of gas composition, temperature, density and pressure by simply integrating a set of chemical kinetic equations.

However, in the regime of interest such a procedure is not meaningful since one is dealing with coupled physicochemical phenomena. In particular, the available kinetic energy of the molecules is redistributed among many different internal modes of energy storage which absorb energy at different rates, but nevertheless in parallel processes and not in series.

The theoretical approach to this problem therefore requires the formulation and numerical solution of the coupled conservation laws, suitable for the description of non-equilibrium chemically reacting fluid flow in which large gradients of velocity, temperature and pressure are present. This type of theoretical model requires the inclusion of molecular transport processes, relaxation phenomena and chemical kinetics. In order to accomplish this task, one must have a knowledge of the various physicochemical quantities which appear as variable coefficients in the governing differential equations.

The experimental approach consists of the development of a shock tube facility in which accurate relaxation rate data and chemical kinetic data may be obtained. These data can then be utilized to supplement and verify the macroscopic predictions of the theoretical investigation.

The following two sections contain the results of Phase I of a theoretical and experimental study of shock wave structure in a relaxing, dissociating diatomic gas. The theoretical study was carried out by Scala and Talbot, and appears as Part I. The experimental investigation was carried out by Cary and appears as Part II.

It should be noted that the theory is quite general and applies to an arbitrary diatomic gas, while the experiments were performed utilizing molecular nitrogen, one of the primary constituents of Earth's atmosphere and the Martian and Venusian atmospheres.

PART I. SHOCK WAVE STRUCTURE WITH ROTATIONAL AND VIBRATIONAL RELAXATION

S. M. Scala

and

L. Talbot

CONTENTS (PART I)

LIST OF FIGURES

ABSTRACT

In an earlier paper (Ref. 1) the authors analyzed the structure of a shock wave in a gas having a long relaxation time for its internal molecular (rotational) degrees of freedom. This analysis has now been extended to the case of a diatomic gas having two relaxation effects, one for the rotational and one for the vibrational degrees of freedom. Departures from thermodynamic equilibrium within the shock wave were studied for two values of the Mach number, M = 4.6 and M = 10. The number of intermolecular collisions required for adjustment of the rotational degrees of freedom was kept fixed, but the number of collisions required for vibrational adjustment was varied parametrically from 300 to 2000.

The relaxation model chosen to supplement the Navier-Stokes equations was a generalization of that used in reference 1, namely, both the rotational and vibrational temperatures T_r and T_v change through the shock wave at a rate which is proportional to the difference between themselves and the other two temperatures, and inversely proportional to the number of intermolecular collisions. In this model, there is direct coupling between T_r and T_v, as well as indirect coupling through the translational temperature T_t.

The calculations provide a more realistic estimate for the distribution of translational temperature T_t through a normal shock wave than is obtained with the neglect of relaxation phenomena. Accurate estimates of T_t are of

importance in determining the onset and initial rates of chemical reactions in strong shocks.

The calculations also give a more realistic value of the effective thickness of the shock transition. This information is of importance in the problem of the merging of the shock wave with the shock layer at the nose of a blunt body in high altitude hypersonic flow.

INTRODUCTION

The shock wave structure problem has been of interest to aerodynamicists for many years, and this interest has been heightened recently with the advent of hypersonic flight. A considerable body of theoretical and experimental work therefore exists which has been reviewed recently by Sherman and Talbot (Ref. 2), Talbot (Ref. 3) and Losev and Osipov (Ref. 4). The bulk of the work is confined, however, to the study of shock wave structure in non-reacting monatomic gases which therefore gives little insight into the problem of the shock structure in a real gas at hypersonic speeds.

In a diatomic gas, one must consider the contributions of the internal degrees of freedom (e.g. rotational, vibrational) as well as translational in studying the approach to thermal equilibrium through a shock wave. Further, the effects of finite chemical kinetics (dissociation and ionization) which begin to appear at the Mach numbers associated with hypersonic flight are coupled with the other physicochemical processes, and thus the problem requires the simultaneous solution of the coupled fluid dynamic and chemical kinetic equations. This is particularly true at the highest flight speeds (highest non-equilibrium temperatures) where the relaxation times for the internal processes and the chemical processes are comparable.

The earliest theoretical studies of shock waves were carried out

for a non-reacting perfect fluid, utilizing the Navier-Stokes equations. For example, Rankine (Ref. 5) solved the problem for the case of zero viscosity and constant thermal conductivity. The classical Navier-Stokes treatment is due to Becker (Ref. 6) who obtained a solution when the viscosity and thermal conductivity were assumed independent of the gas temperature. Later, Thomas (Ref. 7) extended the work of Becker and showed that if the viscosity of the gas is proportional to the square root of the absolute temperature, then a strong shock wave solution results in a non-vanishing shock thickness.

Recently, Grad (Ref. 8) and Gilbarg and Paolucci (Ref. 9) obtained solutions for the Navier-Stokes equations utilizing more realistic values of the specific heats ratio and the Prandtl number, where the viscosity was assumed to follow a power law dependence on the absolute temperature. Their results, when compared with available experimental data, showed the importance of selecting correct transport coefficients in calculating shock wave thickness and have given greater credence to the Navier-Stokes model for shock wave structure, at least for weak shocks.

With regard to internal relaxation phenomena associated with the internal degrees of freedom of the molecules, there is the early work of Bethe and Teller (Ref. 10), Broer (Ref. 11) and Lighthill (Ref. 12) in which, however, the shock transition is considered to occur in two distinct steps.

More recently, studies have been published on relaxing shock waves in which the relaxation phenomena is taken into consideration throughout the entire shock transition. The work of Broer and van der Bergen (Ref. 13) is valid only for very weak shocks, however, the treatment of Talbot and Scala (Ref. 1) based on the Navier-Stokes equations and an auxilliary relaxation equation seems to be phenomenologically correct for strong shock waves.

In reference 1, the authors analyzed the structure of a shock wave in a diatomic gas in which the rotational degrees of freedom were assumed to adjust more slowly than the translational degrees of freedom, and the vibrational degrees of freedom were unexcited. The problem was treated according to both the bulk viscosity and the relaxation equation points of view. It was shown that the bulk viscosity model was limited to such small values of the relaxation time as to preclude its application to most cases of interest, whereas the relaxation equation model yields results which seem reasonable for the full range of relaxation times and Mach numbers treated, $0 < N < 100$ and $1 < M < 10$.

In the present paper, the analysis has been extended to the case of a diatomic gas having two relaxation effects, one for the rotational and one for the vibrational degrees of freedom. Departures from thermodynamic equilibrium within the shock wave were studied for two values of Mach number, $M = 4, 6$ and 10. The number of intermolecular

collisions required for adjustment of the rotational degrees of freedom was kept fixed, but the number of collisions required for vibrational equilibration was varied parametrically from 300 to 2000 in order to study the coupling between the translational, rotational and vibrational temperatures.

For the sake of generality, the fundamental equations have been derived for the one-dimensional flow of a dissociating diatomic gas having rotational and vibrational relaxation. In the present work, however, solutions including finite dissociation rates were not investigated.

NOMENCLATURE

a, b, c, d, e	constants
C	dimensionless specific heat at constant volume
$\overline{C}$	mean molecular speed
C_A	mass fraction of atomic species
C_V	specific heat at constant volume
$\mathcal{D}_{ij}$	binary diffusion coefficient
D_i^T	thermal diffusion coefficient of species i
e	internal energy
$\Delta e_{f_i}^{\circ}$	energy of formation
h	enthalpy, including chemical
$\Delta h_{f_i}^{\circ}$	heat of formation
$\vec{j}$	diffusion flux
K_T	thermal diffusion ratio
$\overline{L}$	mean free path

L_μ	reference length based on viscosity
m	integration constant in continuity equation
M_i	molecular weight of species i
$\overline{M}$	mean molecular weight
N	number of intermolecular collisions
p	static pressure
P	integration constant in momentum equation
Q	integration constant in energy equation
r	dimensionless density
R	universal gas constant
R_i	gas constant of species i
T	temperature
u	velocity
V	diffusion velocity
$\dot{w}$	chemical source term
n	total molar density

x	physical spatial variable
y	dimensionless spatial variable
Z	integration constant in diffusion equation
$\alpha, \beta, \gamma, \delta, \epsilon$	constants
κ	bulk viscosity coefficient
λ	thermal conductivity
μ	viscosity
ρ	density
θ	dimensionless group
τ	dimensionless translational temperature
ϕ	dimensionless rotational temperature
ψ	dimensionless vibrational temperature
σ	dimensionless pressure

Subscripts

A	atoms

i	species i
M	molecules
r	rotational
t	translational
v	vibrational
$-\infty$	upstream
n	mode of energy storage
$+\infty$	downstream

Superscripts

*	reference state

BASIC EQUATIONS

It is assumed that the total thermal energy of the gas is composed of translational, rotational and vibrational modes, and hence upon characterizing these different modes by temperatures T_t, T_r and T_v and specific heats C_{v_t}, C_{v_r} and C_{v_v}, the internal energy of the gas is

$$e = \sum_i C_i e_i \; ; \quad de_i = \sum_n C_{v_{i_n}} dT_{i_n} \tag{1}$$

in which case the ordinary specific heat at constant volume is:

$$C_{v_i} = C_{v_{i_t}} + C_{v_{i_r}} + C_{v_{i_v}} \tag{2}$$

For convenience it is assumed that all specific heats are constant.

For steady, one-dimensional flow, the following conservation laws apply. The conservation of mass is given by:

$$\frac{d}{dx} (\rho u) = 0 \tag{3}$$

which upon integration becomes:

$$\rho u = m \qquad \text{(a constant)} \tag{4}$$

The conservation of momentum is given by:

$$\rho u \frac{du}{dx} = - \frac{dp}{dx} + \frac{d}{dx} \left[\left(\frac{4}{3} \mu + \kappa \right) \frac{du}{dx} \right] \tag{5}$$

which when integrated becomes:

$$mu + p - \left(\frac{4}{3} \mu + \kappa \right) \frac{du}{dx} = P \qquad \text{(a constant)} \tag{6}$$

The conservation of species i is given by:

$$\frac{d}{dx} (\rho u C_i + j_i) = \dot{w}_i \tag{7}$$

which when integrated becomes:

$$mC_i + j_i - \Phi_i = Z \qquad \text{(a constant)} \tag{8}$$

where:

$$d\Phi_i = \dot{w}_i dx \tag{9}$$

and the one-dimensional diffusion flux vector for a binary mixture may be written (Ref. 14):

$$j = -\rho \mathcal{D}_{ij} \left\{ \frac{dC_i}{dx} + \frac{M_i M_j}{\bar{M}^2} \left[\left(\frac{\bar{M} - M_i}{M_i} \right) C_i \frac{d}{dx} \ln p + K_T \frac{d}{dx} \ln T_t \right] \right\} \tag{10}$$

where the thermal diffusion ratio is given by (Ref. 15) :

$$K_T = \frac{\rho}{n^2 M_i M_j} \frac{D_i^T}{\mathcal{D}_{ij}} \tag{11}$$

The energy equation may be written:

$$\rho u \frac{dh}{dx} = \frac{d}{dx} \left(\lambda_t \frac{dT_t}{dx} + \lambda_r \frac{dT_r}{dx} + \lambda_v \frac{dT_v}{dx} \right) - \frac{d}{dx} \left(\sum_i j_i h_i \right) + \left(\frac{4}{3} \mu + \kappa \right) \left(\frac{du}{dx} \right)^2 + u \frac{dp}{dx} + \frac{d}{dx} \left[\frac{RT_t}{n} \sum_i \sum_{j \neq i} \frac{n_j D_i^T}{M_i \mathcal{D}_{ij}} (V_j - V_i) \right] \tag{12}$$

Upon introducing the momentum equation (5) and integrating. this becomes:

$$2mh + mu^2 - 2\lambda_t \frac{dT_t}{dx} - 2\lambda_r \frac{dT_r}{dx} - 2\lambda_v \frac{dT_v}{dx} + 2 \sum_i j_i h_i - 2u \left(\frac{4}{3} \mu + \kappa \right) \frac{du}{dx} - 2 \frac{RT_t}{n} \sum_i \sum_{j \neq i} \frac{n_j D_i^T}{M_i \mathcal{D}_{ij}} (V_i - V_j) = Q \qquad \text{(a constant)} \tag{13}$$

The thermal conductivities λ_t, λ_r and λ_v corresponding to the transport of translational, rotational and vibrational modes of energy are evaluated according to the method of Eucken, (See Ref. 15).

For a binary mixture of atoms and molecules, the Dufour term may be expanded to yield:

$$-2\,\frac{RT_t}{n}\sum_i\sum_{j\neq i}\frac{n_j D_i^T}{M_i \Delta_{ij}}\,(V_j - V_i) = \frac{2pK_T j_A}{\rho C_A (1-C_A)}. \qquad (14)$$

Noting that the enthalpy may be written:

$$h = e + \frac{p}{\rho} \qquad (15)$$

and that the internal energy of the i th species is given by:

$$e_i = \int_o^T C_{v_i}\, dT_i + \Delta e_{f_i}^o \qquad (16)$$

The energy equation becomes:

$$\begin{aligned} &2m\,(C_{v_{M_t}} T_t + C_{v_{M_r}} T_r + C_{v_{M_v}} T_v) + 2pu \\ &\quad + mu^2 - 2\lambda_t \frac{dT_t}{dx} - 2\lambda_r \frac{dT_r}{dx} - 2\lambda_v \frac{dT_v}{dx} \\ &\quad - 2u\left(\frac{4}{3}\mu + \kappa\right)\frac{du}{dx} + 2mC_A \Delta h_{f_A}^o \\ &\quad + 2mC_A\left[(C_{v_A} - C_{v_{M_t}})\,T_t - C_{v_{M_r}} T_r - C_{v_{M_v}} T_v\right] \\ &\quad + 2j_A\left[(C_{v_A} + R_A - C_{v_{M_t}} - R_M)\,T_t - C_{v_{M_r}} T_r\right. \\ &\quad \left. - C_{v_{M_v}} T_v + \Delta h_{f_A}^o + \frac{pK_T}{\rho C_A (1-C_A)}\right] = Q \end{aligned} \qquad (17)$$

The thermodynamic pressure is identified with the translational temperature and hence the equation of state may be written:

$$p = \rho \bar{R} T_t \tag{18}$$

or equivalently:

$$p = \rho R_M (1 + C_A) T_t \tag{19}$$

The relaxation equations, following Wang Chang and Uhlenbeck, (Ref. 16), but extending the concept to a three-temperature model. may be put into a symmetric form (Refs. 17 and 18) which may be written:

$$\frac{u dT_r}{dx} = \frac{T_t - T_r}{\beta_{r_1}} + \frac{T_v - T_r}{\beta_{r_2}} \tag{20}$$

$$\frac{u dT_v}{dx} = \frac{T_t - T_v}{\beta_{v_1}} + \frac{T_r - T_v}{\beta_{v_2}} \tag{21}$$

where the relaxation time β may be related to the mean free path $\bar{L}$, the mean molecular speed $\bar{C}$ and to the number of intermolecular collisions for relaxation N through

$$\beta = \frac{N\bar{L}}{\bar{C}} = \frac{\pi}{4} \frac{N \mu}{p} \tag{22}$$

Also, in the derivation of the equations, it has been assumed throughout that the temperature of the atoms is equal to the translational temperature of the molecules.

SOLUTION OF GOVERNING EQUATIONS

Equations A. 7 through A. 12 given in the Appendix were integrated numerically in phase space by means of an electronic analog computer for two values of the Mach number, 4.6 and 10. In order to examine the coupling between the three temperatures, r, ϕ and ψ, the number of collisions required for vibrational excitation was varied in several steps between 300 and 2000 intermolecular collisions. The results of the phase space integrations are shown in Figures 1 through 6.

It is seen that with the form of relaxation equations given in equations A. 12, the rotational temperature starts to rise almost immediately as the translational temperature rises, however, at a slower rate of excitation. The rotational temperature ϕ very closely approaches the translational temperature r but never exceeds it which is a satisfactory phenomenological result. The vibrational temperature ψ lags furthest behind and its effect is felt at about the same time both the rotational and translational temperature go through a maximum. For the smallest number of collisions considered ($N_{vr} = 300$), ψ actually starts rising before the rotational temperature reaches a maximum.

In general, then, one observes that r and ϕ are strongly coupled while the coupling between ψ and both r and ϕ is weaker. The slower rise in the vibrational temperature acts to produce a relaxation "tail" in both the translational and rotational temperatures which overshoot their final equilibrium values. On the other hand, ψ behaves in a

monotonic fashion for all values of N_{vf} in a range between 300 and 2000 collisions.

Although an increase in Mach number acts to change the downstream boundary conditions relative to the upstream boundary conditions, qualitatively, it was found that there is no significant change in the structure of a normal shock in the range of Mach numbers between 4.6 and 10. The numerical solutions shown in Figures 1 through 6 were transformed back into the spatial plane by quadrature by means of an IBM 7090 digital computer. In the spatial plane, the center of the coordinate system, $y = 0$, was arbitrarily selected to coincide with that point within the shock wave at which the velocity takes on its average value, i.e., $v = 1/2\ (v_{-\infty} + v_{+\infty})$. Here it is seen that although the thermodynamic pressure is associated with the translational temperature, neither the pressure σ nor the density ρ exhibit the overshoot that the translational temperature exhibits. That is, with the exception of ρ and ϕ all physical variables exhibit a monotonic behavior for the full range of conditions considered here (see Figures 7 through 12). In obtaining these solutions it has been assumed that dissociation does not occur.

SHOCK WAVE THICKNESS

One nominal measure of shock thickness is based on the maximum slope of one of the physical variables. That is, for a given property f (which may be taken conveniently as τ, ϕ, ψ, v, σ or r), the maximum slope thickness may be expressed in nondimensional form as

$$\Delta y_{(f)} = \frac{\left| f_{max} - f_{min} \right|}{\left| (df/dy)_{max} \right|}$$

The maximum and minimum values of the vibrational temperature, gas velocity, pressure and density, (i.e. ψ, v, σ and r) occur at $y = \pm \infty$; however, the maximum values of the translational and rotational temperatures (i.e. τ and ϕ) will usually occur at some intermediate location, (unless all of the relaxation times are assumed to be identically zero). The term $\left| (df/dy)_{max} \right|$ represents the absolute value of the maximum gradient of f, regardless of where within the shock wave it occurs.

Figs. 13 and 14 show that the maximum slop thicknesses based on τ, ϕ, v, σ and r are essentially independent of N_V, for a given Mach number and N_r, whereas $(\Delta y)_\psi$ increases directly and almost linearly with N_{Vf}. Since N_r was held fixed while N_{Vf} was varied parametrically, it is not surprising that $(\Delta y)_\phi$ behaves differently for the three-temperature model treated here than in the two temperature model treated earlier in reference 1. That is, it is found here that in spite of the direct coupling between the rotational and vibrational temperatures in the two relaxation equations, ϕ

primarily follows τ and goes through a maximum. Thus, the primary effect of an increase in $N_{v\tau}$ is to increase the maximum-slope thickness based on ψ, and to simultaneously add a long relaxation "tail" to τ and ϕ, which cannot appreciably affect the value of $(\Delta y)_\phi$.

In order to obtain an appreciation of the implications of these new results upon the thickness of a shock wave in Earth's atmosphere, the values of the dimensionless shock thickness $(\Delta y)_\psi$ shown in Figure 13 were transformed into the physical thicknesses $(\Delta x)_\psi$ shown in Table II. Simulated initial conditions corresponding to a range of altitudes between 200,000 and 400,000 ft. were utilized, and it was found that at a Mach number of 10, and $N_{v\tau}$ = 2000 collisions, the thickness of the shock wave corresponding to equilibration of the translational, rotational and vibrational degrees of freedom varied by five orders of magnitude, i.e. $10^{-3} < (\Delta x)_\psi < 10^{2}$ ft.

CONCLUSIONS

A new theoretical model for shock wave structure in a diatomic gas with rotational and vibrational excitation was developed here, and numerical integrations have been carried out employing high speed electronic computing equipment. The model which is based on the use of symmetric relaxation equations yields results which seem reasonable for the full range of relaxation times and Mach numbers treated.

More realistic estimates are provided for the distribution of translational temperature through a normal shock wave than would have been obtained with the neglect of relaxation phenomena. These results will be of use in further theoretical studies of the rates of chemical reactions (e.g. thermal dissociation) in strong shocks.

The new calculations give more realistic values for the effective thickness of the shock transition, which will yield better criteria for the determination of the condition of "viscous merging" at the nose of a blunt body in high altitude hypersonic flow. Examination of the concept of nominal shock wave thickness according to the symmetric relaxation model shows that values based on the maximum gradients of velocity, pressure, density, translational temperature and rotational temperature are relatively insensitive to the magnitude of the vibrational relaxation time, whereas the thickness which is based on the maximum gradient of the vibrational temperature is directly proportional to the number of intermolecular

collisions required for vibrational equilibration.

It can also be inferred from these calculations that in the initial steep part of the shock wave, direct coupling between T_t and T_v is not of importance, and that in general these coupling effects affect the temperature distribution only in the relaxation "tail", at least in the range of parameters and flow conditions investigated. The coupling between T_r and T_v is not as strong as between T_t and T_r, but does exist and depends critically on the magnitude of N_{vr}.

APPENDIX

We will now derive the non-dimensional form of the governing equations. Following Grad (Ref. 8), we introduce the following dimensionless variables

$$v = \frac{mu}{P} \; ; \qquad r = \frac{P\rho}{m^2}$$

$$\tau = \frac{m^2 R_M T_t}{P^2} \; ; \qquad \sigma = \frac{p}{P} \tag{A.1}$$

$$\phi = \frac{m^2 R_M T_r}{P^2} \; ; \qquad \bar{a} = \frac{mQ}{P^2}$$

$$\psi = \frac{m^2 R_M T_v}{P^2} \; .$$

Let us introduce the transport lengths

$$L_\mu = \frac{\mu}{m}$$

$$L_\vartheta = \frac{m \vartheta_{AM}}{P}$$

$$L_t = \frac{\lambda_t}{m R_M} \tag{A.2}$$

$$L_r = \frac{\lambda_r}{mR_M}$$

$$L_v = \frac{\lambda_v}{mR_M} \quad .$$

Now, let us put the transport property equations in the form:

$$\mu = a(T_t)^{\alpha}$$

$$\mathcal{D}_{AM} = b(T_t)^{\beta}/p$$

$$\lambda_t = c(T_t)^{\gamma} \qquad \text{(A. 3)}$$

$$\lambda_r = d(T_t)^{\delta}$$

$$\lambda_v = e(T_t)^{\epsilon}$$

where a, b, c, d, e, α, β, γ, δ and ϵ are assumed to be constants and the α in the exponent of the viscosity law is not to be confused with the $\bar{\alpha}$ appearing in equation A.1.

Upon selecting a reference temperature T_t^*, we can introduce the non-dimensional spatial variable:

$$y = \frac{(\rho^*)^{\alpha} x}{L_\mu^*} \tag{A.4}$$

where

$$\rho^* = \frac{m^2 R_M T_t^*}{P^2} \tag{A.5}$$

$$L_\mu^* = -\frac{\mu^*}{m}$$

so that in terms of the new variables the governing equations become for the case of difficult energy exchange with $\kappa = 0$

mass:

$$\rho v = 1 \tag{A.6}$$

momentum:

$$\frac{4}{3} \rho^{\alpha} v \frac{dv}{dy} = v^2 + \rho(1 + C_A) - v \tag{A.7}$$

species:

$$j_A = \Phi_A - m(C_A - C_{A_\infty}) \tag{A.8}$$

where

$$j_A = -m\theta_{\mathcal{D}} \rho^{(\beta - 1)} \left[\frac{1}{1 + C_A} \frac{dC_A}{dy} + \frac{C_A(1 - C_A)}{2} \frac{1}{\sigma} \frac{d\sigma}{dy} + \frac{1 + C_A}{2} \frac{K_T}{\rho} \frac{d\rho}{dy} \right] \tag{A.9}$$

and

$$\Phi_A = \int \dot{w}_A \frac{L \mu^*}{(r^*)^{\alpha}} dy \qquad (A.10)$$

energy:

$$\theta_t r^{\gamma} \frac{dr}{dy} + \theta_r r^{\delta} \frac{d\phi}{dy} + \theta_v r^{\epsilon} \frac{d\psi}{dy}$$

$$= \frac{j_A}{m} \left[C_i r - C_{M_r} \phi - C_{M_v} \psi + \Delta H + \left(1 + \frac{K_T (1 + C_A)}{C_A (1 - C_A)}\right) r \right]$$

$$+ C_A \left[C_i r - C_{M_r} \phi - C_{M_v} \psi + \Delta H \right]$$

$$+ C_{M_t} r + C_{M_r} \phi + C_{M_v} \psi + v - \frac{v^2}{2} - \frac{a}{2} \qquad (A.11)$$

The non-dimensional form of the relaxation equations is

$$v^2 \frac{d\phi}{dy} = \frac{4r^{(1-a)}(1 + C_A)}{\pi} \left[\frac{r - \phi}{N_{rr}} + \frac{\psi - \phi}{N_{r\psi}} \right]$$

$$v^2 \frac{d\psi}{dy} = \frac{4r^{(1-a)}(1 + C_A)}{\pi} \left[\frac{r - \psi}{N_{vr}} + \frac{\phi - \psi}{N_{v\phi}} \right] \qquad (A.12)$$

In the above equations,

$$\Delta H = \frac{m^2}{P^2} \Delta h_{f_A}^{\circ} \qquad (A.13)$$

$$C_i = \frac{C_{v_A} - C_{v_{M_t}}}{R_M}; \quad C_{M_r} = \frac{C_{v_{M_r}}}{R_M}$$

$$C_{M_t} = \frac{C_{v_{M_t}}}{R_M} ; \qquad C_{M_v} = \frac{C_{v_{M_v}}}{R_M}$$

The dimensionless ratios θ_t, θ_r, θ_v and $\theta_{\mathcal{D}}$ are defined by:

$$\theta_t = \frac{L_t^*}{L_\mu^* (\tau^*)^{\gamma-a}} ; \qquad \theta_r = \frac{L_r^*}{L_\mu^* (\tau^*)^{\delta-a}}$$

$$\theta_v = \frac{L_v^*}{L_\mu^* (\tau^*)^{\epsilon-a}} ; \qquad \theta_{\mathcal{D}} = \frac{L_{\mathcal{D}}^*}{L_\mu^*} \frac{\sigma^*}{(\tau^*)^{\beta-a}} \qquad \text{(A.14)}$$

It may readily be verified that the ratios θ_t, θ_r and θ_v have the behavior of reciprocal Prandtl numbers, whereas, $\theta_{\mathcal{D}}$ has the behavior of the reciprocal of the Schmidt number.

The boundary conditions corresponding to the Rankine-Hugoniot jump relations in non-dimensional form may be obtained by setting all the derivatives with respect to y equal to zero in equations (A. 7) through (A. 12).

ACKNOWLEDGEMENTS

The authors would like to acknowledge the capable assistance of several personnel at the General Electric Company, Missile and Space Division, including Mr. Frank Bosworth who obtained the numerical results on an IBM 7090 digital computer, Mr. Paul Gordon who assisted with the numerical analysis, Messrs. J. Young and D. Cuzzocrea who obtained some of the initial numerical results on an EA 231 R electronic analog computer, Mr. C. Cook who programmed the analog to digital computations on the LGP 30 and Messrs. L. Zeiger and J. Wilson who performed additional numerical computations and prepared the figures.

This analysis is based on work sponsored by the AF Office of Scientific Research of the Office of Aerospace Research under Contract No. AF 49(638)-931 with Mr. Milton Rogers acting as contract monitor.

REFERENCES

1. Talbot, L. and Scala, S.M., "Shock Wave Structure in a Relaxing Diatomic Gas", Rarefied Gas Dynamics, Second International Symposium, (L. Tabot, Ed.), Academic Press, N.Y., pp. 603-622, 1961.

2. Sherman, F. S. and Talbot, L., "Experiment versus Kinetic Theory for Rarefied Gases", Rarefied Gas Dynamics, First International Symposium (F.M. Devienne, Ed.), Pergamon Press, pp. 161-191, London, 1958.

3. Talbot, L., "Recent Research on the Shock Structure Problem", Paper 61-1, Western States Section, Combustion Institute Conference, California, April 10-11, 1961.

4. Losev, S.A. and Osipov, A.I., "The Study of Non-equilibrium Phenomena in Shock Waves", Usp. Fiz. Nauk, Vol. 74, No. 3, pp. 393-434, July 1961.

5. Rankine, W., "On the Thermodynamic Theory of Waves of Finite Longitudinal Disturbance", Phil. Trans. Roy. Soc., London, Series A, Fol. 160, p. 227, 1870.

6. Becker, R., "Stozzwelle and Detonation", Zeit. fur Physik, Vol. 8, p. 321, 1922.

7. Thomas, L.H., "Note on Becker's Theory of the Shock Front", J. Chem. Phys., Vol. 12, p. 499, 1944.

8. Grad, H., "The Profile of a Steady Plane Shock Wave", Comm. Pure and Applied Math., Vol. 5, p. 257, 1952.

9. Gilbarg, D. and Paolucci, D., "The Structure of Shock Waves in the Continuum Theory of Fluids", J. Rational Mech. and Anal., Vol. 2, p. 617, 1953.

10. Bethe, H.A. and Teller, E., "Deviations from Thermal Equilibrium in Shock Waves", Ballistic Research Lab. Rept., Aberdeen Proving Ground, Maryland, 1941. Reproduced by University of Michigan Engineering Research Institute.

11. Broer, L.J.F., "On the Influence of Acoustical Relaxation in Compressible Flow", Appl. Sci. Research, Ser. A 2, pp. 447-468, 1951.

12. Lighthill, M. J., "Viscosity Effects in Sound Waves of Finite Amplitude" Surveys in Mechanics, (G. K. Batchelor and R. M. Davies, Eds.) pp. 342-350, Cambridge Univ. Press, London and New York, 1956.

13. Broer, L. J. F., and van den Bergen, A. C., "On the Theory of Shock Structure II", Appl. Sci. Research, Ser. A 4, pp. 157-170, (1954).

14. Scala, S. M., "Thermal Diffusion Ratio in Dissociated Air", ARS Journal, Vol. 31, No. 10, pp. 1441-1443, October 1961.

15. Hirschfelder, J. O., Curtiss, C. F. and Bird, R. B., Molecular Theory of Gases and Liquids, John Wiley and Sons, Inc., New York, 1954.

16. Wang Chang, C. S. and Uhlenbeck, G. E., "Transport Phenomena in Polyatomic Gases", University of Michigan Engineering Research Institute, Rept. CM-681, July 1951.

17. Herzfeld, K. F., "Relaxation Phenomena in Gases", Section H, Thermodynamics and Physics of Matter, (F. D. Rossini, Ed.), Vol. I, High Speed Aerodynamics and Jet Propulsion, Princeton University Press, Princeton, New Jersey, 1955.

18. Herzfeld, K. F. and Litovitz, T. A., Absorption and Dispersion of Ultrasonic Waves, Academic Press, New York and London, 1959.

19. The 1959 ARDC Atmospheric Model, Air Force Cambridge Research Center, Surveys in Geophysics No. 115, 1959.

TABLE I. CONSTANTS

α (exponent) $= \gamma = \delta = \epsilon = 1/2$

β (exponent) $= 3/2$

$\theta_t = 5.303$

$\theta_r = 1.172$

$\theta_v = 1.172$

$C_{M_t} = 3/2$

$C_{M_r} = 1$

$C_{M_v} = 1$

$N_{r\tau} = 10$

$N_{r\psi} = 100$

$N_{v\tau} = 300, 500, 2000$

$N_{v\phi} = 4000$

$\bar{\alpha}$ (M = 4.6) = 1.238

$\bar{\alpha}$ (M = 10) = 1.054

TABLE II - SHOCK WAVE THICKNESS (M=10)

SIMULATED ALTITUDE (Ft.)	AMBIENT DENSITY (particles/c.c.)	AMBIENT PRESSURE (Atm.)	SHOCK THICKNESS* (Ft.)
200,000	6.56×10^{15}	2.23×10^{-4}	2.40×10^{-3}
250,000	8.30×10^{14}	2.06×10^{-5}	1.89×10^{-2}
300,000	4.42×10^{13}	1.00×10^{-6}	3.55×10^{-1}
350,000	2.44×10^{12}	7.44×10^{-8}	6.45
400,000	2.54×10^{11}	1.78×10^{-8}	6.1×10^{1}

*Based on maximum slop thickness of the vibrational temperature.

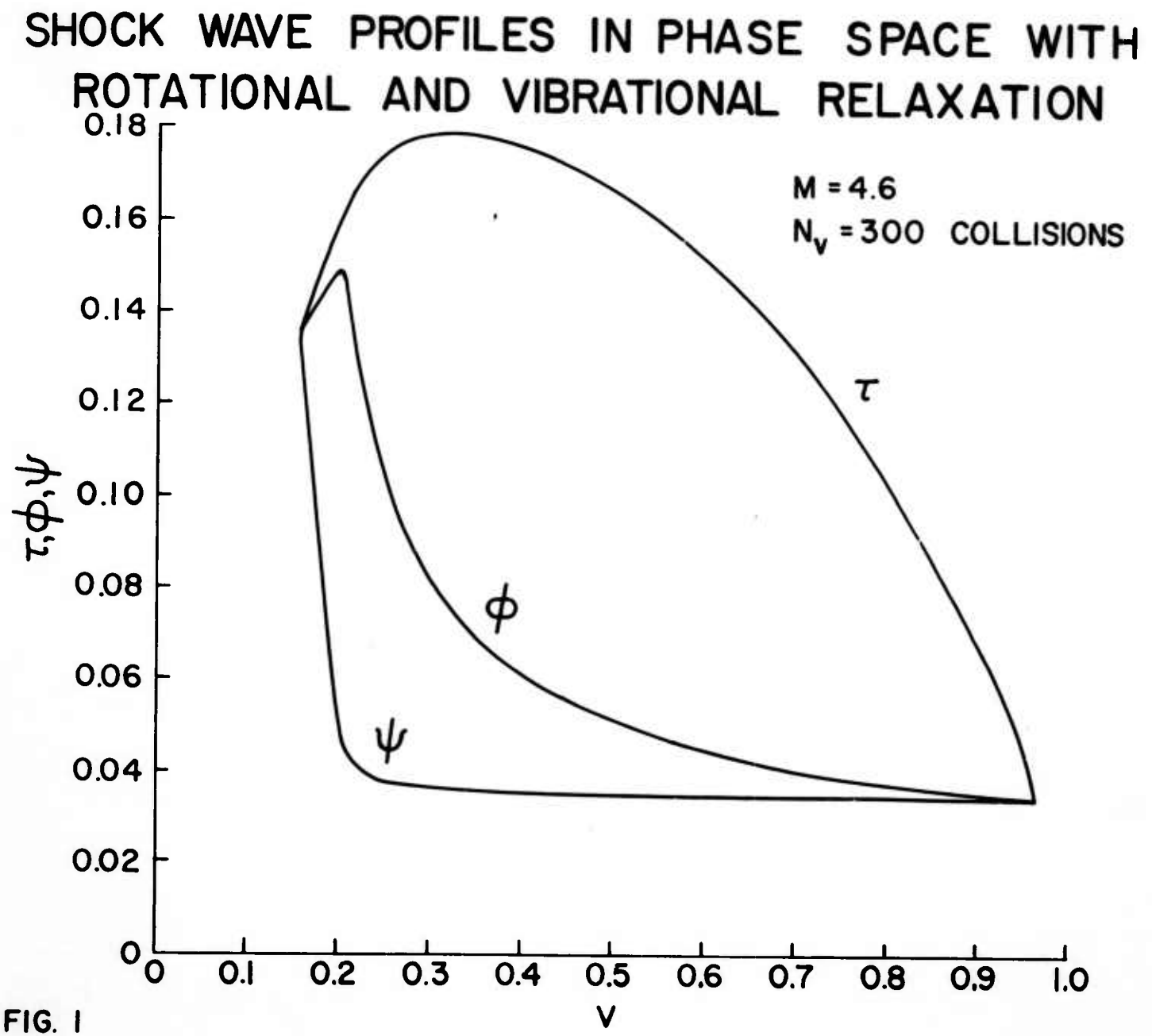
SHOCK WAVE PROFILES IN PHASE SPACE WITH ROTATIONAL AND VIBRATIONAL RELAXATION
M = 4.6
N_v = 300 COLLISIONS
τ
φ
ψ
τ,φ,ψ
0.18
0.16
0.14
0.12
0.10
0.08
0.06
0.04
0.02
0
0
0.1
0.2
0.3
0.4
0.5
0.6
0.7
0.8
0.9
1.0
V

FIG. 1

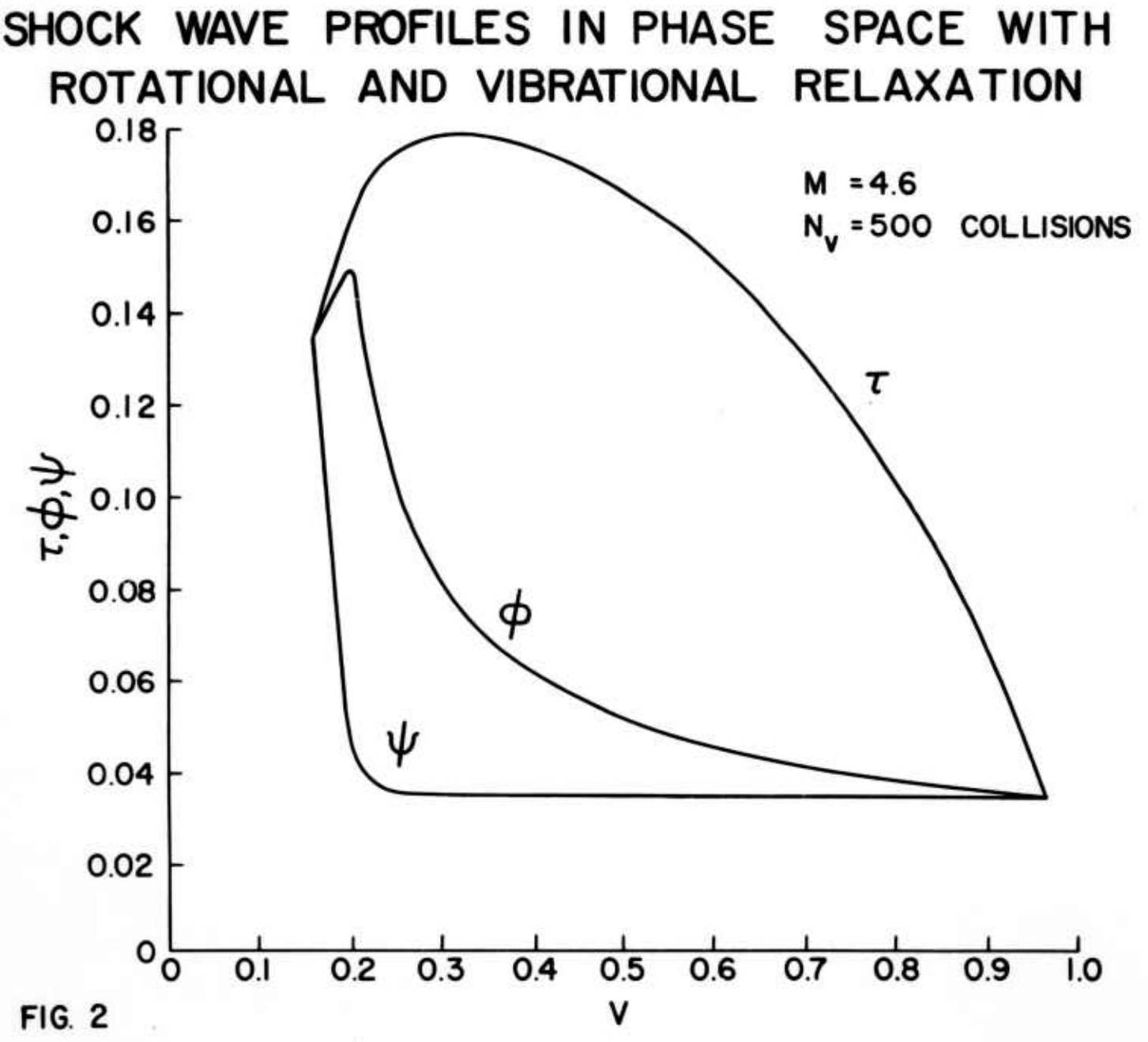
SHOCK WAVE PROFILES IN PHASE SPACE WITH ROTATIONAL AND VIBRATIONAL RELAXATION
M = 4.6
N_v = 500 COLLISIONS
τ
φ
ψ
τ,φ,ψ
V
0.18
0.16
0.14
0.12
0.10
0.08
0.06
0.04
0.02
0
0.1
0.2
0.3
0.4
0.5
0.6
0.7
0.8
0.9
1.0

FIG. 2

SHOCK WAVE PROFILES IN PHASE SPACE WITH ROTATIONAL AND VIBRATIONAL RELAXATION

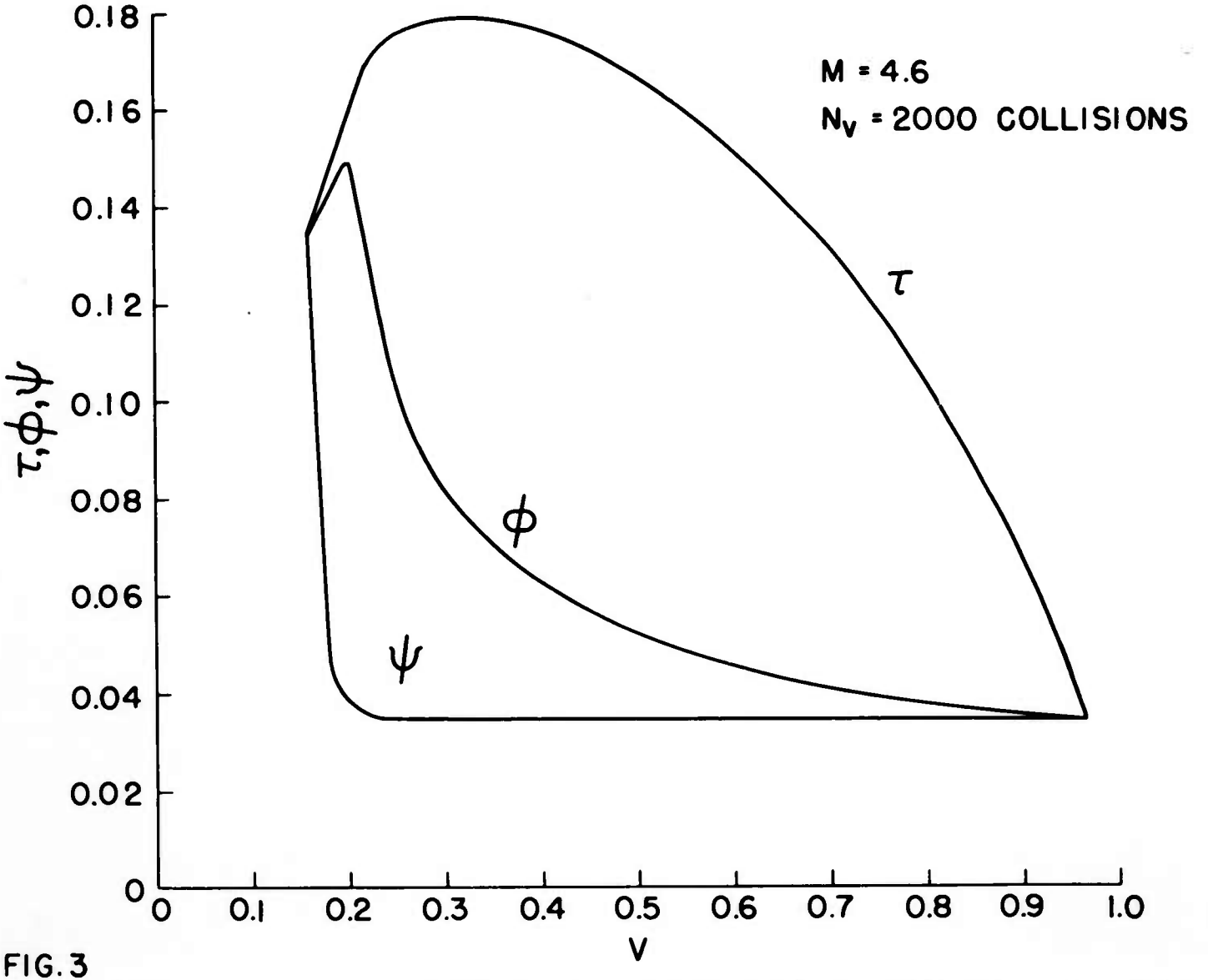

FIG. 3

SHOCK WAVE PROFILES IN PHASE SPACE WITH ROTATIONAL AND VIBRATIONAL RELAXATION

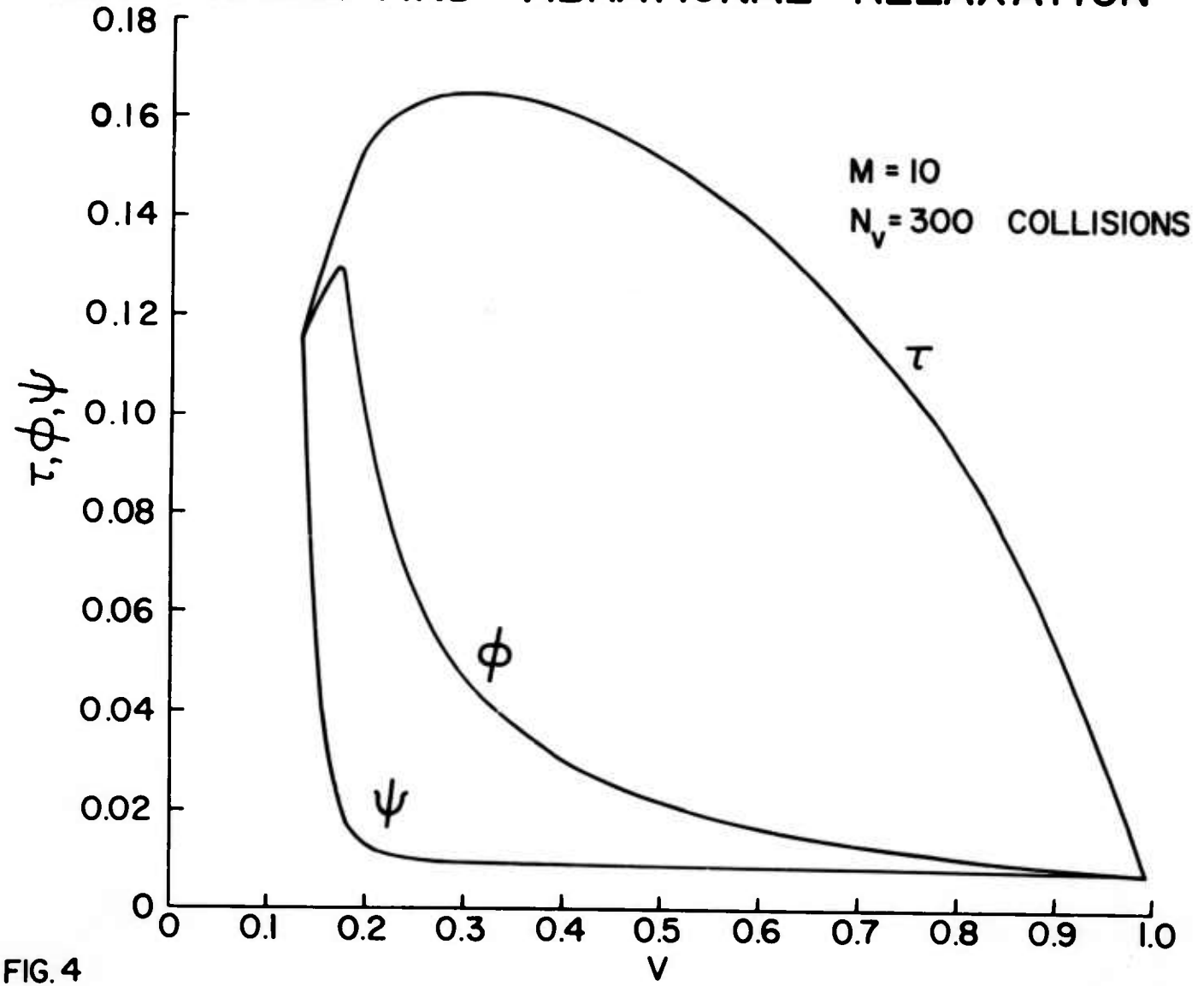

FIG. 4

SHOCK WAVE PROFILES IN PHASE SPACE WITH ROTATIONAL AND VIBRATIONAL RELAXATION

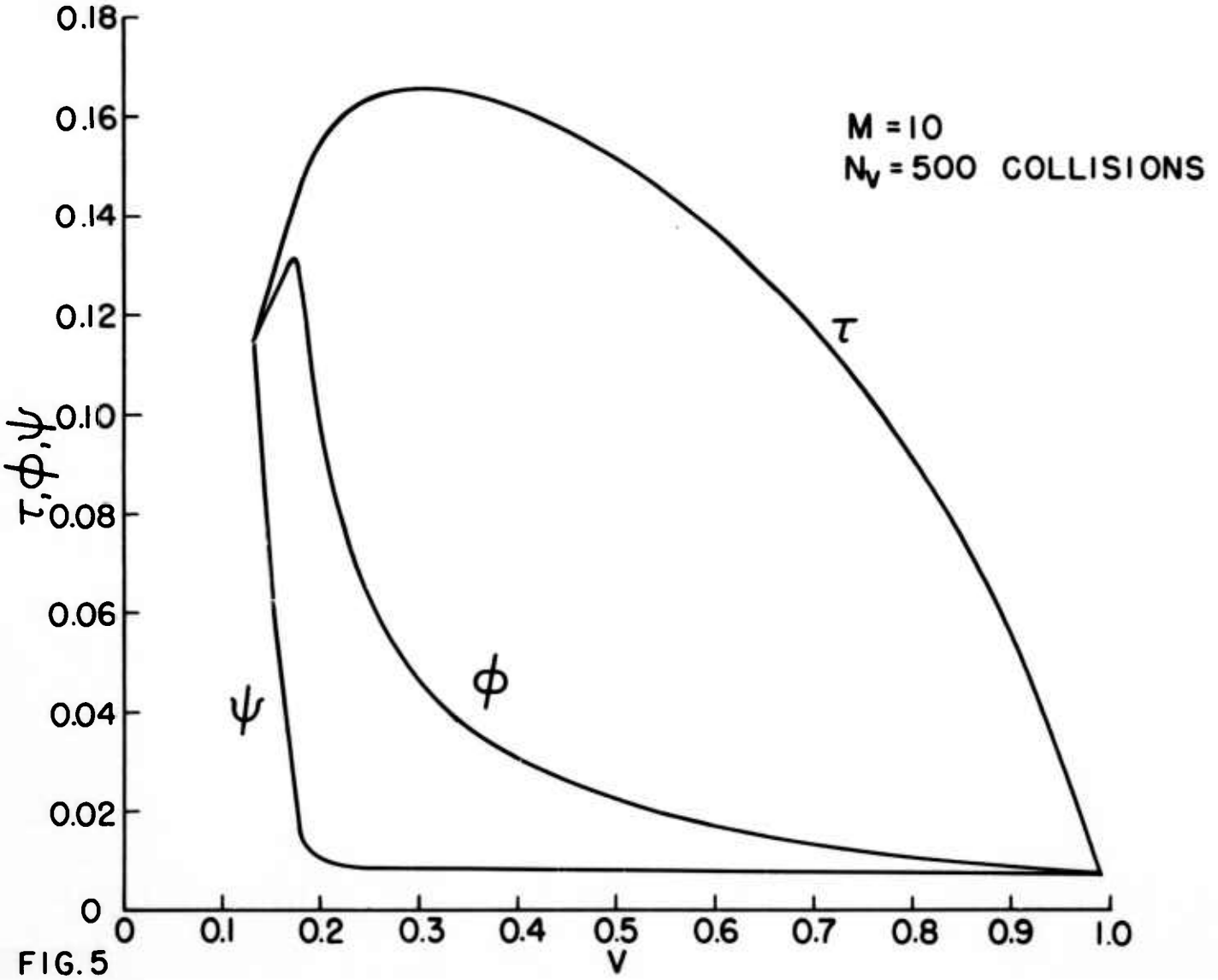

FIG. 5

SHOCK WAVE PROFILES IN PHASE SPACE WITH ROTATIONAL AND VIBRATIONAL RELAXATION

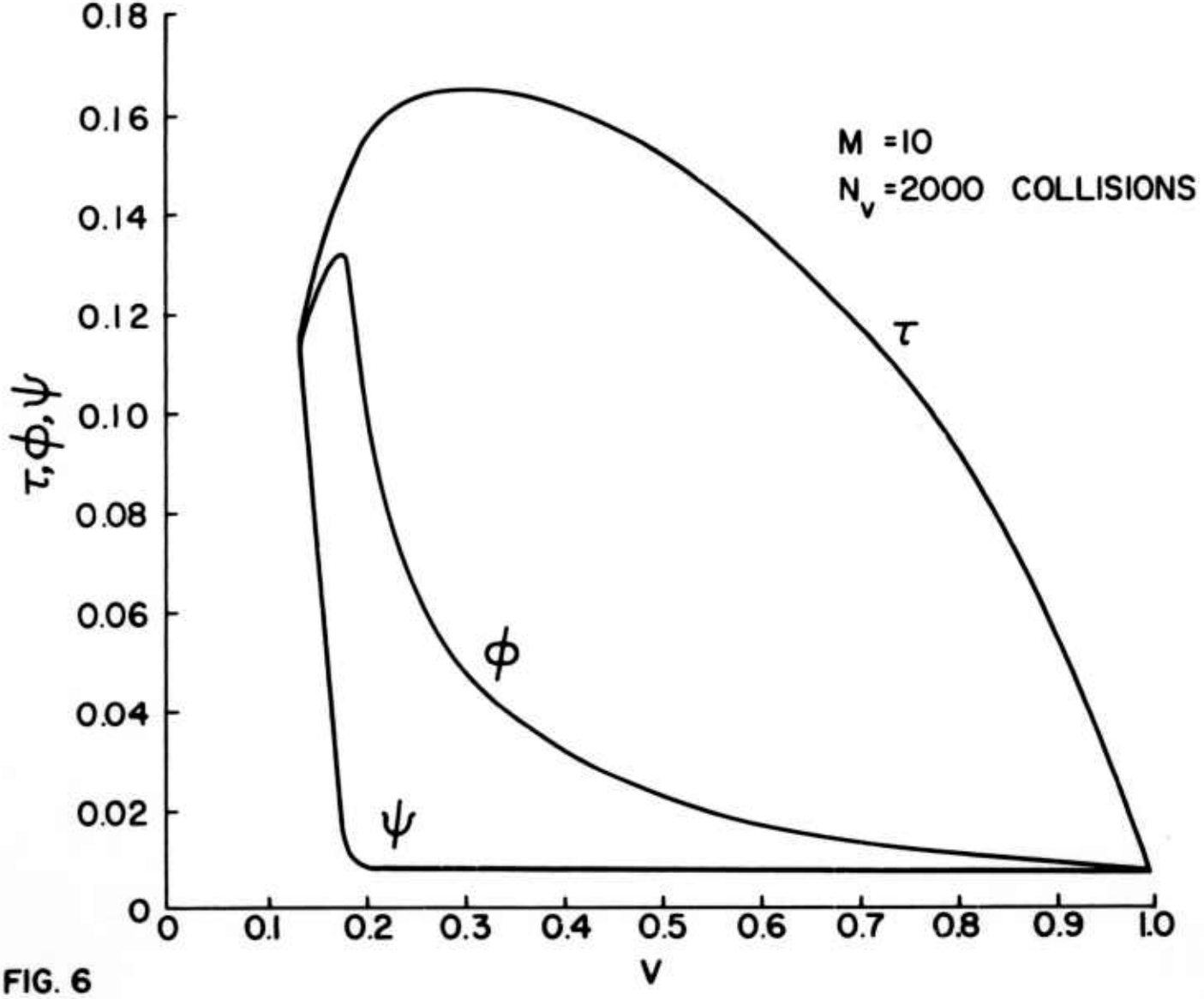

FIG. 6

SHOCK WAVE STRUCTURE IN THE SPATIAL PLANE WITH ROTATIONAL AND VIBRATIONAL RELAXATION

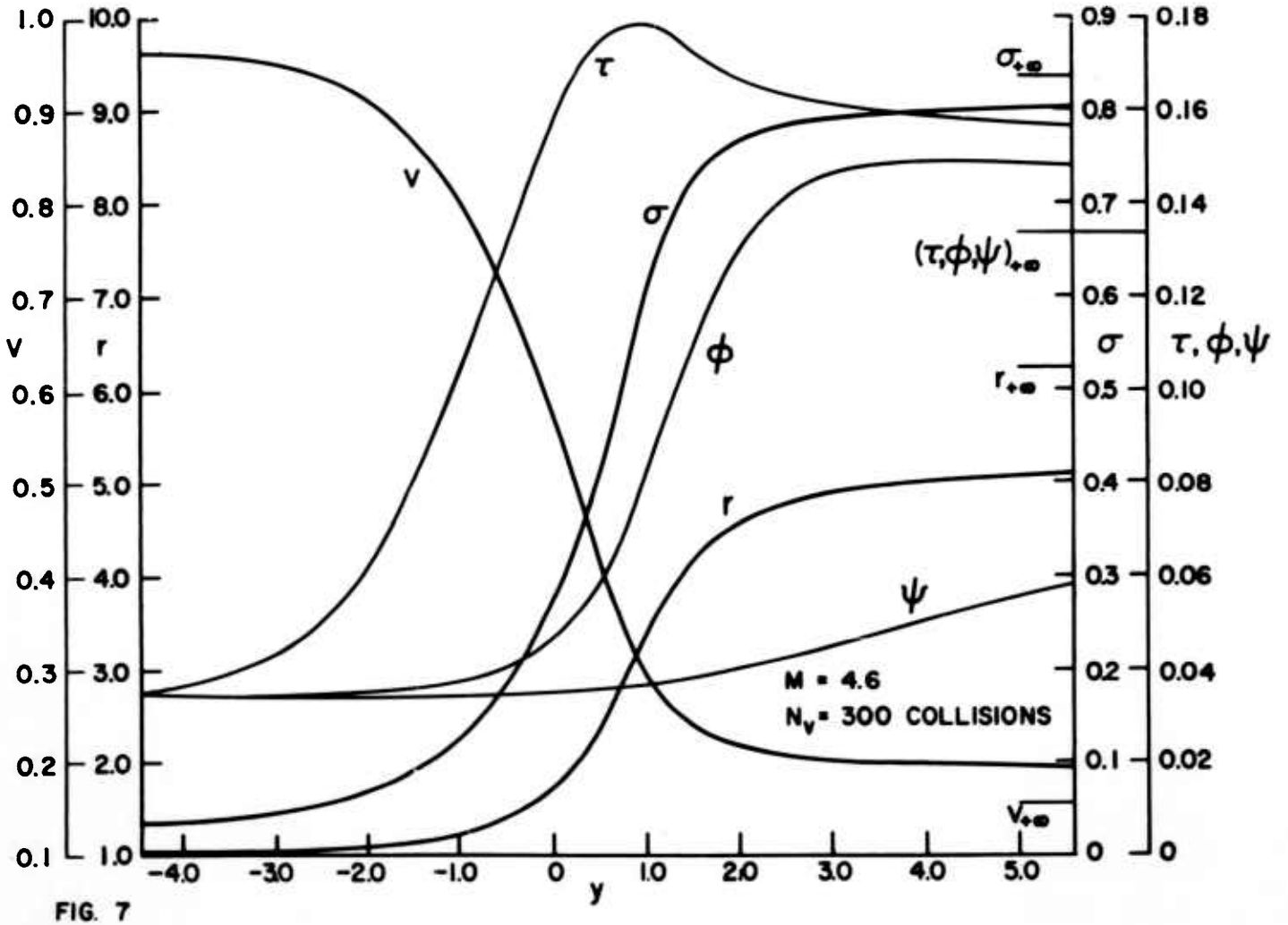

FIG. 7

SHOCK WAVE STRUCTURE IN THE SPATIAL PLANE WITH ROTATIONAL AND VIBRATIONAL RELAXATION

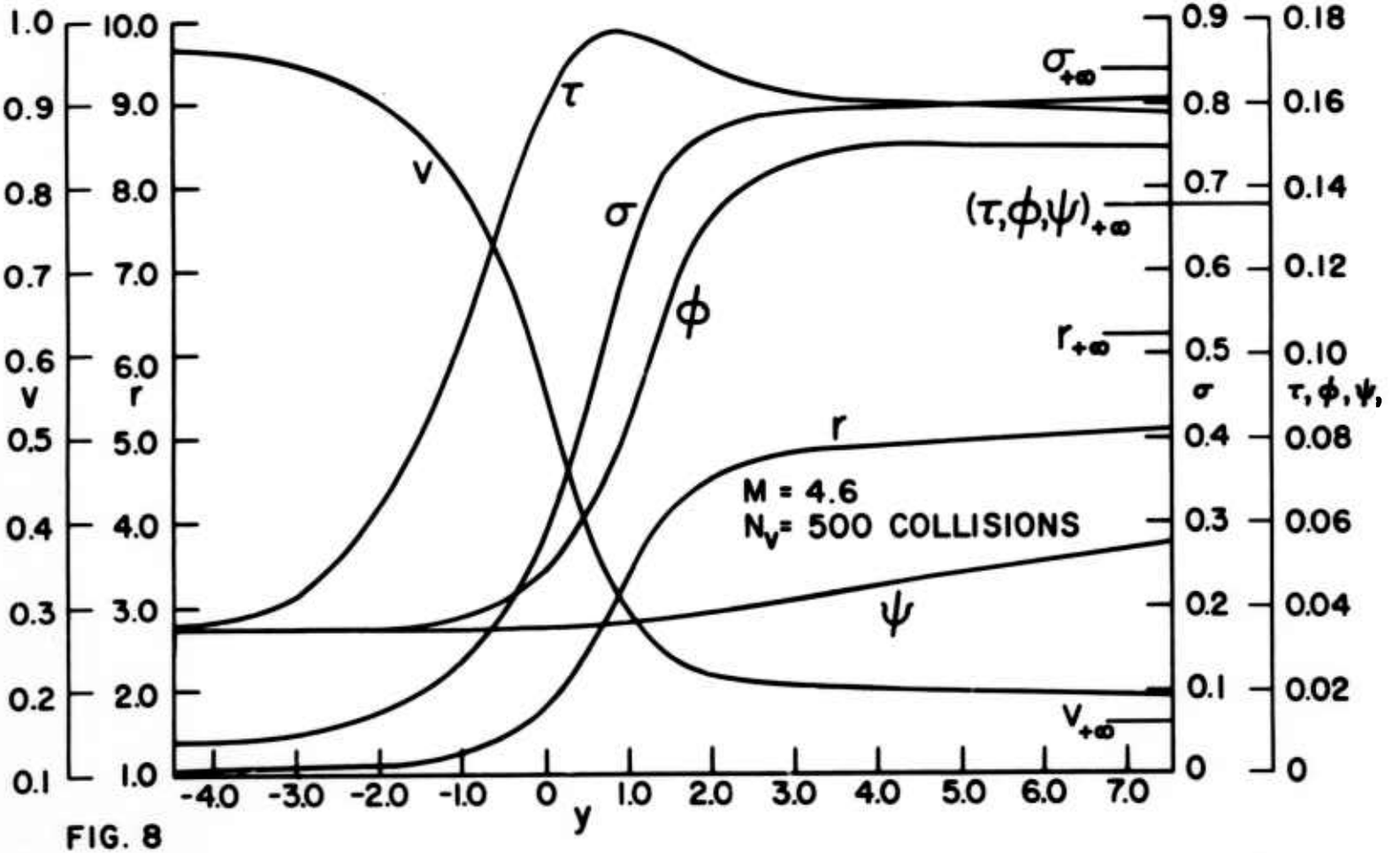

FIG. 8

SHOCK WAVE STRUCTURE IN THE SPATIAL PLANE WITH
ROTATIONAL AND VIBRATIONAL RELAXATION

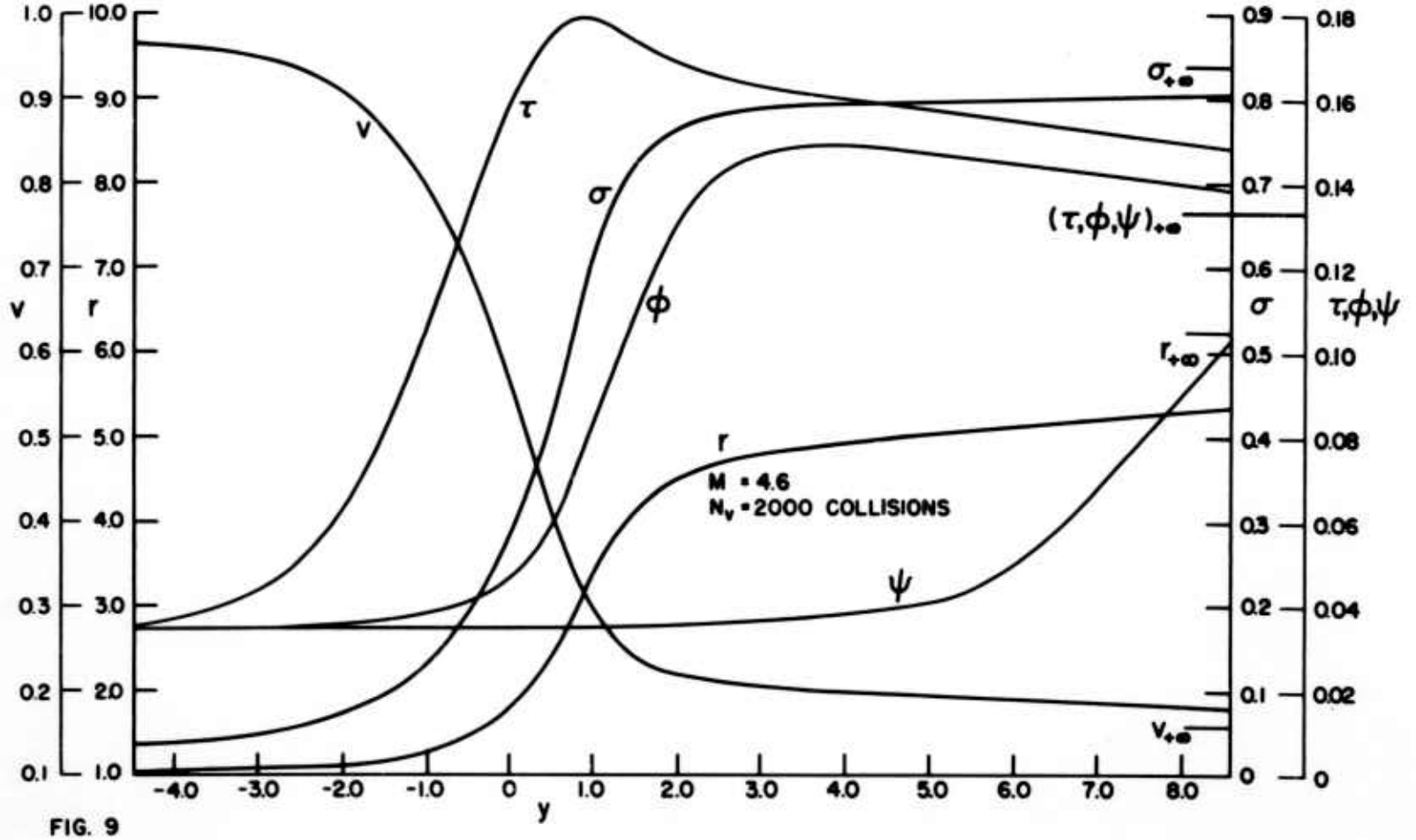

FIG. 9

SHOCK WAVE STRUCTURE IN THE SPATIAL PLANE WITH ROTATIONAL AND VIBRATIONAL RELAXATION

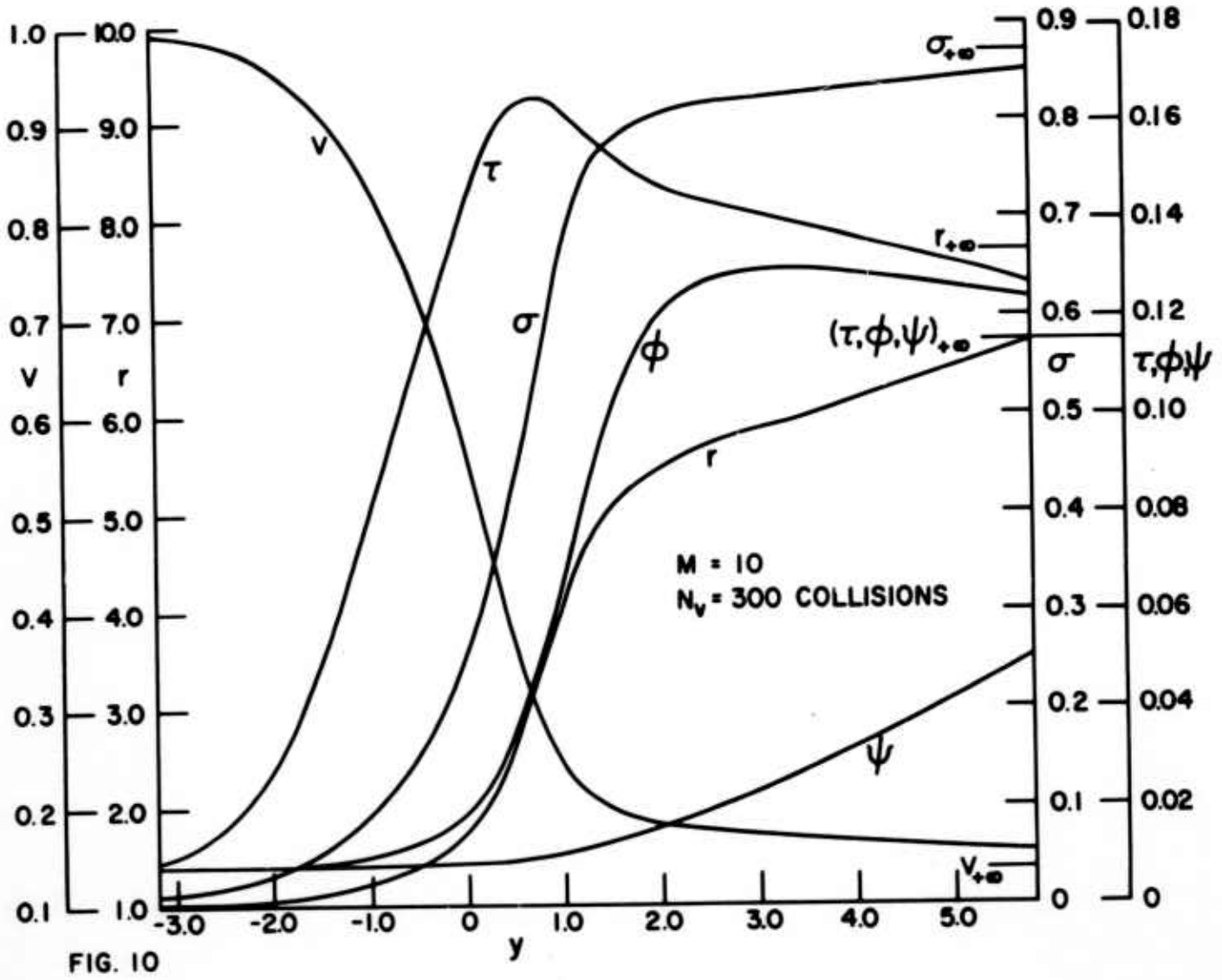

FIG. 10

SHOCK WAVE STRUCTURE IN THE SPATIAL PLANE WITH ROTATIONAL AND VIBRATIONAL RELAXATION

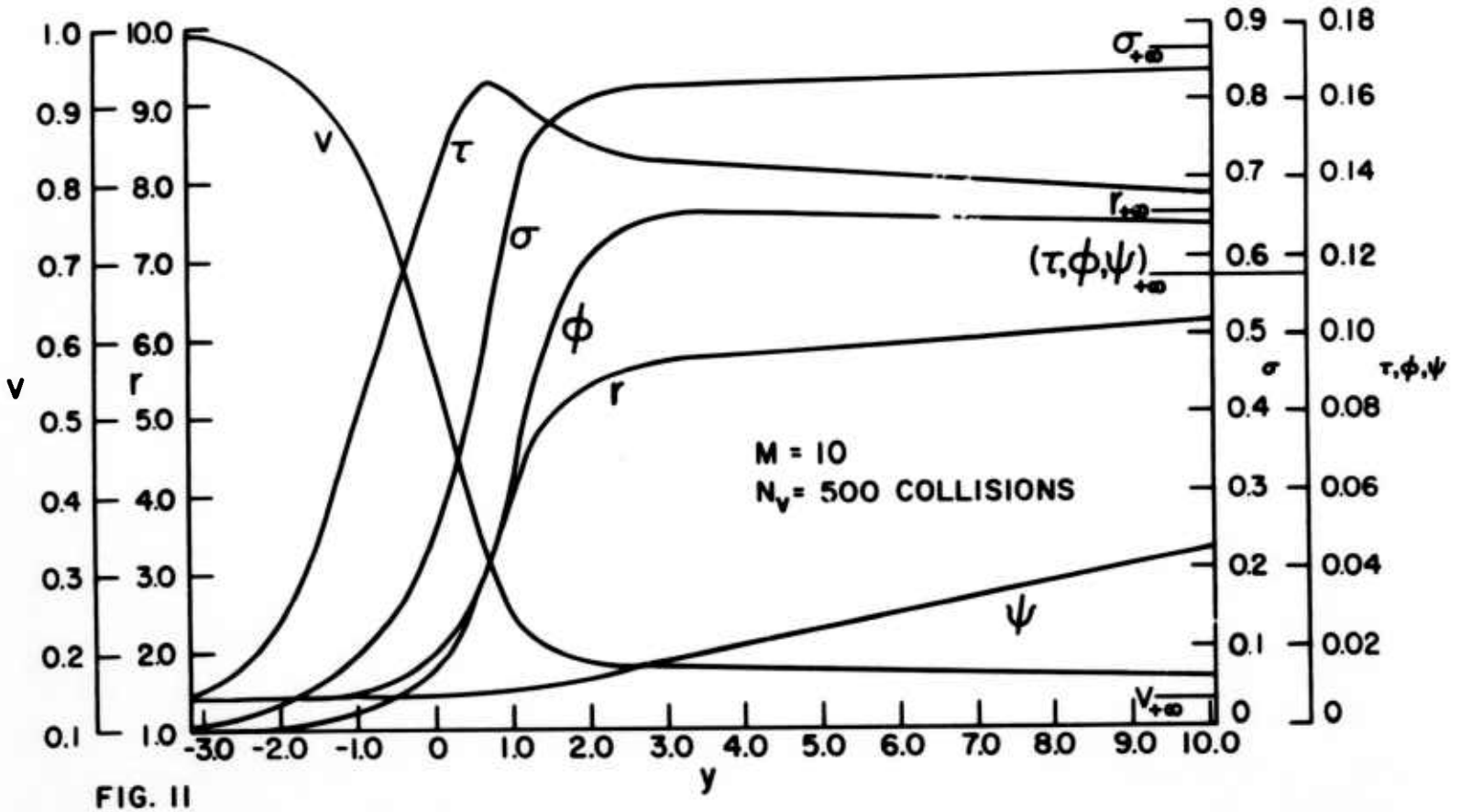

FIG. 11

SHOCK WAVE STRUCTURE IN THE SPATIAL PLANE WITH ROTATIONAL AND VIBRATIONAL RELAXATION

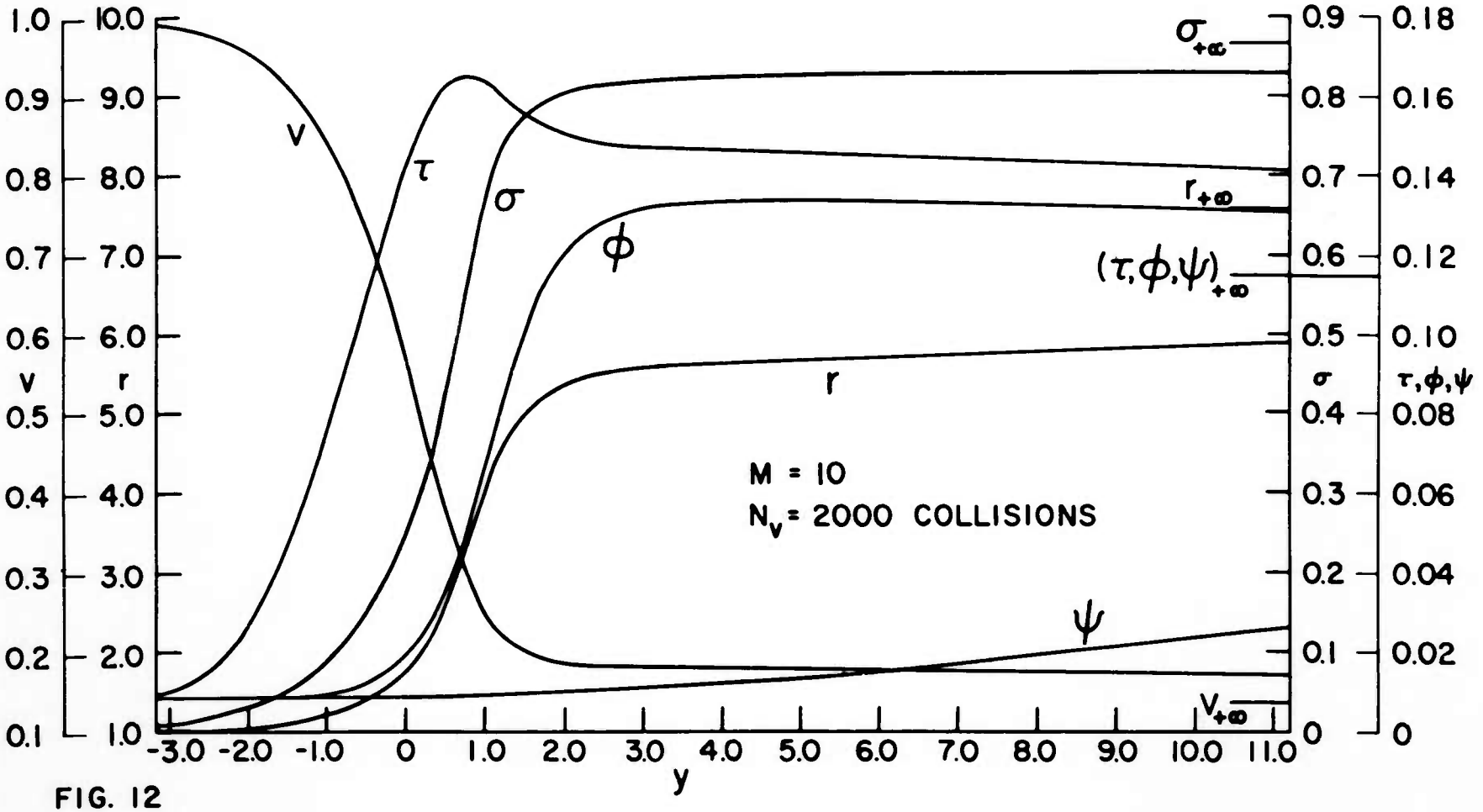

FIG. 12

CHARACTERISTIC SHOCK WAVE THICKNESS

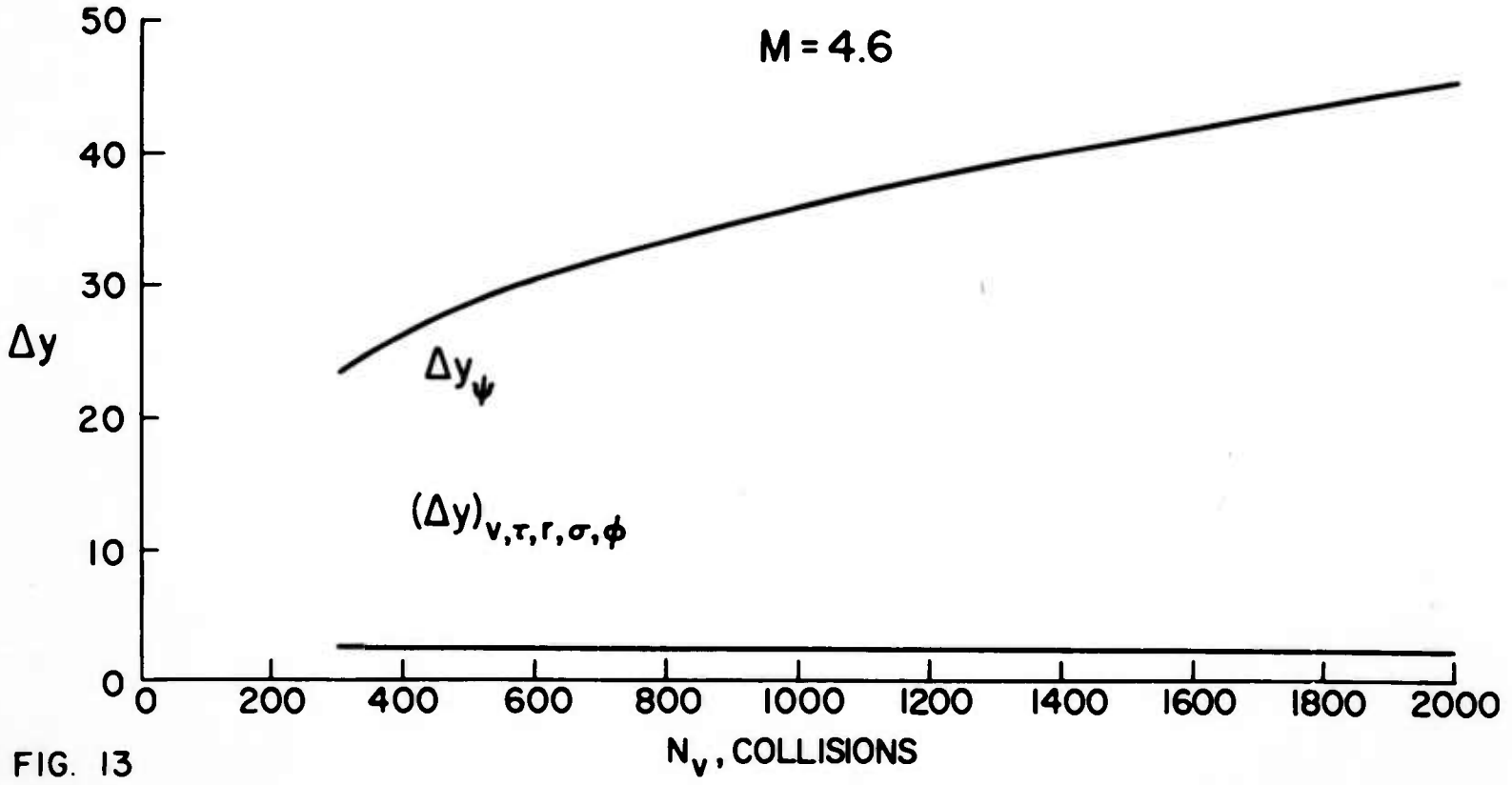

FIG. 13

CHARACTERISTIC SHOCK WAVE THICKNESS

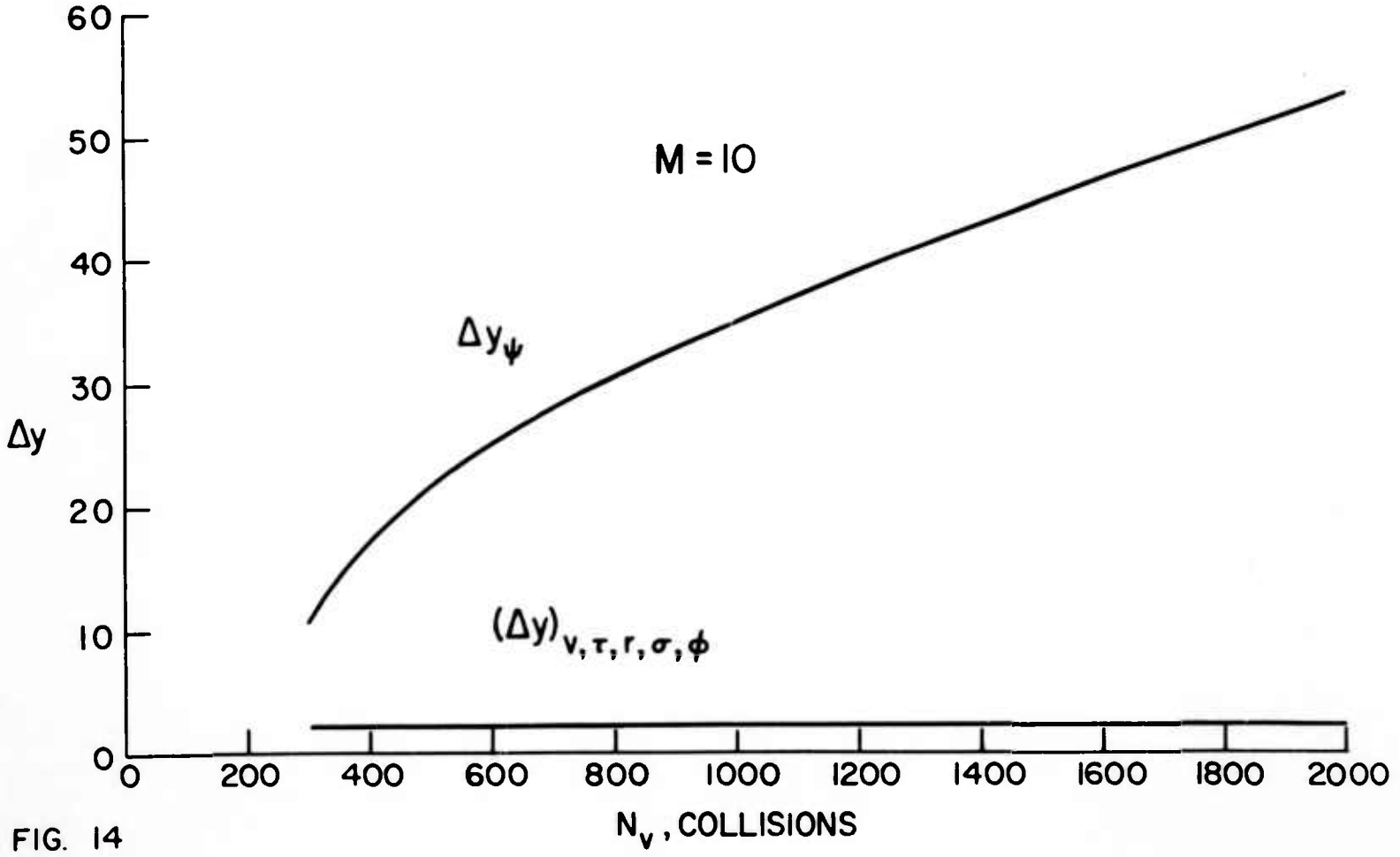

FIG. 14

PART II. A SHOCK TUBE STUDY OF THE THERMAL DISSOCIATION OF NITROGEN

B. B. Cary

CONTENTS (PART II)

LIST OF FIGURES

INTRODUCTION

This investigation was undertaken with two primary objectives. The first objective was to see if chemical reaction rates can be determined to about the same accuracy behind combustion driven shock waves as that previously attained[1, 2, 3] behind shock waves generated by high pressure hydrogen or helium. The second was to obtain chemical rate data for nitrogen. The following reaction has been studied:

$$N_2 + M \rightleftharpoons N + N + M$$

where $M = N_2$, N, Ne, or A.

The above reaction becomes of increasing importance in the air system for re-entry Mach numbers of 25 and upwards at an altitude of 100,000 feet and above.

The earliest experimental study of nitrogen dissociation at high temperatures was carried out by Eckerman[4]. A hypervelocity gun was used to fire small spheres into N_2 - Xe mixtures at high velocities. Shadowgraphs were recorded by a rotating mirror camera. These photographs allowed a determination of the distance from the front of the sphere to its bow shock wave. Eckerman has developed a method for relating the shock detachment distance to the bimolecular dissociation rates of a diatomic gas.

In 1959, Byron[5] reported interferometric measurements of the time to reach 50% of equilibrium dissociation behind shock waves in nitrogen-argon mixtures. His technique was identical to that used previously for a study of oxygen dissociation.[2]

Allen and Camm[6] have made a measurement of the recombination rate of nitrogen with the nitrogen atom and molecule as third bodies. The recombination rate can be related to the rate of decay of the intensity of non-equilibrium radiation behind the shock front. Hammerling[7] has developed a theoretical model for the origin of this non-equilibrium radiation.

At low temperatures, Herron[8], Wentinck[9], and Harteck[10] have obtained recombination rates. Herron measured the decrease of nitrogen atom concentration as a function of distance from a microwave discharge over a temperature range of 195°K-453°K. The atom concentrations were measured by "titration" with NO_2 and determination of the resulting NO by mass spectrometry. Wentinck measured the recombination rate at room temperature in a non-flow system by using an electrodeless discharge to partially dissociate the nitrogen in a spherical pyrex flask at room temperature. A platinum resistance thermometer was centered in the flask. Rate of change of the wire resistance could be correlated with the rate of disappearance of nitrogen atoms. Harteck carried out a measurement of the atom recombination rate at room temperature employing a discharge and following the radiative decay of the yellow nitrogen afterglow. To determine the recombination rate, it is necessary to measure the absolute atom concentration at one point. Harteck accomplished this by "titration" with NO.

The results obtained in this experiment will be compared with those just obtained in the final section.

THEORETICAL CONSIDERATIONS

If thermal and mass diffusion are not large throughout the dissociation zone, and moreover, if the vibrational degrees equilibrate before appreciable dissociation occurs, then it is possible to measure inferred specific rate constants.

The equation adopted for the net rate of decrease in the concentration of nitrogen molecules in a mixture of a rare gas and nitrogen is

$$\left(\frac{\partial [N_2]}{\partial t}\right)_\rho = -k_{d_1} [N_2]^2 - k_{d_2} [N_2] [N] - k_{d_3} [N_2] [\text{Rare}]$$

$$+ k_{r_1} [N_2] [N]^2 + k_{r_2} [N]^3 + k_{r_3} [N]^2 [\text{Rare}] \qquad (1)$$

The number of unknown rate constants in (1) can be reduced from six to three, if the usual assumption is invoked that at equilibrium

$$\frac{kd_1}{kr_1} = \frac{kd_2}{kr_2} = \frac{kd_3}{kr_3} = K$$

where K is the equilibrium constant. Eq. (1) must be expressed in terms of the degree of dissociation and the density in the reaction zone behind the shock front for comparison with interferometric measurements. Mathews[1] has given a form of Eq. (1) which, with the conservation equations of mass, energy, and momentum, the shock velocity, and the equation of state, yields the variation of the density of a dissociating diatomic gas as a function of distance behind the shock front. This formulation can be readily extended to include mixtures of a rare and a diatomic gas. The Appendix gives the equations

that were used in this study as well as the IBM 1620 program. Since the specific refractivity of the nitrogen atom differs from that of the molecule the program was set up to generate the index of refraction as a function of distance behind the shock front.

The equilibrium constant has to be evaluated over the temperature range of these experiments (6,000°K - 8,500°K). Treanor's[11] values are tabulated in 1,000°K steps up to 8,000°K. Baulknight's[12] tables range up to 15,000°K in smaller steps; hence, they were used throughout.

Evans[13] has shown that the density in the reaction zone can be expressed as a function of the shock velocity, initial gas state ahead of the shock, and a dimensionless parameter β defined by

$$\beta = \frac{H - E_o^o}{RT}$$

E_o^o = the enthalpy of an ideal gas at 0°K

H = the enthalpy of the gas at temperature T

R = the universal gas constant in $\frac{cal}{mol\,^oK}$ if H is expressed in $\frac{cal}{mol}$.

Fickett[14] has tabulated the values of β for the nitrogen molecule up to 12,000°K which is adequate for the temperature range carried in these experiments.

β for atomic nitrogen was calculated from 5,000°K to 12,000°K using the following relation:

$$\beta_n = 5/2 + \left\{ \frac{\sum_{n=1}^{4} g_n \frac{E_n}{k_o T} e^{-\frac{E_n}{k_o T}}}{\sum_{n=1}^{4} g_n e^{-\frac{E_n}{k_o T}}} \right\} \qquad (2)$$

g_n = statistical weight of the nth energy level of the nitrogen atom

E_n = the energy of the nth energy level of the nitrogen atom

k_o = the Boltzmann factor

T = the absolute temperature

Collision rate expressions were used for k_{d_1}, k_{d_2}, and k_{d_3} given in Eq. (1). These are:

$$k_{\substack{d_1 \\ N_2 - N_2}} = \frac{2\phi_1 N_o \delta_1^2}{\Gamma(S_1+1)} \left(\frac{\pi R}{MW_{N_2}}\right)^{1/2} T^{1/2} \left(\frac{D}{RT}\right)^{S_1} \exp\left[-\frac{D}{RT}\right]$$

$$k_{\substack{d_2 \\ N_2 - N}} = \frac{2\phi_2 N_o \delta_2^2}{\Gamma(S_2+1)} \left(\frac{6\pi R}{MW_{N_2}}\right)^{1/2} T^{1/2} \left(\frac{D}{RT}\right)^{S_2} \exp\left[-\frac{D}{RT}\right]$$

$$k_{\substack{d_3 \\ N_2 - Rare}} = \frac{2\phi_3 N_o \delta_3^2}{\Gamma(S_3+1)} \left(\frac{\frac{2\pi R}{MW_{N_2} \cdot MW_{Rare}}}{MW_{N_2} + MW_{Rare}}\right)^{1/2} T^{1/2} \left(\frac{D}{RT}\right)^{S_3} \exp\left[-\frac{D}{RT}\right] \quad (3)$$

where the rate constants are expressed in $\frac{cm^3}{mol - sec}$

ϕ_1, ϕ_2, ϕ_3 = collision efficiency factors

N_o = Avogadro's number

δ_1 = diameter of the molecule

δ_2 = diameter of the nitrogen atom taken equal to δ_1

δ_3^2 = the average of the squares of the diameters of the molecule and rare gas atom

D = dissociation energy

R = universal gas constant

T = absolute temperature

S_1, S_2, S_3 = one-half of the square terms available in internal energy of the molecule, nitrogen atom, and rare gas atom respectively.

The above expressions are based upon the assumption that only the relative translational energy along the line of centers at the time of impact is available for dissociation. Limits can be placed upon the value of S_1. It can range in value from 0 when none of the internal degrees contribute to the dissociation energy up to an upper limit of 3. Byron[2] found in oxygen that S_1 was 2.0 by a best fit of the data. He had sufficient sensitivity to show that a value of 2.0 for S_1 gave a better fit of the experimental data than a value of 2.5. Since the atoms cannot contribute to the dissociation energy from rotational and vibrational degrees, the values of S_2 and S_3 should range between the limits of 0 to 1.5. The upper limit of 1.5 arises from the fact that at least one of the rotational degrees of freedom of the molecule is not free to contribute to the dissociation energy in order to conserve angular momentum. However, an excited atom can have a larger value for S.

The limitations of such a simple theory of reaction rates have already been fully discussed in the literature.[1, 2] It would be ideal to have static sources for the study of high temperature reactions. But at present there is no such source available for temperatures in the vicinity of 5000°K. Even if

one had such a source, so that very careful reaction rate measurements could be made, this knowledge alone would not be sufficient for a full understanding of a shock transition. The principal motivation of this research is toward a better understanding of shock structure in a diatomic gas. Accordingly then, the philosophy has been one of compromise wherein shock reaction zone data has been employed to infer values for the specific dissociation rates in nitrogen. It is hoped that the insertion of these rates into a shock structure model which includes the differential equations of fluid motion, relaxation equations, and diffusion effects will lead to more insight into shock front structure.

EXPERIMENTAL PROCEDURE

The shock tube and associated equipment used for this study are shown in Figure 1. The stainless steel tube has a cross section of 2" x 2". The driven part of the tube is about 25 feet long while the driver (not shown) has a length of 5 feet. The driver section is equipped with 5 spark plugs distributed alternately along the tube walls. In addition, 5 fill ports are uniformly distributed along the driver for the purpose of loading the combustible mixture. The mixture used was 10% O_2, 20% H_2, and 70% He at initial load pressures of about 300 psi, 600 psi, and 800 psi absolute. The combustible gases were allowed to mix for 8 minutes prior to ignition. Water pumped, commercial grade gases were used throughout for the driver loads.

Station 1 in Figure 1 shows a light screen which was used to trigger a tungsten exploded wire light source (4). If the light screen photomultiplier fed directly into a resistive load, appreciable pre-triggering occurred owing to the luminosity of the strong shocks generated. In order to reduce this effect an inductive load was inserted, so that the light screen was more sensitive to high frequencies. Triggering by a shock roughly corresponds to a high frequency signal input whereas triggering by the luminosity of the approaching shock wave might be considered to correspond to a lower frequency signal input. In practice, the inductive load kept the pre-triggering of the light screen to a maximum of 20-30 microseconds for all shock strengths generated in this study.

As Figure 1 shows, both beams of the Mach-Zehnder interferometer pass through the test section similar to Byron's[2] arrangement. The distance downstream from the light screen (1) to the upstream beam of the interferometer (2) is 2 feet and the distance downstream to the other interferometer beam (3) from (2) is 1 foot. At (2) there is a window port in the top center of the test section in which a Kistler SLM pressure gauge could be mounted.

A tungsten wire (4) exploded by the discharge of a delay line which had 16 kilojoules of stored energy provided the light source for the recording of time-resolved interferograms. This source has a rise time of 50 microseconds and a useful duration of about 800 microseconds. By actual spectrographic observation, narrow wavelength bands could be isolated with the aid of Bausch and Lomb interference filters. These bands were never wider then 100 $\mathring{A}$. Consequently, good monochromatic fringes could be obtained in the blue, green, and red regions. The time-resolution was accomplished by use of a 60 micron slit imaged at the windows at locations (2) and (3) in conjunction with an air turbine driven camera. A beam splitting arrangement inside the rotating drum camera permitted the simultaneous recording of white and monochromatic fringes. The 60 micron slit width gave good space resolution and the ultimate time resolution was .15 microseconds. All the interferograms were read on an optical comparator which has a linear accuracy along both axes of 1 part in 14,000. Distances could be measured accurately down to 10 microns. Generally, the drum was rotated so that the film had a time scale of 50 microseconds per cm (the limit is 30 microseconds per cm). Ansco 70 mm

super hy-pan film was employed. Since this film has 100 grains per millimeter, it is concluded that an actual time resolution of about .25 microseconds was attained in laboratory coordinates.

The shock velocity was measured over the 1 foot distance from the upstream beam (2) to the one downstream (3) from the interferogram. Simultaneously, the shock velocity was measured over the 2 feet from the light screen (1) to the Kistler pressure gauge at (2). The optical method was accurate to .2% while the pressure gauge method has an accuracy of $\frac{1}{2}$ - 1%. All runs indicated that the maximum local attenuation was no larger than 1% of a Mach number per foot which was surprisingly good. However this attenuation agrees well with that observed by Wittliff[15] and Waldron[16] for constant volume combustion about 20 feet downstream of the diaphragm. Stainless steel and copper diaphragms were used with about 30%-40% scribe depth. The x scribes were held to a tolerance of + .001" and -.000". The initial combustible load was carefully matched to yield a peak pressure equal to the burst pressure of the diaphragm. A pressure gauge was mounted in the driver for the purpose of attaining a good match between load and diaphragm. The material for the diaphragm was carefully controlled and the scribe marks were cut 45° to the grain. Very reproducible breaks were obtained. One series of 3 runs repeated under the same conditions indicated that the shock velocity at the test section could be reproduced to about 2%.

After acquiring good control of the constant volume technique, it was still a moot question whether the flow region behind the shock front would be steady enough in time to permit a quantitative study of the reaction zone. Byron[2]

and Rose[17] have observed a rapid decay in gas density behind the shock wave as it passed a given point even when it was certain that a shock and not a detonation wave had been generated. Byron[18] attributed this decay to the arrival of many expansion waves from the hot driver gases which expand down the tube. Alternatively, Rose[17] emphasized the importance of the cooling of the shock heated sample gas by rapid heat transfer to the walls through the turbulent boundary layer. Another possible source of these expansion waves is the continued burning of the driver gases as they expand along the driver tube approaching constant pressure burning[15]. Some evidence was found to support this view. On two runs the diaphragms were defective and opened long before the burning was complete. The interferograms seemed to show a larger decay. Consequently, it was believed that by exercising great care in matching loads and diaphragms, and also in the fabrication of the diaphragms, this decay might be reduced. The first interferograms taken with good combustion control showed a promisingly small decay. But it was decided that a further check was necessary before the flow could be assumed steady enough for quantitative studies. A necessary condition for steady flow is that the reaction zone density profile be unchanging in time as it proceeds past the slit at the upstream interferometer window (2). In order to demonstrate that the flow fulfilled this requirement two slits placed 1 cm apart were employed. The anticipated reaction zone length prompted this choice of slit spacing. In order to avoid double photographic exposures the upper half of the upstream slit was masked off simultaneously with the lower half of the downstream slit. Figure 2 shows a monochromatic interferogram taken with the

double slit showing a M 11.0 shock in nitrogen with a time resolution of 55 microseconds per cm. The reaction zone can be clearly seen at both slits. Comparative measurements indicated that the profile shape is unchanged as the shock traverses the 1 cm slit separation; hence, it appears that these shock induced flows are sufficiently steady in time for measurements to be taken. Returning to Figure 2, note that a vibrational relaxation zone can be distinguished from the dissociation zone owing to the relatively low Mach number. A compression wave can be seen following about 20 cm behind the shock. This wave was primarily observed only for combustion runs in nitrogen. Combustion runs into the mixtures and cold hydrogen pressure breaks into nitrogen did not generate any sizeable secondary waves.

The presence of such waves pursuing the shock wave along the tube attests to the desirability of examining the flow field behind combustion driven shock waves prior to making other types of measurements, for example, spectrographic.

The fringe shifts could be read accurately to at least .1 of a fringe width. However, in adjacent regions along the profile the fringes were sensitive to displacements of only .03 fringe which agrees with the conclusion reached by Mathews[2].

Figure 3 shows a M 10.3 wave in a 13% nitrogen-87% neon mixture. For simplicity only the white interferogram is shown. When the shock arrives at the upstream window the fringes jump up corresponding to the rise in density. Then there is a small decay which is quite linear until the shock arrives at the downstream window. Here the fringes jump back below the original position,

because the density jump turns out to be exactly the same as it was when the shock was at the upstream window. This is consistent with the shock velocity measurements which indicated that there was no more than a 1% decrease in Mach number of the shock as it traversed the one foot distance between the two windows. The vibrational relaxation zone can also be seen in Figure 3.

Figure 4 shows a monochromatic interferogram of a M 11.5 shock in a 15% nitrogen-85% argon mixture. The decay is again relatively small. Throughout this study the decay was generally small enough, so that its effect was negligible on the reaction zone. However, in the neon mixtures the decay began to have some influence as equilibrium was approached. Therefore in these runs the reaction profile could only be followed up to about 70% of equilibrium. The interferometric sensitivity was smallest in the neon mixture. To partially offset this fact, all the runs with the neon mixture were made at initial pressures of about 2 cm.

Fundamentally, the interferometer measures changes in the index of refraction of the gas. These can be linearly related to density changes through the Gladstone-Dale relation provided the mean specific refractivity is known. White[19] has measured the specific refractivity of the nitrogen atom and found good agreement with a calculation made by Dalgarno[19]. Since he used an interferometer it may be argued that perhaps dissociative equilibrium is not obtained behind the shock. If Dalgarno's calculation is good to an order of magnitude, and it appears to be so, then one can select degrees of equilibrium dissociation for which the specific refractivity of the nitrogen atom will play a negligible role as long as its order of magnitude is known. For example,

if the shock leads to only 6% equilibrium dissociation, then the index of refraction measurements can be directly converted into densities safely neglecting the specific refractivity of the nitrogen atom. In this way, ar unambiguous demonstration can be made showing that equilibrium is attained at lower Mach numbers (and therefore temperatures); it is even more certainly attained at higher Mach numbers where for higher degrees of dissociation (10% and upwards) one must take into account the nitrogen atom refractivity. White's measured value of .31 $\frac{cm^3}{gm}$ for the specific refractivity of the nitrogen atom was incorporated into the theoretical profiles of the index of refraction as a function of distance behind the shock front in shock fixed coordinates. The distances measured on the film were converted to distances in shock fixed coordinates by the following relation

$$(\text{shock fixed}) = \frac{x \cdot U_s}{\text{film speed}} \tag{4}$$

where U_s is the shock velocity and x is the distance measured along the time axis of the film from the shock front. The film speed which was measured by a Berkeley counter and the shock velocity were known to an accuracy of $\frac{1}{2}$ %. This conversion introduced no error since owing to the limitations of film grain, measurements taken in shock fixed coordinates would not be better than $\frac{1}{2}$ %. Film shrinkage after development was monitored and found to introduce negligible error in the measurements.

It will be instructive to consider the actual magnitude of the numbers involved in two cases in order to gain insight into the influence of changing refractivity versus changing density upon the index of refraction.

Case I: 100% nitrogen

Mach No. = 13.5; 9.95% of the molecules dissociated at equilibrium

The Gladstone-Dale relation is

$$(n - 1) = b\rho \tag{5}$$

where b is the specific refractivity, ρ the density, and n the total index for any point on the reaction profile. Since the interferometer measured changes in total index let b_o, ρ_o, and n_o represent the same quantities at the point where vibration is equilibrated and no dissociation has begun. The quantities in Eq. (5) may be defined as

$$\begin{aligned} n &= n_o + \Delta n \\ p &= \rho_o + \Delta \rho \\ b &= b_o + \Delta b \end{aligned} \tag{6}$$

Substituting into (5)

$$(n_o - 1) + \Delta n = b_o \rho_o + \rho_o \Delta b + b_o \Delta \rho + \Delta \rho \Delta b$$

$$\therefore \Delta n = b_o \Delta \rho + \Delta b \left[\rho_o + \Delta \rho\right] \tag{7}$$

Since $n_o - 1 = b_o \rho_o$ by (5)

The change Δn from the point corresponding to vibrational equilibrium and no dissociation up to full equilibrium is 8.14×10^{-6}. The corresponding values of b_o, Δb, $\Delta \rho$, and ρ_o are,

$$(\lambda = 4549\ \text{Å}) : b_o = .241 \frac{cm^3}{gm}\ ;\ \Delta b = 6.50 \times 10^{-3}; \frac{cm^3}{gm}\ ;\ = 30.28 \times 10^{-6}\ gm/cm^3$$

$$\rho_o = 98.51 \times 10^{-6}\ gm/cm^3$$

Substituting into Eq. (7)

$$8.14 \times 10^{-6} = (.241)(30.28)\,10^{-6} + (6.50)\,10^{-3}\,[98.51 \times 10^{-6}$$

$$+ 30.28 \times 10^{-6}] = 7.30 \times 10^{-6} + .84 \times 10^{-6}$$

Note that the $b_o \Delta\rho$ term is about 9 times larger than the term involving Δb.

Case II: 15% nitrogen-85% argon

Mach No. = 11.7; 80% of the molecules dissociated at equilibrium

The differences between the values at full equilibrium and vibrational equilibrium are:

$$\Delta n = 15.10 \times 10^{-6};\ \Delta\rho = 77.05 \times 10^{-6}\ \text{gm/cm}^3;\ \Delta b = 6.26 \times 10^{-3}\ \frac{\text{cm}^3}{\text{gm}}$$

Substituting into Eq. (7):

$$15.10 \times 10^{-6} = (.169)(77.05)\,10^{-6} + (6.26)\,10^{-3}\,[252.77 \times 10^{-6}$$

$$+ 77.05 \times 10^{-6}] = 13.03 \times 10^{-6} + 2.07 \times 10^{-6}$$

Consequently, while the first term on the right still dominates it is now only about 6 times larger than the second term on the right. If the error in White's value were as large as 5% it would still only produce a 1% error in the change in total index in Case II above.

The initial pressure of the sample gas prior to shock heating was measured by a Wallace and Tiernan absolute manometer, and pressures above 2 cm of mercury were read on an absolute mercury manometer with a cathetometer. The manometer was isolated from the system by a liquid nitrogen trap. The initial temperature of the gas was measured with a calibrated thermometer which could be read directly to tenths of a degree.

In regard to the pre-mixing of driver and test gas by diffusion across the contact zone, Hooker[26] has shown by spectrographic absorption measurements for initial gas pressures of .5 cm and upwards that 40% of the ideal test time is free from driver gas contamination. The initial gas pressure ranged from about 9 mm - 27 mm in the present study. In all of the interferograms a sharp rise in index of refraction could be seen entering the upstream beam of the interferometer after the shock had already arrived at the downstream beam. In Figures 3 and 4 this is easily seen and probably represents the arrival of the driver gases. In all cases the actual test time appeared to be from 33%-50% of the ideal. The Kistler pressure gauge records indicated that the average value of the pressure was constant over this whole zone of flow up to 50% of the ideal flow duration. As far as boundary layer effects are concerned they are negligible in all cases over the length of reaction zones observed here (1 cm-3 cm). Interferograms of shocks in pure argon at Mach numbers of about 6 conveniently reveal information on rate of growth of the boundary layer.

Throughout this study Matheson pre-purified water pumped nitrogen and argon were used. These were guaranteed to have impurity levels less than 20 ppm. The neon was of research grade. In the early pure nitrogen runs the system was evacuated to about 1 micron and in the later runs to .6 micron. This was followed by a continuous flush at the initial pressure chosen for each run up to within 20 seconds of ignition. The total leak rate averaged between 1-2 microns per minute. When the mixtures were run a larger diffusion pump was put into the system and the system was pumped down to about .2 micron

read on a Phillips gauge. All diffusion pumps were isolated by liquid nitrogen traps. To further check the cleanliness of the system, a glass tonometer tube was fuzed into the tube. A typical pre-run cycle was carried out and then the tonometer vessel was brought up to atmospheric pressure with the sample gas and sealed off. Crippen laboratories made a mass spectrometric analysis. They found that oxygen, hydrocarbons, and water vapor were present in quantities less than 25 ppm which is in good agreement with levels expected from a knowledge of the vacuum system and gas purity.

A spectrographic window was inserted in the top of the tube above the upstream interferometer beam in place of the pressure gauge. An f-3 time-resolved spectrograph (See 5 in Figure 1) was utilized to examine the luminosity emitted behind shocks in nitrogen and the nitrogen-argon mixture. The violet band system of CN was not observed since it would have to be present at levels of about 150 ppm in order to be observed with the present spectrograph. The first negative band system of N_2^+ was not observed in pure nitrogen shocks up to Mach numbers of 14.

Since the combustion technique produces large amounts of water in the tube it was felt advisable to manually clean the tube prior to repumping. Wooden blocks covered with a relatively lint-free paper were pushed through the tube. After this was done a careful inspection was made by shining a light down the driven section of the tube to be certain that no dust or lint remained.

RESULTS

Tables I and II give the pertinent data for fourteen final data runs yielding information on vibrational relaxation times and dissociation rates. The vibrational relaxation times obtained in pure nitrogen were about a factor of two longer than Blackman's[20]. Previous experimentation has shown that the vibrational relaxation time can be shortened considerably if there are small amounts of water vapor and hydrocarbons present. The longer times observed here may be a direct result of better impurity control. The pure nitrogen data of Table I do not cover a sufficient temperature range to distinguish between Widom's[21] and Landau's[20] theories.

Turning from the results for pure nitrogen to the mixtures, the neon mixture dissociation runs had a surprisingly long vibrational relaxation zone. Within the precision of the measurements neon seemed to be less than 10% as effective as nitrogen molecules in exciting nitrogen vibrationally. The argon mixture data given in Table I implied that argon was about as efficient as the nitrogen molecule in exciting nitrogen vibrationally. The argon efficiency was inferred by comparing the actual relaxation time in the mixture to an extrapolated time based on the lower temperature nitrogen data, assuming that the argon played no role. Extrapolation by either Widom's or Landau's theory inferred that the argon atom is as efficient in vibrationally exciting nitrogen as the nitrogen molecule itself. This result checks well with the observation by Blackman that the nitrogen molecule was only 40% as effective as the oxygen molecule in exciting oxygen vibrationally. Byron[18] found that the argon atom was about 30% as efficient as the oxygen molecule in exciting oxygen vibrationally.

Concerning the question of vibrational equilibration in the dissociation runs the following procedure was adopted. First, the time was measured behind the shock front to the point which had the index of refraction corresponding to vibrational equilibrium. This time was then compared with the relaxation time extrapolated by the Landau theory (predicting slightly longer times that Widom's), and in every case the observed time was no longer than Landau's. For the higher temperature runs in the argon-nitrogen mixture the vibrational relaxation zone was so short that it coalesced with the shock front. In closing this discussion of the vibrational relaxation, it may safely be concluded that vibration was equilibrated before any measurable dissociation occurred. Therefore, there was no detectable coupling between the vibrational and dissociative processes over the temperature and pressure ranges of these experiments.

Referring to Table II it is seen that the highest temperature obtained for vibrational equilibrium and no dissociation was 10,963°K (no reaction). The experimentally inferred rates imply that even in this case only about 1 in 10,000 collisions produces a dissociation. Therefore, the assumption that the vibration and rotational degrees maintain equilibrium with the local kinetic temperature throughout the dissociation process is valid, since it takes only about 1,000 collisions to equilibrate vibration, and less than 100 collisions to equilibrate rotation at these temperatures. Consequently, use of the collision rate expressions given in Eq. (3) which ignore coupling between the dissociation and vibrational processes is justified in this study.

The initial values that were chosen for S_1, S_2, and S_3 in Eq. (2) were 2.0, 1.0, and 1.0 respectively. These were the values reported by Byron[5] from data taken in nitrogen-argon mixtures. The IBM 1620 could run twelve different profiles simultaneously for various choices of ϕ_1, ϕ_2, and ϕ_3. A good over-all fit of the nine runs of Table I was not obtained for these values of S. Figures 5, 6, 7, and 8 show the experimental profiles for runs 3, 5, 6, and 7. A theoretical profile is shown in each of the figures which has the S and ϕ values obtained by Byron. A glance at Table II shows that runs 3, 5, 6, and 7 cover almost a 3,000°K range in the no reaction temperature. Further, owing to the higher dissociation energy of nitrogen, the temperature drop between the no reaction point and dissociative equilibrium is greater than that occurring in oxygen for the same degree of equilibrium dissociation. In view of the fact that a good fit could not be obtained for Byron's values of S_1, S_2, and S_3, it was decided to vary these parameters. The value of S_1 was varied between 1.7 and 2.5 in incremental steps. The corresponding values of S_2 and S_3 were set equal to $(S_1 - 1.0)$ in each case.

Then twelve profiles were generated for runs 3, 6, and 7 for each set of S values by varying the ϕ values. An optimum set of ϕ values could be picked for every set of S values. After plotting the profiles, the following set appeared to hold promise for obtaining a good compromise fit for the profiles of Figures 5, 6, 7, and 8:

$$S_1 = 2.2;\ S_2 = S_3 = 1.2;\ \phi_1' = .08;\ \phi_2 = .3;\ \phi_3' = .08$$

At this point it was discovered that there was an erroneous factor of $\sqrt{3}$ multiplying the expression for k_{d3}. Therefore the correct value of ϕ_3 was

that cited above multiplied by 1.73; hence, in these three cases the true values of ϕ_3 were larger than the ϕ_1 values. This was a disturbing result, since if the classical collision theory has any validity at all, it is expected that the efficiency parameter ϕ_3 for collisions with rare gas atoms should be no larger than ϕ_1 which pertains to collisions with nitrogen molecules. Therefore it was decided to vary S_2 and S_3 (letting $S_2 = S_3$) while S_1 was held fixed at values of 1.7, 2.0, 2.2, 2.3, 2.4, and 2.5. The argon-nitrogen mixtures offered the best chance for detecting any sensitivity to variation of S_2 and S_3, since they had the largest degrees of dissociation and covered a temperature range of 3,000°K. With the values of $\phi_3' = .08$ and $S_3 = 1.3$ the magnitude of the product $\phi_3' \left(\frac{D}{RT}\right)^{S_3} \sqrt{3}$ was determined for the hottest run (6). Recalling that $\phi_3 = \phi 3' \sqrt{3}$, a series of ϕ_3 and S_3 values were calculated that kept the value of $\phi_3 \left(\frac{D}{RT}\right)^{S_3}$ fixed, so that a good fit of the upper part of the profile in Figure 7 (run 6) was maintained. These choices were then fitted to the coolest nitrogen-argon run in Figure 6: The profile seemed to favor the following:

$$S_1 = 2.2;\ S_2 = S_3 = 1.5;\quad \phi_1 = .08\ ;\quad \phi_2 = .15;\quad \phi_3 = .08$$

This fits slightly better at the top of the profile than does $S_1 = 2.2$; $S_2 = S_3 = 1.2$; $\phi_1 = .08$; $\phi_2 = .3$; $\phi_3 = .18$. Admittedly, there is no great precision in getting the best value for S_2 and S_3; However, the data suggested that the values of S_2 and S_3 were nearer to 1.5 than 1.0. The value adopted here for S_2 and S_3 of 1.5 is still consistent with the predictions of classical collision theory.

In regard to the determination of S_1, Figures 5, 7, and 8 show that 2.3 was slightly better than 2.0 or 2.5. The final set of values adopted here was:

$$S_1 = 2.2;\ S_2 = S_3 = 1.5;\ \phi_1, = .08 \quad \phi_2 = .15;\ \phi_3 = .08$$

Hence the final values for the rate constants inferred here are:

$$(N_2 - N_2) : k_{d_1} = (6.8 \times 10^{22}) \times T^{-1.7} \times \exp\left(-\frac{113,260}{T}\right) \pm 25\% \ \frac{cc}{mole\text{-}sec.}$$

$$(N_2 - N) : k_{d_2} = (5.5 \times 10^{19}) \times T^{-1.0} \times \exp\left(-\frac{113,260}{T}\right) \pm 40\% \ \frac{cc}{mole\text{-}sec.}$$

$$(N_2 - Ne) : k_{d_3} = (1.5 \times 10^{19}) \times T^{-1.0} \times \exp\left(-\frac{113,260}{T}\right) \pm 40\% \ \frac{cc}{mole\text{-}sec.}$$

$$(N_2 - A) : k_{d_4} = (2.1 \times 10^{19}) \times T^{-1.0} \times \exp\left(-\frac{113,260}{T}\right) \pm 40\% \ \frac{cc}{mole\text{-}sec.}$$

The ratio of the two ϕ_3 values for neon and argon as third bodies was determined from the conservation equations of energy and momentum. The fraction of energy transferred to a nitrogen molecule on impact was calculated for both rare atoms. Equating the initial kinetic energies of the two rare atoms before they undergo impact with the nitrogen molecule allows one to estimate a relative efficiency for each in transferring energy to the nitrogen molecule. Argon and neon turned out to be equally efficient by this calculation and so ϕ_3 was taken to have the same value for both argon and neon. This estimate of efficiencies is purely classical and rests upon the assumption that the rare atoms can be treated as rigid spheres. This is a fair assumption for neon owing to its high excitation potentials, but was somewhat weaker for argon. An examination of the luminosity behind the shocks in the nitrogen-

argon mixtures by means of the f-3 spectrograph indicated no evidence of argon excitation.

Table III gives the values of the inferred recombination rates at 6, 400°K for the four third bodies (N_2, N, A, Ne). Byron's[5] values with N_2, N, and A as third bodies are shown also, as well as Eckerman's[4] value with Xe as the third body, and Camm's[22] value for N_2 and N as third bodies. Recently Allen[6] has collected more data using the same technique as Camm. While the value for the recombination rate constant k_{r_2} is still about the same with N as the third body the value of k_{r_1} is at least 13 times smaller than k_{r_2}. This result does not seem reasonable. The success of their method rests upon the validity of the kinetic model for the origin of the radiative decay that is observed. Hammerling's[7] proposed kinetic scheme has been criticized[23]. This is an ingenious experiment, but it appears that there is need for further experimental studies of the origin of the luminosity behind strong shocks in nitrogen.

In addition to presenting the inferred rate constants at 6,400°K in Table III, the extrapolated values for k_{r_1} (N_2 third body) and k_{r_3} (A third body) adopted in this paper and those of Byron are listed for comparison with the measurements of Harteck[10], Heron[8], and Wentick[9] made at 300°K. The rate constant k_{d_1} obtained in this paper is about 13-20 times larger at 300°K than the other values. This failure of rate constants inferred from shock tube measurements to extrapolate down to the values obtained at 300°K has caused criticism of the shock tube measurements. Therefore, some discussion of this point is warranted. If we wished to choose the appropriate value of S_1

in the expression for k_{d_1} at 300°K, we must consider how many internal degrees of freedom can contribute to the dissociation of one nitrogen molecule upon colliding with another. Since the vibrational characteristic temperature of nitrogen is high (3,337°K), only about 1 in 66,000 nitrogen molecules will possess the full classical vibration.

Classically, probably only 2 rotational degrees and the vibrational degree of the dissociating molecule can contribute to the energy of dissociation; hence, S_1 takes on a value of 2.0. Then by making a reduction in ϕ_1, from .08 to .03 and setting S_1 equal to 2.0, the calculated rate k_{r_1} will agree fairly well with the measurements of Herron, Wentinck, and Harteck. Since the collision theory is only classical, it is unreasonable to demand that ϕ_1, and S_1 remain constant over a temperature range of 6,000°K. The changes in S_1 and ϕ_1, suggested here (.2 and .05) between 6,400°K and 300°K are not totally inconceivable. At the high temperatures, an S_1 of 2.2 seems to give a better fit than an S_1 of 2.0. If the vibrational energy of both colliding molecules were available for dissociation, S_1 would be 2.5. The fact that a value of 2.2 seems to be favored at the high temperatures is therefore not unreasonable, implying that some of the vibrational energy of the undissociating molecule is available. Recall that over the temperature range of these experiments almost all of the nitrogen molecules possess their full classical vibration.

Another criticism of shock tube dissociation measurements is the reported anonomously high efficiency for dissociation of the parent molecules by the daughter atoms. All of the shock tube measurements in oxygen and the recent work of Gardiner[24] in hydrogen have yielded this result. The present

study differs from those measurements in that the results here imply that the nitrogen atom is about as efficient as the nitrogen molecule in promoting the dissociation of nitrogen molecules at 6,400°K. It should be emphasized that the different nitrogen atom rate constant found here is not a direct consequence of the fact that the data favors values nearer to 1.5 for S_2 and S_3 than 1.0. The rate k_{d_2} is proportional to the product $\phi_2\left(\frac{D}{RT}\right)^{S_2}$. Therefore, the fact that k_{d_2} is of the same order as k_{d_1} at 6,400°K is independent of the ability to select S_2 or S_1 precisely. The fact that there seemed to be a tendency of the data to favor S_2 nearer to 1.5 than 1.0 can be attributed to the use of the combustion technique which allows one to achieve high degrees of dissociation (80%) at high initial pressure (3 cm) for mixtures that are not too lean (15% N_2-85% A). This fact helps the sensitivity of any optical method of study. A comparison of the sensitivity of the measuring techniques, of tube widths, initial pressures, composition, and percent change in density throughout the reaction zone for the same degree of equilibrium dissociation between this study and that of Rink[3] indicates that there was 3-4 times the over-all sensitivity in this study. It is not to be implied that the results here cannot be improved upon. More data and higher Mach number shocks, especially in the neon mixtures at higher initial pressures of about 3 cm, would be of considerable aid in determining more precisely values for S_1, S_2, S_3, and ϕ_1, ϕ_2, ϕ_3.

One final remark should be made in connection with the curve fitting procedure. The neon mixture runs were more sensitive to variations in ϕ_1, S_1 and ϕ_3, S_3 than ϕ_2, S_2. Whereas in the argon mixture the initial part of the

profile was sensitive to S_3 and ϕ_3 but not too sensitive to S_1 or ϕ_1, the upper part of the curve was very sensitive to S_2 and ϕ_2. The pure nitrogen runs were very sensitive to ϕ_1 and S_1 throughout the entire profile. They showed sensitivity to ϕ_2 and S_2 only at the top.

Returning to Table III, Eckerman's[4] implied high third body efficiency for xenon may possibly be a direct consequence of excitation of the xenon, since its first excited state lies at about 8.3 e.v. The result of Harteck[10] that the argon is equally efficient is the nitrogen molecule as a third body is in disagreement with Herron's[8] work and with Britton's[25] data for the relative efficiencies of atoms and molecules in promoting the dissociation of iodine.

Returning to Byron's studies in nitrogen-argon mixtures, a few specific differences should be pointed out between his study and the present one. Byron only matched one point of the profile, neglected to take into account the change in refractivity with increasing nitrogen atom population, and took his measurements from the central white fringe shift. Profiles were generated for his highest Mach number run generated in his leanest mixture (5% N_2-95% A). The results showed that his neglect of the recombination rate up to the point of apparent 50% dissociation led to no significant error. Further, calculations based upon room temperature dispersion data for nitrogen indicated that the overshifting of the central white fringe did not affect the accuracy of his measurement. But the neglect of the increasing refractivity indicated that his apparent 50% dissociation time might be 20% too long, thus causing an underestimate of the rate for his hottest mixture. This error would be negligible for his cooler runs, so that it would not affect his over-all choice of

ϕ values. On the contrary, if one neglected the change in refractivity or read the white fringe shifts rather than the monochromatic shifts for the argon-nitrogen mixtures in this study, sizeable errors would be introduced even into the measurement of the 50% dissociation time, and the apparent profile would be distorted. Therefore, the prime reason for the results of this paper differing from those of Byron is the greater sensitivity here and the greater temperature span covered.

The very fact that a theoretical model which neglects diffusion effects gives such a fair fit of the observed data over a wide temperature range is in itself strong evidence that diffusion effects played no significant role. For example, the principal transport phenomenon is expected to be heat conduction rather than mass diffusion. Heat conduction is largest at the steep beginning of the profile. Calculation based upon the maximum initial temperature gradient at the beginning of the reaction profile of run number 3 in pure nitrogen indicated that heat transport affected the index of refraction profile by less that 1/2% even at the steepest part. Over the major portion of the profile the effect was negligible. In the neon mixtures the gradients were much smaller, so that heat transport played no measurable role.

Since the theory assumes that vibration is equilibrated prior to dissociation in those runs where a vibration zone was detected, the origin of the profiles was shifted along the X axis to the point at which vibrational equilbrium was attained. In Figures 6 and 7 in the argon-nitrogen runs, the vibrational zone was coalesced with the shock front, so that the origin was not shifted. The relative and absolute errors in measurement are indicated on Figures 5

through 8. The error in fixing the position of the shock front is shown in Figures 6 and 7. Although only nine runs were used to infer the dissociation rate measurement, many more runs were made in the over-all study. At least a half-dozen were made using pressure gauges in the window ports for the interferometer beams in order to measure attenuation of the shock. Another half dozen interferometer runs were made. These for the most part attested to the good control of the combustion technique. They were not used for data reduction for other reasons: small fringe shifts in the reaction zone, uncertain initial pressure owing to failure of the vacuum valve to fully close, underexposure of the optical image, and splitting of the optical image across the butted ends of the film. Out of the twenty-six interferometric runs made with combustion driven shocks, on one occasion two shocks were observed and the diaphragm showed signs of a bad opening. On another occasion a wave was seen overtaking the shock front in the reaction zone itself; however, no visible evidence was found of faulty diaphragm opening.

CONCLUSIONS

1. It has been experimentally demonstrated that combustion generated shocks may be used for shock structure studies providing that the peak burning pressure of the combustible loads is carefully matched to the burst pressure of the diaphragms. The flow field behind the shock should be monitored simultaneously with the recording of other types of data for the most reliable results.

2. Owing to the greater sensitivity attained by operating with not too lean mixtures, higher initial pressures (1 cm- 3 cm) and high shock Mach numbers, a more reasonable value was obtained for the ratio of the efficiency of the nitrogen atom to the nitrogen molecule in promoting the molecular dissociation. This ratio of about unity at $6,400^{\circ}K$ is more consistent with the results of careful room temperature measurements.

3. In view of the over-all good fit of the data, it is concluded that the naive picture of vibrational relaxation being completed ahead of the onset of dissociation appears to be valid for the temperature and density ranges covered in this study. Consequently, it would appear that the inferred rate constants here approximate the true values quite well over the temperature range in this study. However it would be a mistake to use these inferred rate constants at higher temperatures where coupling between the vibrational relaxation and dissociation cannot be ignored. If the inferred rate constants are used at temperatures intermediate between room temperature and the range here ($5,795^{\circ}K$ - $10,963^{\circ}K$), they will be in error (not owing to coupling between

vibration and dissociation,) because the correct values of S_1 and ϕ_1 will probably be smaller.than those reported here.

ACKNOWLEDGEMENTS

The author is pleased to acknowledge the skillful assistance of Mr. William Nickels who contributed so much to the successful completion of this study. I wish to thank Mr. David Rogers for developing most of the electronic equipment. The f-3 spectrograph was designed and constructed in this laboratory by Mr. Richard Harner and Mr. Harry Sadjian. Dr. Bortner and Mr. Golden contributed helpful discussions in regard to the chemical kinetical aspects of this study. A special acknowledgement goes to Dr. W. King who programmed all of the computations for the IBM 1620 and ran most of the theoretical profiles.

This analysis is based on work sponsored by the AF Office of Scientific Research of the Office of Aerospace Research under Contract No. AF 49(638)-931 with Mr. Milton Rogers acting as contract monitor.

REFERENCES

1. Mathews, D., "Interferometric Measurement in the Shock Tube of the Dissociation Rate of Oxygen," Phys. of Fluids, Vol. 2, No. 2, p. 170, 1959.

2. Byron, S., "Measurement of the Rate of Dissociation of Oxygen," J. Chem. Phys., Vol. 30, No. 6, p. 1380, 1959.

3. Rink, J., et al., "Shock Tube Determination of Dissociation Rates of Oxygen," J. Chem Phys., Vol. 34, No. 6, p. 1942, 1961.

4. Eckerman, J., "A Study of the Relaxation Time for Thermal Dissociation of Nitrogen Using Free-Flight Techniques, "NAVORD Report No. 5704, Vol. 1, May, 1958.

5. Byron, S., "Interferometric Measurement in a Shock Tube of Dissociation Rates for Air and Its Component Gases," Proceedings of the Ninth General Assembly of AGARD, NATO, Aachen, Germany, Sept., 1959.

6. Allen, R. et al., "Non-Equilibrium Radiation from Shock Heated N_2 and a Determination of the Recombination Rate," AVCO Laboratory Report No. 110, June, 1961.

7. Hammerling, P. et al., "Theory of Radiation from Luminous Shock Waves in Nitrogen," Phys. of Fluids, Vol. 2, No. 4, p. 422, 1959.

8. Herron, J. et al., "Kinetics of N_2 Recombination," J. Chem. Phys., Vol. 29, p. 230, 1958.

9. Wentinck, T. et al., "Nitrogen Atom Recombination at Room Temperature," J. Chem Phys., Vol. 29, p. 231, 1958.

10. Harteck, P. et al., "Rate of Recombination of N_2 Atoms," J. Chem. Phys., Vol. 29, p. 608, 1958.

11. Treanor, C. and Logan, J., "Thermodynamic Properties of Nitrogen from 2,000°K to 8,000°K," Cornell Aeronautical Laboratory Report No. BE-1007-A-5, January, 1957.

12. Private communication. G.E. Aerospace Laboratory Report in preparation.

13. Evans, J., "Method for Calculating Effects of Dissociation of Flow Variables in the Relaxation Zone Behind Normal Shock Waves," NACA TN 3860, December, 1956.

14. Fickett, W. and Cowan, R. "Values of Thermodynamic Functions to 12,000°K for Several Substances," J. Chem. Phys., Vol. 23, p. 1349, 1955.

15. Wittliff, C. and Wilson, M., "Shock Tube Driver Technique and Attenuation Measurements," Cornell Aeronautical Laboratory, Inc., Report No. AD-1052-A-4, August, 1957.

16. Waldron, H., "An Experimental Investigation of the Flow Properties Behind Strong Waves in Nitrogen," Institute of Aerophysics, Univ. of Toronto, Report No. 50, March, 1958.

17. Rose, P. and Nelson, W., "On the Effect of Attenuation on Gas Dynamics Measurements Made in Shock Tubes," AVCO Laboratory Report No. 24, April, 1958.

18. Byron, S., "Interferometric Measurement of the Dissociation Rate of Oxygen Heated by Strong Shock Waves," Doctoral Thesis, Cornell University, February, 1958.

19. White, D., "Optical Refractivity of High Temperature Gases Part I", Phys. of Fluids, Vol. 2, No. 2, p. 153, 1959.

20. Blackman, V., "Vibration Relaxation in Oxygen and Nitrogen," J. Fluid. Mech., Vol. 1, p. 61, 1956.

21. Widom, B., "Inelastic Molecular Collisons with a Maxwellian Interaction Energy," J. Chem. Phys., Vol. 27, p. 940, 1957.

22. Camm, J. and Keck, J., "Experimental Studies of Shock Waves in Nitrogen," AVCO Laboratory Report No. 140, June, 1959.

23. Kivel, B., "Radiation from the Non-Equilibrium Region of Normal Shocks in O_2, N_2, and Air," Proceedings of the Physical Chemistry Conference (Jointly Sponsored by GE MSVD and AFOSR), p. 132, September, 1959.

24. Gardiner, W., and Kistiakowski, G., "Thermal Dissociation Rate of H_2," J. Chem. Phys., Vol. 35, No. 5, p. 1765, 1961.

25. Britton, D. et al., "Shock Waves in Chemical Kinetics," J. Chem. Phys. Vol. 25, No. 5, p. 804, 1956.

26. Hooker, W., "Testing Time and Contact-Zone Phenomena in Shock-Tube Flows," Phys. of Fluids, Vol. 4, No. 12, p. 1451, 1961.

TABLE I

Vibrational Relaxation Data

No.	Composition	Shock Velocity mm/μsec	T_1 °K	P_1 mm Hg	Relaxation time for 1 atmosphere of pressure in shock fixed coordinates μsec
1	100% N_2	3.52	290.9	9.51	10.3
2	"	2.90	292.0	17.00	54.1
3	"	3.32	293.5	13.10	16.9
4	"	3.52	292.3	10.60	10.8
5	15.5% N_2-84.5% A	2.69	293.0	11.32	.6

TABLE II

Data Pertinent to the Dissociation Runs

No.	Composition	T_o °K	P_o mm Hg	Shock Velocity mm/μsec	Equilibrium % of Dissoc. N_2	Equilibrium Temperature °K	No Reaction Temperature °K
1	100% N_2	292.1	10.34	4.43	6.8	5969	7651
2	"	294.9	8.10	4.31	5.9	5795	7264
3	"	293.8	8.57	4.64	8.9	6107	8312
4	15.5% N_2-84.5% A	293.2	16.27	3.67	74.2	7690	10,597
5	"	292.5	29.3	3.35	44.5	7073	8990
6	"	294.0	26.7	3.74	76.4	8005	10,963
7	13.1% N_2-86.9% Ne	294.4	15.72	4.48	48.8	7070	9077
8	"	293.5	18.58	4.19	37.3	6593	7993
9	"	290.9	17.57	4.14	35.0	6515	7845

TABLE III

Inferred Recombination Rates $\frac{k_r \text{ cm}^6}{\text{mole}^2 - \text{sec}}$

Source	Third Body	300°K	6,400°K
This paper	N_2	$1.6 \cdot 10^{17}$	$4.2 \cdot 10^{14}$
	N	$2.0 \cdot 10^{16}$	$4.7 \cdot 10^{14}$
	Ne	$5.4 \cdot 10^{15}$	$1.3 \cdot 10^{14}$
	A	$8.0 \cdot 10^{15}$	$1.9 \cdot 10^{14}$
Byron[5]	N_2	$8.6 \cdot 10^{16}$	$4.4 \cdot 10^{14}$
	N	$1.9 \cdot 10^{16}$	$2.0 \cdot 10^{15}$
	A	$1.5 \cdot 10^{15}$	$1.6 \cdot 10^{14}$
Eckerman[4]	Xe	$5.1 \cdot 10^{17}$	$2.7 \cdot 10^{15}$
Camm[22]	N_2	--------	$< 1.1 \cdot 10^{15}$
	N	--------	$8.7 \cdot 10^{15}$
Allen[6]	N	--------	$6.5 \cdot 10^{15}$
Herron[8]	N_2	$5.7 \cdot 10^{15}$ (297°K)	--------
	A	$3.3 \cdot 10^{15}$ (297°K)	--------
Wentinck[9]	N_2	$1.2 \cdot 10^{16}$	--------
Harteck[10]	N_2	$6.1 \cdot 10^{15}$	--------
	A	$6.1 \cdot 10^{15}$	--------

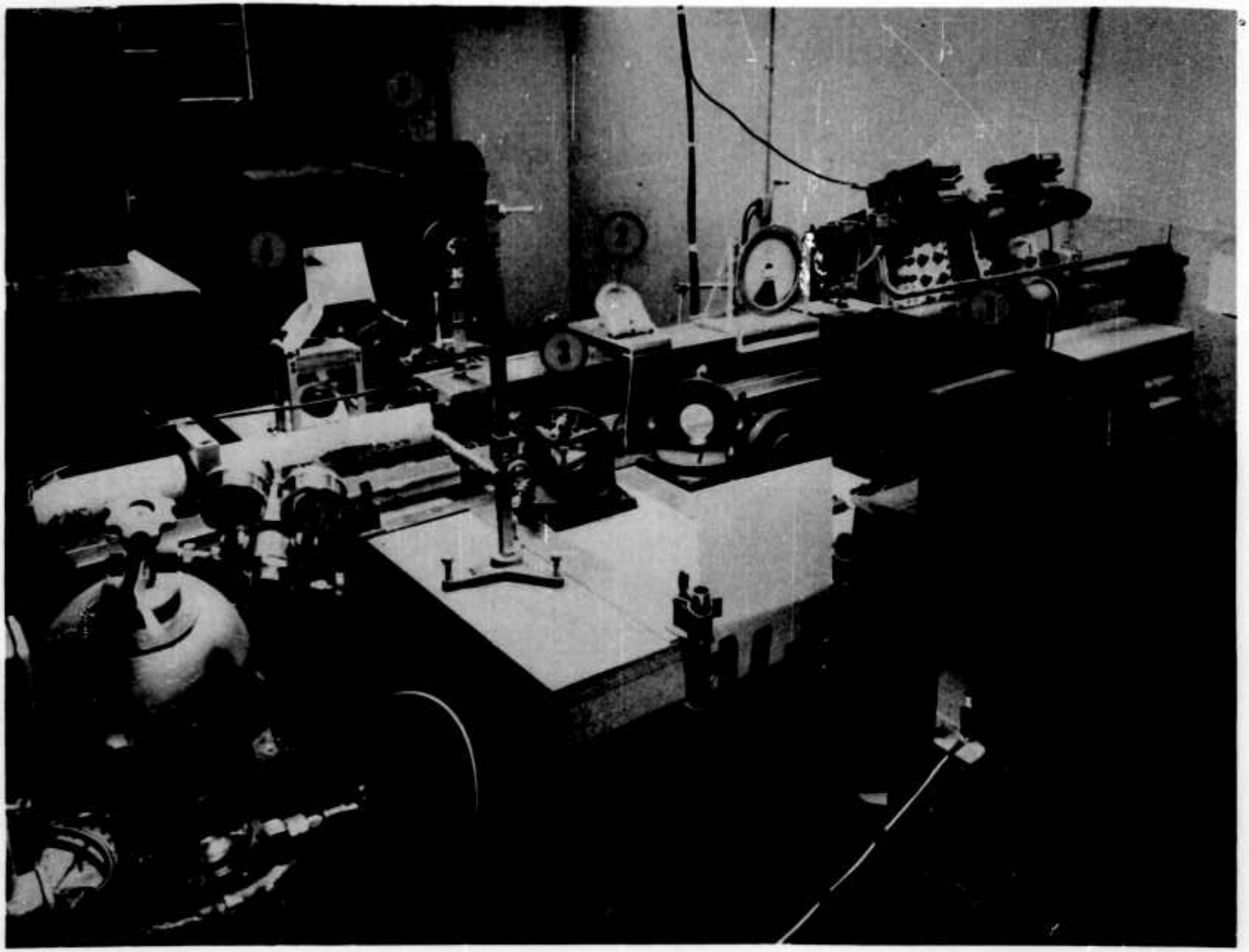

Figure 1 The Shock Tube and Associated Instrumentation

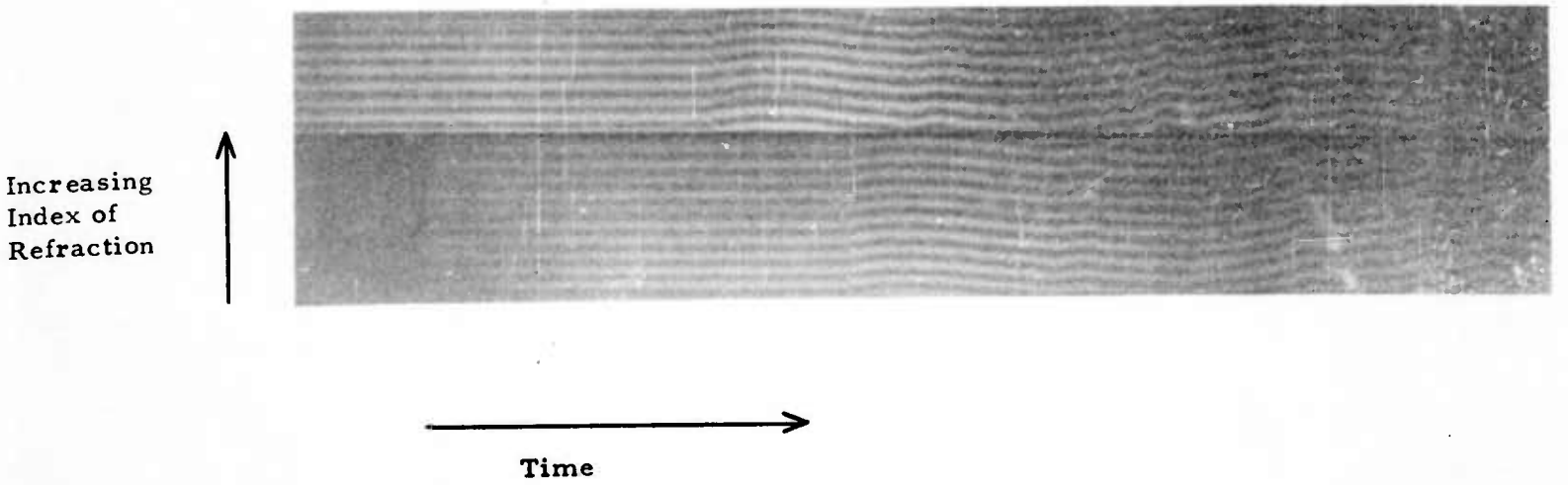

Figure 2 "Double Slit" Monochromatic Interferogram of a M 11.0 Shock Wave Propagating into N_2

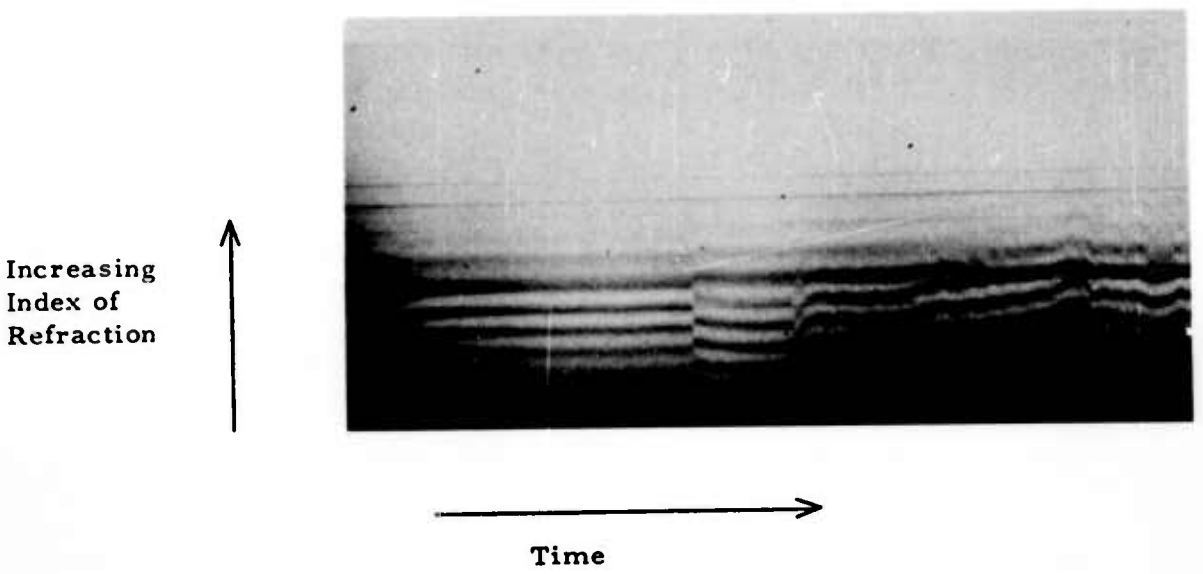

Figure 3 White Light Interferogram of a M 10.3 Shock Wave Propagating into a 13% N_2-87% Ne Mixture

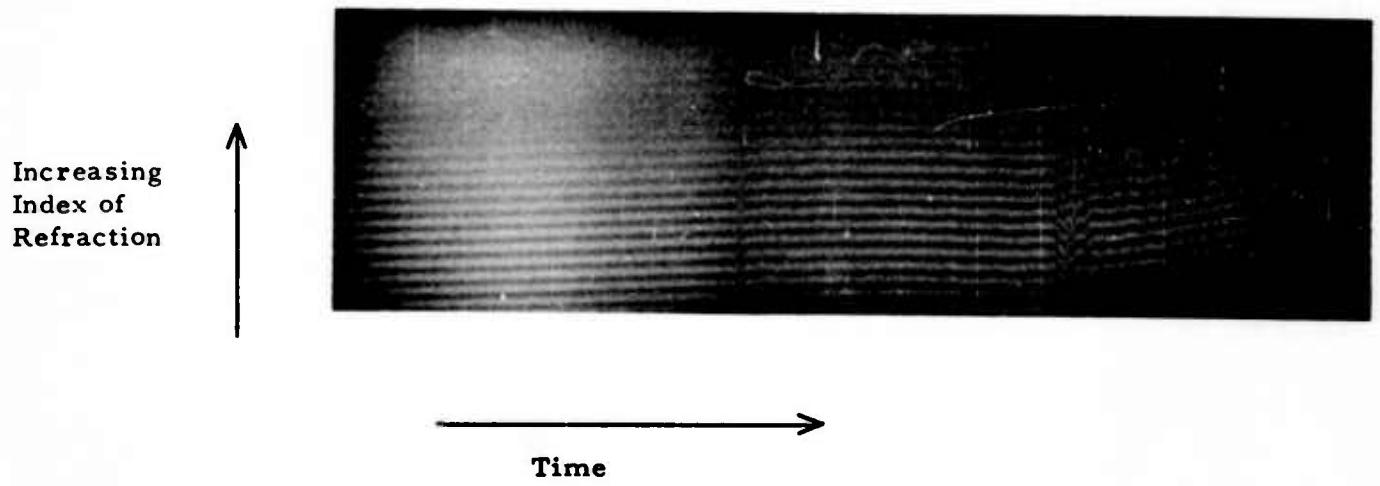

Figure 4 Monochromatic Interferogram of a M 11.7 Shock Wave Propagating into a 15.5% N_2-84.5% A Mixture

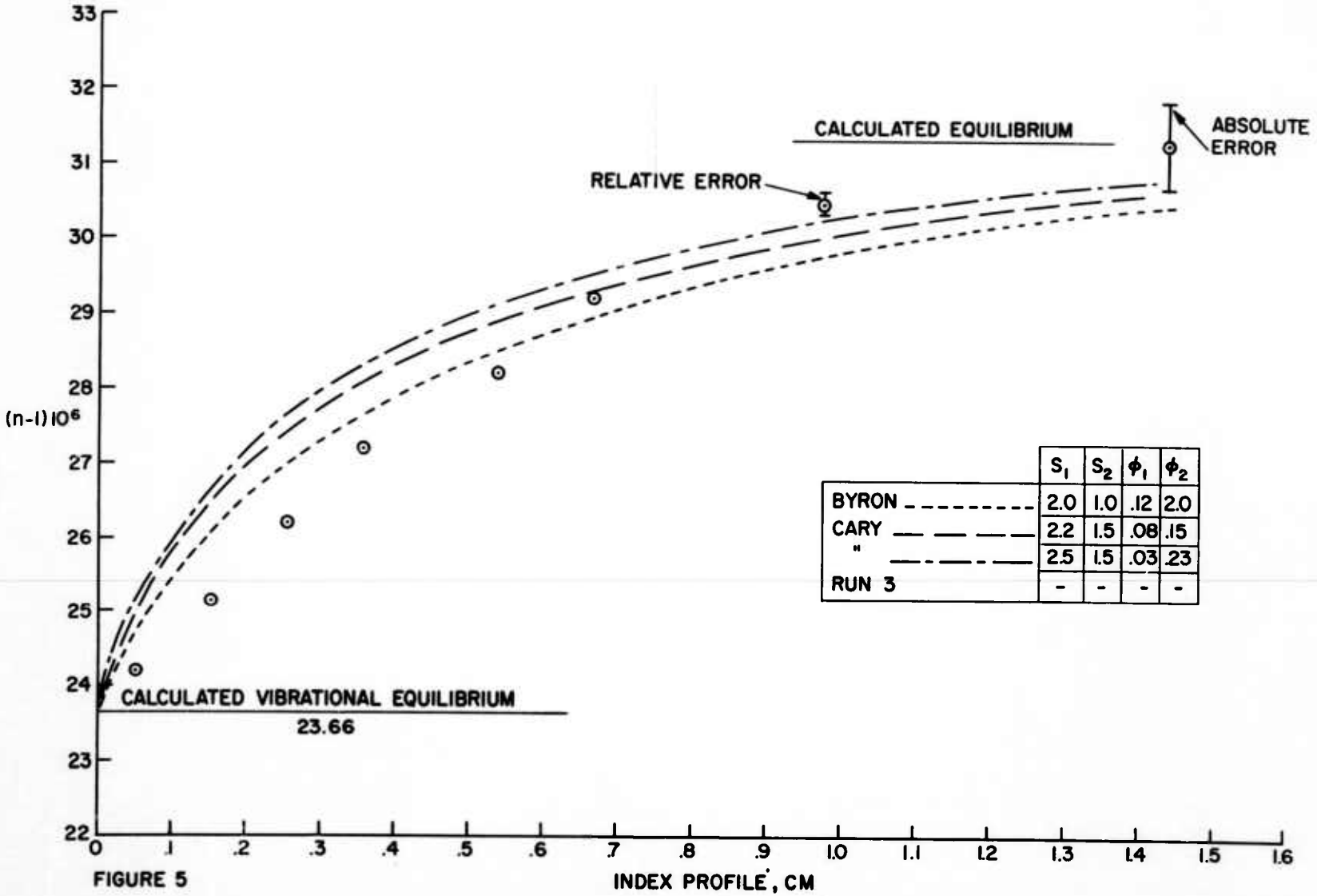
33
32
31
30
29
28
27
26
25
24
23
22
(n-1) 10⁶
CALCULATED EQUILIBRIUM
ABSOLUTE ERROR
RELATIVE ERROR
CALCULATED VIBRATIONAL EQUILIBRIUM
23.66
0
.1
.2
.3
.4
.5
.6
.7
.8
.9
1.0
1.1
1.2
1.3
1.4
1.5
1.6
INDEX PROFILE, CM
S1 S2 ϕ1 ϕ2
BYRON 2.0 1.0 .12 2.0
CARY 2.2 1.5 .08 .15
" 2.5 1.5 .03 .23
RUN 3 - - - -

FIGURE 5

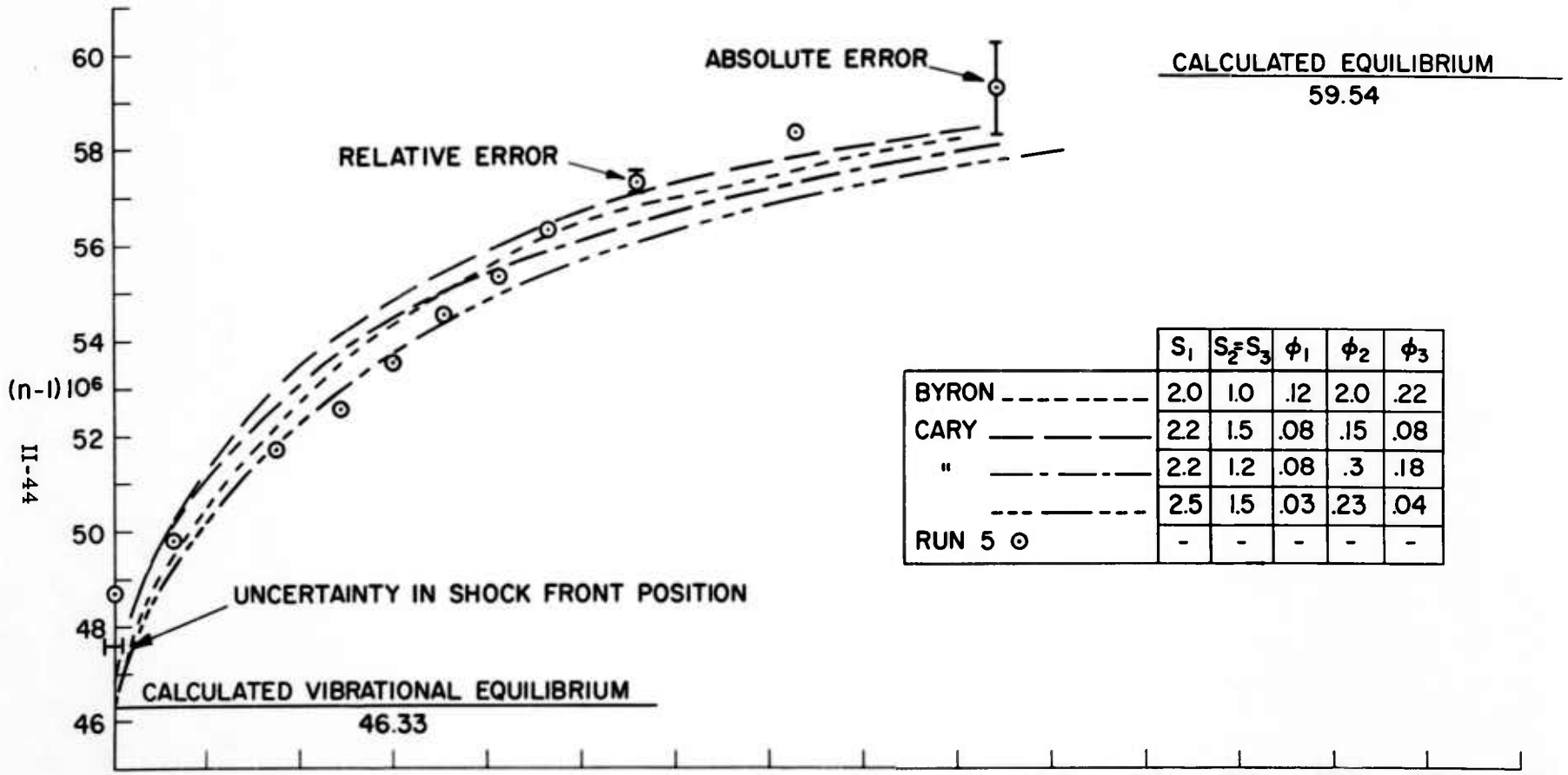

	S_1	$S_2=S_3$	ϕ_1	ϕ_2	ϕ_3
BYRON - - - - - - - -	2.0	1.0	.12	2.0	.22
CARY ——— ——— ———	2.2	1.5	.08	.15	.08
" ——— - ——— - ———	2.2	1.2	.08	.3	.18
- - - ——— - - -	2.5	1.5	.03	.23	.04
RUN 5 ⊙	-	-	-	-	-

FIGURE 6

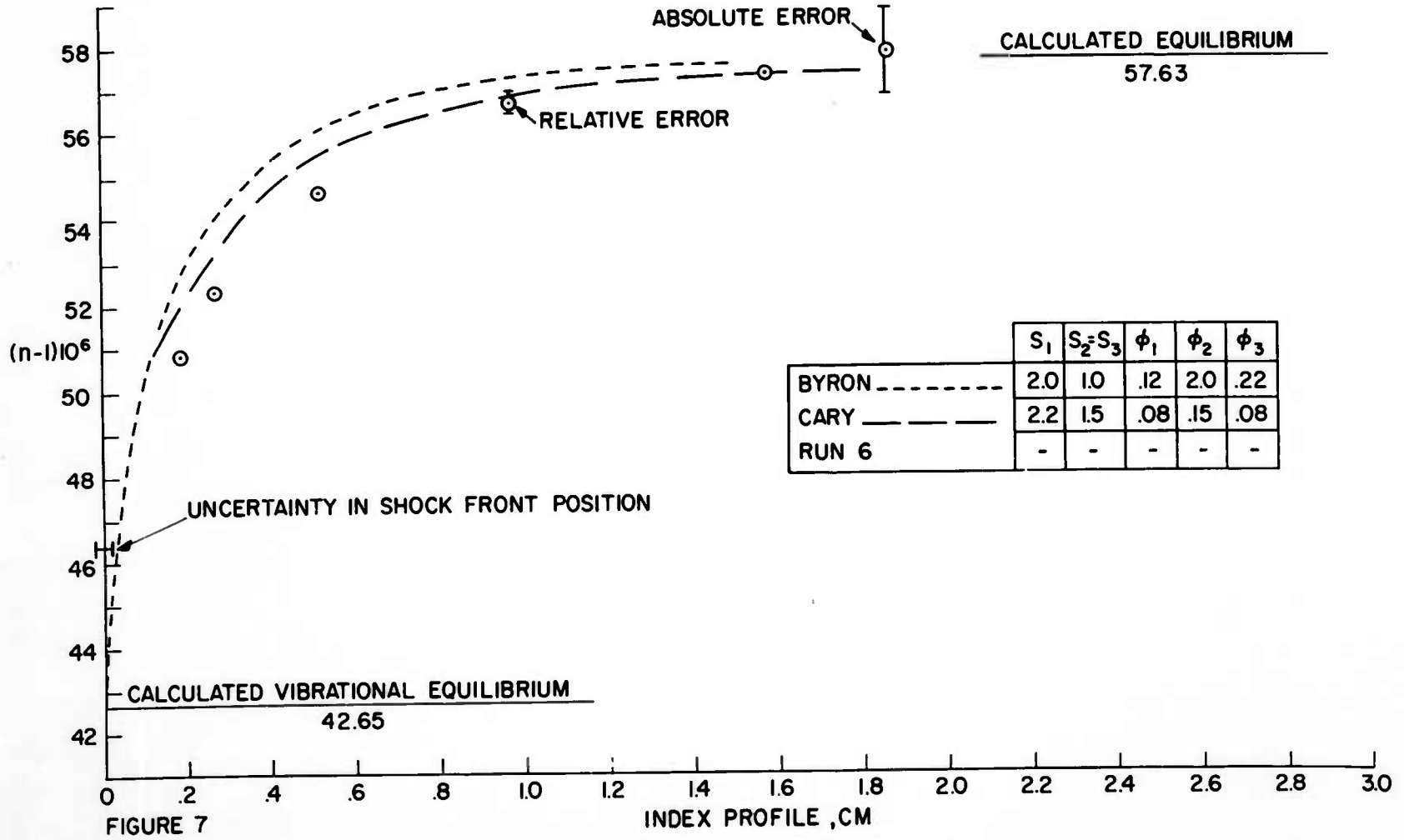

	S_1	$S_2=S_3$	ϕ_1	ϕ_2	ϕ_3
BYRON - - - - - - - -	2.0	1.0	.12	2.0	.22
CARY ———	2.2	1.5	.08	.15	.08
RUN 6	-	-	-	-	-

FIGURE 7

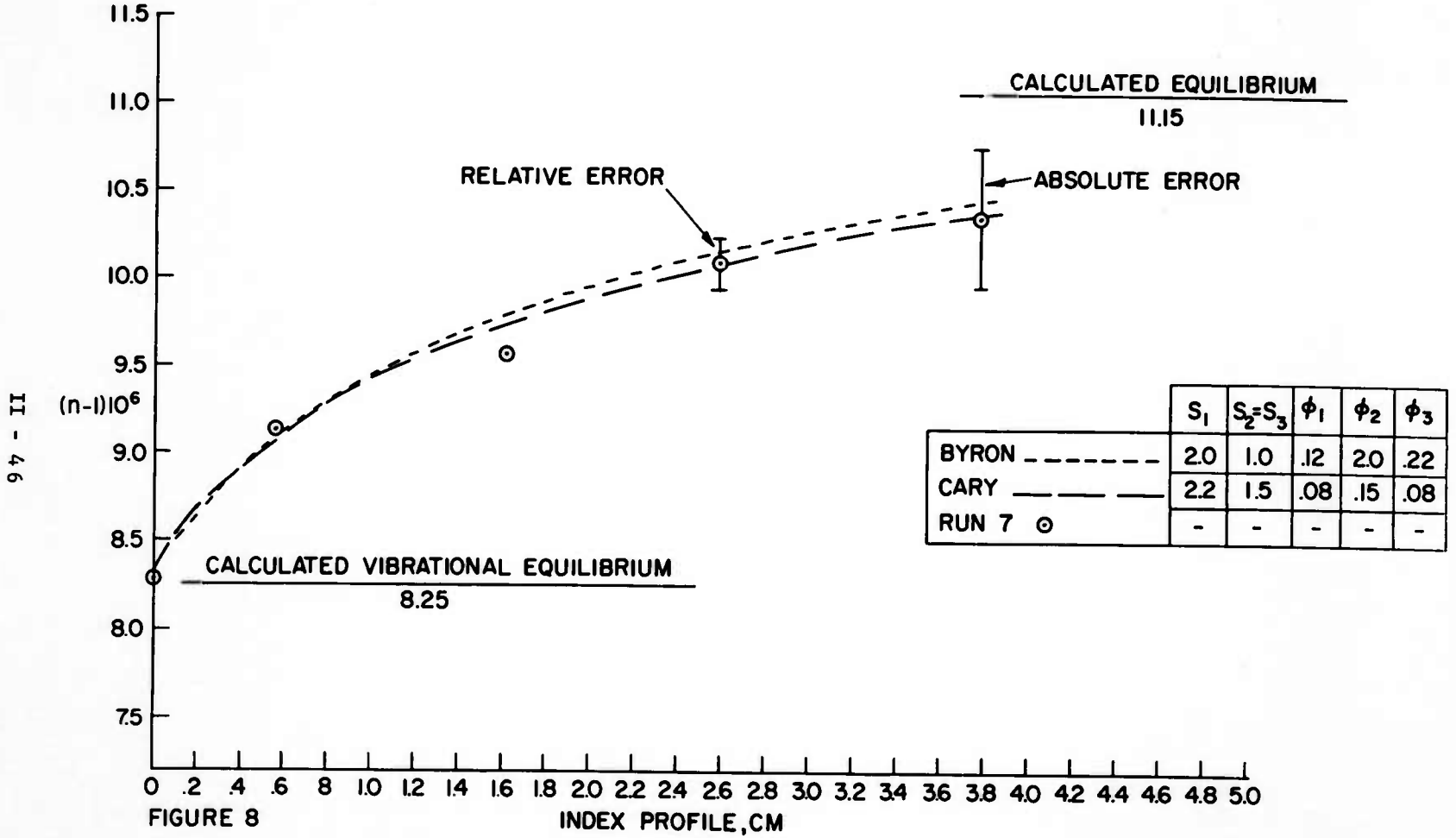

	S_1	$S_2=S_3$	ϕ_1	ϕ_2	ϕ_3
BYRON - - - - - - -	2.0	1.0	.12	2.0	.22
CARY ———	2.2	1.5	.08	.15	.08
RUN 7 ⊙	-	-	-	-	-

FIGURE 8

APPENDIX

A computer program for the IBM 1620 computer has been formulated to calculate index of refraction profiles behind a normal shock. Coding of the program is for use with the IBM three-address interpretive routine known as TAISSIT. The basic equations and the logic used in the program are discussed in this section, and a complete listing of the program is contained in a later section, together with detailed statements of the operations performed at each step, nomenclature of intermediate results, lists of working storage addresses, and other information. The listing is complete enough so that any interested person may use or modify the program with a minimum of effort.

There are three essentially separate functions performed in the computation. First, the equilibrium values of temperature and degree of dissociation (and related variables) are obtained. Second, the temperature, density, index of refraction (and other quantities) are calculated which correspond to a series of predetermined values of dissociation (α'). Then an expression for $dx/d\alpha'$ is obtained for each value of α, and integrated over α' to obtain the value of linear distance x corresponding to each set of values (α', T, ρ, $\overline{M}$, N). Storage is provided so that up to 14 integrations, each utilizing different sets of temperature functions and efficiency factors, can be carried out during a single run.

I. EQUILIBRIUM CALCULATION

A. In order to start the iterative loop used to find the equilibrium dissociation and temperature, estimates of α_e' and T_e are required. These are

part of the input data. The value of α_e' is momentarily considered to be fixed, and the closed T Subroutine is used to find the corresponding values of T in the following way:

1. Using T_e' and α_e', evaluate

$$\bar{\beta}' = \frac{1 - \alpha'}{1 + \alpha'} \beta_{N2} + \frac{\alpha'}{1 + \alpha'} \left(\frac{D_o/R}{T} + 2\beta_N \right)$$

2. $$\bar{M}' = \frac{\frac{1 + \gamma_1' M_1^2}{\gamma_1' M_1} \bar{\beta}' - \left[\left(\frac{1+\gamma_1' M_1^2}{\gamma_1' M_1} \bar{\beta}' \right)^2 - \left(2\bar{\beta}' - 1 \right) \left(M_1^2 + \frac{2}{\gamma_1' - 1} \right) \right]^{\frac{1}{2}}}{2\bar{\beta}' - 1}$$

where $\gamma_1' = C\gamma_d + (1-C)\gamma_i$

and C = mole fraction of diatomic gas in mixture.

(Subscript i denotes inert gas, d diatomic.)

3. $$T = T_1 \frac{\gamma_1' \bar{M}'}{1 + \sigma'} \left(\frac{1 + \gamma_1' M_1^2}{\gamma_1' M_1} - \bar{M} \right)$$

$$\rho = \rho_1 M_1 / \bar{M}'$$

4. The subroutine then compares the T calculated at step 3 with the initial guess value of T, T_i. If the difference exceeds the tolerance stated in the input, the calculated value of T replaces T_i and becomes the guess value for the next iteration starting again at step 1.

This loop converges quite rapidly. The difference $\Delta T = |T - T_i|$ decreases by a factor of 5 or more with each iteration, provided that the initial guess value of T is within 2000°K of the actual value.

When a value of T is found which satisfies the established criterion (0.2°K was used in the work reported here), exit from the subroutine occurs with the final value of T, ρ and $\overline{M}'$ available for further computation.

B. The value of T determined above is used by the K_e Subroutine in a 7-point Stirling interpolation formula* to obtain ln K_e (T) and then K_e (T). This value is stored and available for later use.

C. The f Subroutine then evaluates the expression

$$f = 1 - \frac{4\alpha'^2 \rho}{(c - \alpha') M_{w_{mix}} K_e}$$

It can be shown that this function is a monotonically decreasing function of α', and that f = 0 is a necessary and sufficient condition for equilibrium.

D. The program tests the sign of f and then increments or decrements (as appropriate) the initial value of α_e' by the amount $\Delta\alpha_e' = 0.01$, calculated as a new starting temperature from the relations

$$\Delta T = -\frac{\Delta\alpha'}{9 + \alpha'} \left[2 D_o/R + T\right] ,$$

$$T_1 = T_o + \Delta T,$$

and repeats the calculation.

---

*Scarborough, Numerical Mathematical Analysis, 3rd Ed., The Johns Hopkins Press, Baltimore, 1955. pp 70-74.

E. When f changes sign, indicating that α' has passed the equilibrium value, Newton's method is applied. The values of f immediately above and below zero are used to determine the slope and the approximate value of the root:

$$\alpha' = \alpha'_n + \delta\alpha'$$

$$\delta\alpha' = f_n \frac{\alpha'_n - \alpha'_{n-1}}{f_n - f_{n-1}}$$

This $\delta\alpha'$ is then used in the equation of step D to obtain an approximate value of T corresponding to the root. The value of $\Delta\alpha'_e$ in (D) is reduced by a factor of 10, and the program returns to (A) and repeats.

F. When four significant digits of α'_e have been obtained in this manner the calculation is concluded. The final values of α'_e and T_e, as well as all pertinent intermediate results. are retained in memory for later use.

II. PROFILE CALCULATION

Following calculation and pointing of the equilibrium values the program proceeds to the computation of the index of refraction profile.

A. At the shock front $\alpha' = 0$. The starting value of T is obtained from the expression

$$T_o = T_1 \frac{\left(\frac{\gamma_k' + 1}{\gamma_k' - 1}\right) + \left(\frac{p_o}{p_1}\right)}{\left(\frac{\gamma_k' + 1}{\gamma_k' - 1}\right)\left(\frac{p_o}{p_1}\right) + 1}$$

where $$\frac{p_o}{p_1} = \frac{2 M_1^2 \gamma_1'}{\gamma_k' + 1} - \frac{\gamma_k' - 1}{\gamma_k' + 1}$$

$$\gamma_k' = c\gamma_k + (1-c)\gamma_i$$

$$\gamma_k = 9/7$$

This expression assumes complete translational, rotational, and classical vibrational equilibrium. At best it gives only an approximation to the value of T behind the front, but only a crude approximation is needed to start the iterative loop. The accuracy of the final answer does not depend at all upon the accuracy of the assumed starting value.

B. The T Subroutine then evaluates T and ρ as described in I. A.

C. Using the value of K_e calculated during the final iteration of the Equilibrium Calculation and the T from (B) above, the f Subroutine evaluates the expression given in I. C.

D. The program then calculates N and certain intermediate results needed for the evaluation of $\left(\frac{dx}{d\alpha'}\right)$. All intermediate results are listed in the working storage assignment list. The nomenclature utilized is a purely arbitrary one: the k's are quantities which remain constant throughout a run, and the q's are functions of T and α' as shown in the listing.

E. The quantity $\left(\frac{dx}{d\alpha'}\right)$ is calculated from the relationship:

$$\gamma = \frac{dx}{d\alpha'} = \frac{1}{\frac{d\alpha'}{dx}}$$

$$\frac{d\alpha'}{dx} = \frac{\rho'^2}{M_{w_{mix}} \rho_1 U_s} \left[(c-\alpha')^2 c^2 k_{d_1} + 2\alpha'(c-\alpha')k_{d_2} + (c-\alpha')(1-c)k_{d_3}\right]$$

$$\left[1 - \frac{4\alpha'^2 \rho}{(c-\alpha')M_{w_{mix}} K_e}\right]$$

where the k_d's are as indicated in Equations 3 of the text.

At the time the program was originally written, the values $S_1 = 2$, $S_2 = S_3 = 1$ were assigned, the Γ functions evaluated, and the numerical value combined with other constants. The resulting expression was

$$\gamma = \frac{q_5}{q_3 \varphi_1 + q_{10} \varphi_2 + k_{13} \varphi_3} .$$

When it became necessary to include variations of S_1 and $S_2 = S_3$ in the computation this expression was modified to the form

$$\gamma = \frac{q_5 (D/RT)^{-n_1}}{q_3 \varphi_1' + (D/RT)^{n_2} (q_{10} \varphi_2' + k_{13} \varphi_3')}$$

The effect of this change is to set

$$S_1 = 2 + n_1$$

$$S_2 = S_3 = 1 + n_1 + n_2$$

as far as the exponent of (D/RT) is concerned, but it does not take into account the change in the value of the Γ function in Equation 3. Thus the numerical value labelled $\hat{\varphi}_1$ in the latter expression is the equivalent of $\varphi_1 \frac{\Gamma(3 + n_1)}{\Gamma(2)}$, with similar relationships existing for the other φ's:

$$\hat{\varphi}_1 = \varphi_1 \frac{\Gamma(3 + n_1)}{\Gamma(3)}$$

$$\hat{\varphi}_2 = \varphi_2 \frac{\Gamma(2 + n_1 + n_2)}{\Gamma(2)}$$

$$\hat{\varphi}_3 = \varphi_3 \frac{\Gamma(2 + n_1 + n_2)}{\Gamma(2)}$$

This fact was overlooked in the original computation and necessitated "ex post facto" modification of the φ values associated with a given profile, but otherwise caused no difficulty. Anyone contemplating use of this program in the future should modify it to remove this possibility of misunderstanding.

This calculation is carried out in a closed subroutine ("Special Program") starting at Location 200. In the program listing, the program shown utilizes

a set (n_1, n_2, $\hat{\varphi}_1$, $\hat{\varphi}_2$, $\hat{\varphi}_3$) for each profile desired. The γ values corresponding to each set are calculated and placed in a storage file for use in forming the integrals.

F. To obtain the value of X corresponding to each pair of α' and N values, we use

$$\Delta a_n = \int_{\alpha'_{n-1}}^{\alpha'_n} \left(\frac{dx}{d\alpha'}\right) \, d\alpha' \quad ,$$

$$a_n = \sum_{i=o}^{n} \Delta a_n \quad .$$

This computation is performed by the Integration Subroutines. After the first four steps ($\alpha' = \alpha'_o, \ldots, \alpha'_3$) have been carried out, Simpson's Rule is used to compute a_2, and the four point integration formula

$$\Delta a_n = \frac{\Delta\alpha'}{2} \left[\frac{(\gamma_{n-1} + \gamma_n) - (\gamma_{n-2} + \gamma_{n+1})}{12} + (\gamma_{n-1} + \gamma_n)\right]$$

is used to evaluate Δa_2. Then

$$a_1 = a_2 - \Delta a_2 .$$

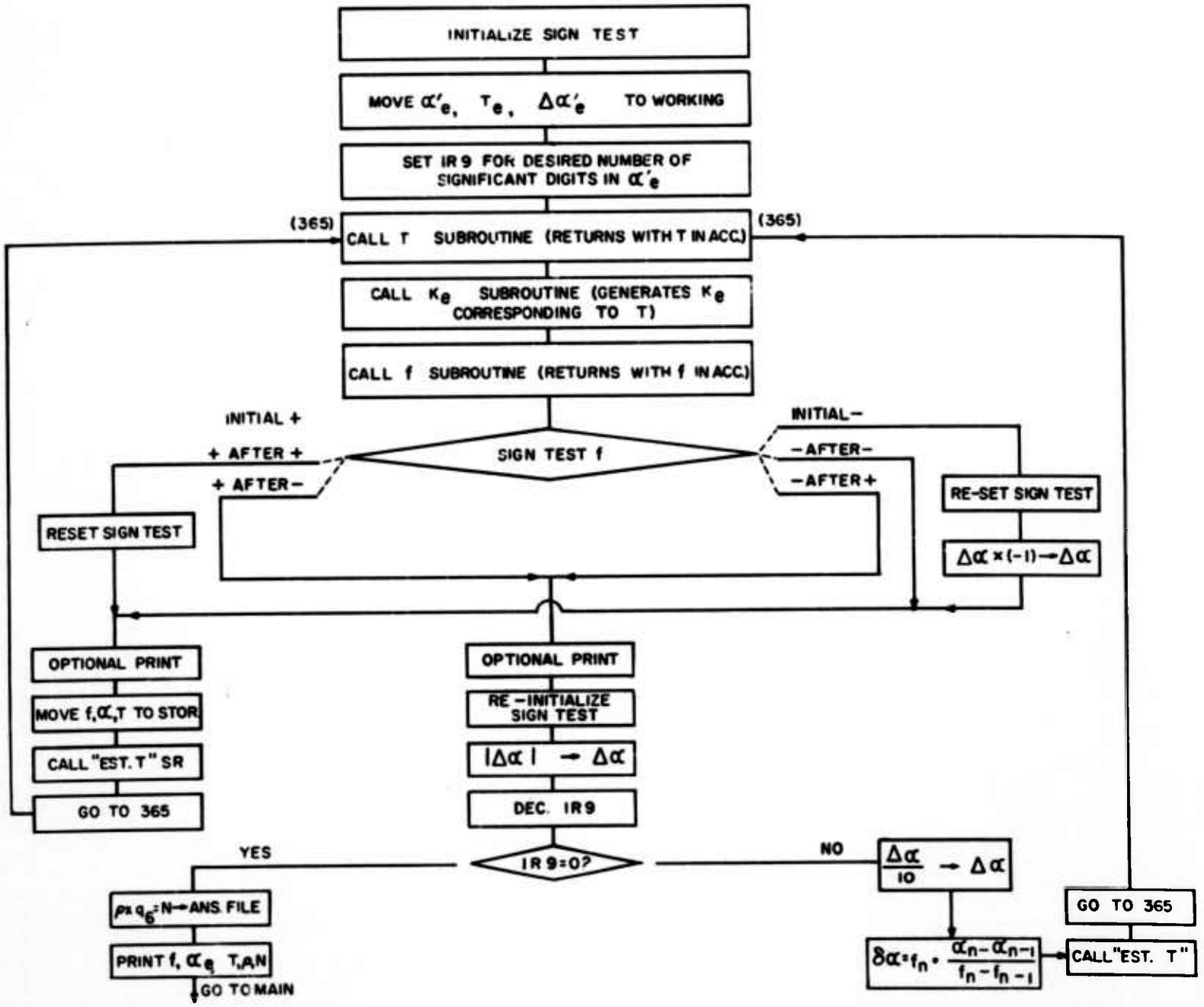
INITIALIZE SIGN TEST
MOVE α'_e, T_e, $\Delta\alpha'_e$ TO WORKING
SET IR 9 FOR DESIRED NUMBER OF SIGNIFICANT DIGITS IN α'_e
(365)
CALL T SUBROUTINE (RETURNS WITH T IN ACC.)
(365)
CALL K_e SUBROUTINE (GENERATES K_e CORRESPONDING TO T)
CALL f SUBROUTINE (RETURNS WITH f IN ACC.)
INITIAL +
+ AFTER +
+ AFTER −
SIGN TEST f
INITIAL −
− AFTER −
− AFTER +
RESET SIGN TEST
RE-SET SIGN TEST
$\Delta\alpha \times (-1) \rightarrow \Delta\alpha$
OPTIONAL PRINT
MOVE f, α, T TO STOR
CALL "EST. T" SR
GO TO 365
OPTIONAL PRINT
RE-INITIALIZE SIGN TEST
$|\Delta\alpha| \rightarrow \Delta\alpha$
DEC. IR 9
YES
IR 9=0?
NO
$\frac{\Delta\alpha}{10} \rightarrow \Delta\alpha$
$p \times q_6 = N \rightarrow$ ANS. FILE
PRINT f, α_e, T, A, N
GO TO MAIN
GO TO 365
$\delta\alpha = f_n \cdot \frac{\alpha_n - \alpha_{n-1}}{f_n - f_{n-1}}$
CALL "EST. T"

The computation then proceeds, using the four-point form to compute successive Δa's until a value of α' is reached which causes the function f to become negative, indicating that the equilibrium value has been exceeded. This causes the integration routine to discard the invalid computation, and Simpson's Rule is again used to compute $(\Delta a_{f-1} + \Delta a_f)$, where the subscript f denotes the final area strip in the integral. Since Δa_{f-1} was obtained from the last valid four-point integration, Δa_f can be computed. The program then returns to the beginning and seeks new input.

"BOOT STRAP PROGRAM"

100	$\overline{9}$ 155 103 103	Read 1 word from tape.
101	$\overline{9}$ 580 103 103	Print the word.
102	$\overline{7}$ 661 000 103	HALT if SW 1 is ON. Proceed to 103 when "START" is pushed.
103	$[\overline{0}$ 000 000 000$]$	Word read from tape.
104	$\overline{7}$ 700 000 100	Transfer to 100 and repeat.

SPECIAL PROGRAM

200	6	063	221	[000]	Set exit.
201	6	064	000	932	Set integration counter (882 + 5N)
202	6	063	217	886	Initialize answer file address.
203	6	062	205	230	Initialize move order.
204	8	864	775	224	$\ln q_1 \rightarrow$ temp. stor.
205	0	005	[000]	225	Move (n_1, n_2, $\hat{\varphi}_1$, $\hat{\varphi}_2$, $\hat{\varphi}_3$) to wkng location.
206	5	225	224	000	$- n_1 \ln q_1$
207	8	874	000	000	$\frac{1}{(q_1)^{n_1}}$.
208	3	779	000	799	$q_5 \times \frac{1}{(q_1)^{n_1}} \rightarrow q_5$.
209	3	226	224	000	$n_2 \times \ln q_1$.
210	8	874	000	223	$q_1^{n_2} \rightarrow$ temp. stor.
211	3	784	228	222	$q_{10} \times \varphi_2 \rightarrow$ temp. stor.
212	3	773	229	000	$k_{13} \times \varphi_3$
213	1	000	222	000	$+ q_{10} \varphi_2$
214	3	000	223	223	$\times (q_1^{n_2}) \rightarrow$ temp. stor.

215	3	777	227	000	$q_3 \times \varphi_1$
216	1	000	223	000	$+ q_1^{n_2} (q_{10} \varphi_2 + k_{13} \varphi_3)$
217	4	799	000	[000]	$(q^5 q_1^{-n_1}) \div [216] \rightarrow \gamma_i \rightarrow$ ans file
218	6	012	205	005	Increment move.
219	6	013	217	005	Increment answer file address.
220	6	134	217	205	If ans add $\leq$ final ans ads, repeat.
221	7	700	000	[000]	Exit.

300	7 661 300 301	HALT if SW 1 is ON
301	9 155 800 816	Load data from tape
302	6 061 000 000	Set IR 1 to 000
303	6 062 000 000	Set IR 2 to 000
304	6 063 000 000	Set IR 3 to 000
305	7 661 305 306	HALT if SW 1 is ON
306	9 155 307 307	Read "Special Integration" load command from tape
307	[9 155 200 225]	(Command read from tape)
308	7 661 308 309	HALT if SW 1 is ON
309	9 155 311 313	Read three words from tape (print commands)
310	9 580 800 816	Print input data ALTERNATE ENTRY POINT
311	[9 580 211 211]	(Print ϕ_1's)
312	[9 580 221 223]	(Print ϕ_2's)
313	[9 580 231 233]	(Print ϕ_3's)
314	7 661 314 315	HALT if SW 1 is ON
315	2 840 804 750	$1 - c_1 \rightarrow$ wkng storage
316	3 000 848 799	$(1-c_1) \times \gamma_i \rightarrow$ temp storage
317	3 804 849 000	$c_1 \times \gamma_d$
318	1 000 799 751	$(c_1 \times \gamma_d) + (1-c_1)\gamma_i = \gamma_1' \rightarrow$ wkng storage
319	3 804 850 000	$c_1 \times \gamma_k$
320	1 000 799 752	$(c_1 \gamma_k) + (1-c_1)\gamma_i = \gamma_k' \rightarrow$ wkng storage
321	1 000 840 799	$\gamma_k' + 1 \rightarrow$ temp storage
322	2 752 840 000	$\gamma_k' - 1$
323	4 000 799 762	$(\gamma_k' - 1) \div (\gamma_k' + 1) = k_2 \rightarrow$ wkng storage
324	3 841 751 000	$2 \times \gamma_1'$
325	4 000 799 761	$(2\gamma_1') \div (\gamma_k' + 1) = k_1 \rightarrow$ wkng storage
326	3 750 847 763	$(1-c_1) \times 2.5 = k_3 \rightarrow$ wkng storage
327	3 751 801 799	$\gamma_1' \times M_1 \rightarrow$ temp storage
328	3 000 801 000	$\times M_1$
329	1 000 840 000	$+ 1$

330	4 000 799 764	$(\gamma_1' M_1^2 + 1) \div \gamma_1' M_1 = k_4 \rightarrow$ wkng storage
331	3 801 801 760	$M_1 \times M_1 = M_1^2 \rightarrow$ wkng storage
332	2 751 840 000	$\gamma_1' - 1$
333	4 841 000 000	$2 \div (\gamma_1' - 1)$
334	1 000 760 765	$+ M_1^2 = k_5 \rightarrow$ wkng storage
335	3 802 751 766	$T_1 \times \gamma_1' = k_6 \rightarrow$ wkng storage
336	3 800 801 767	$\rho_1 \times M_1 = k_7 \rightarrow$ wkng storage
337	3 750 810 799	$(1 - C_1) \times M_{wi} \rightarrow$ temp storage
338	3 804 805 000	$C_1 \times M_{wd}$
339	1 000 799 753	$+ (1 - C_1) M_{wi} = M_{w\,mix} \rightarrow$ wkng storage
340	4 851 000 798	$10^6 \div M_{w\,mix} \rightarrow$ temp storage
341	3 000 799 000	$\times M_{wi} (1 - C_1)$
342	3 000 811 768	$\times K_i = k_8 \rightarrow$ wkng storage
343	3 798 805 000	$(10^6 / M_{w\,mix}) \times M_{wd}$
344	3 000 806 769	$\times K_d = k_9 \rightarrow$ wkng storage
345	8 835 805 000	$\sqrt{M_{wd}}$
346	3 000 753 000	$\times M_{w\,mix}$
347	3 000 800 000	$\times \rho_1$
348	3 000 803 000	$\times U_s$
349	4 000 852 770	$\div \left[N_o (\pi R_w^2) \right] = k_{10} \rightarrow$ wkng storage
350	4 843 753 771	$4 \div M_{w\,mix} = k_{11} \rightarrow$ wkng storage
351	3 841 809 759	$2 \times (D_o / R) \rightarrow$ wkng storage
352	7 661 352 360	HALT if SW 1 is ON.
353	0 000 000 000	
354	0 000 000 000	
355	0 000 000 000	
356	0 000 000 000	NOT USED BY PROGRAM
357	0 000 000 000	
358	0 000 000 000	
359	0 000 000 000	

360	6 062 366 370	Initialize sign test
361	6 063 366 377	Initialize sign test
362	0 002 813 754	Move initial α_e', T_e to wkng loc
363	0 000 853 757	Move initial $\Delta\alpha_e'$ to $\Delta\alpha'$ wkng loc
364	6 069 000 004	Set IR 9 to 4 (number of sig digits in α_e)
365	7 820 367 480	Call T Subroutine. (Returns with T in acc)
366	7 760 [000] [00]	Sign test f and transfer
367	7 820 368 445	Call K_e Subroutine
368	7 820 366 545	Call f Subroutine, return to 366
369	7 600 000 000	(Not used)
370	6 063 366 381	HERE IF f IS + ON FIRST PASS Re-set sign transfer for break-out
371	7 733 373 372	HERE IF f IS − ON 2nd-Nth PASS
372	9 580 869 871	(Optional print f, α', T if SW 3 is ON)
373	0 003 869 865	Move f, α', T to storage location
374	0 000 757 000	Bring $\Delta\alpha'$ to acc
375	7 820 365 467	Call "Estimate T" subroutine, return to 365
376	7 600 000 000	NOT USED
377	6 062 366 381	HERE IF f IS − ON FIRST PASS Re-set sign test for break-out
378	6 063 366 371	Re-set sign test for 2nd-Nth pass negative
379	3 855 757 757	Set $\Delta\alpha_e'$ negative ($\Delta\alpha_e' \times -1 \rightarrow \Delta\alpha_e'$)
380	7 700 000 371	Go to 371
381	7 733 383 382	HERE WHEN SIGN OF f CHANGES
382	9 580 869 871	(Optional print f, α', T if SW 3 is ON)
383	6 062 366 370	Re-initialize sign test
384	6 063 366 377	Re-initialize sign test
385	8 894 757 757	Set $\Delta\alpha'$ positive
386	6 029 000 001	Decrement IR 9
387	7 661 387 388	HALT if SW 1 is ON
388	6 509 389 396	If IR 9 = 0, Equilibrium calc is finished. If IR 9 ≠ 0, decrement $\Delta\alpha'$ and continue
389	4 757 854 757	$\Delta\alpha' \div 10 \rightarrow \Delta\alpha'$

390	2 869 865 799	$f_n - f_{n-1}$ → temp storage
391	2 866 870 000	$\alpha'_n - \alpha'_{n-1}$
392	4 000 799 000	$\div (f_n - f_{n-1})$
393	3 000 869 758	$\times f_n = \delta\alpha'$ → wkng storage
394	7 820 365 467	Call "Estimate T" sub-routine, return to 365
395	7 600 000 000	(Not used)
396	3 872 780 873	HERE WHEN FINISHED $\rho' \times q_6 = N$ → answer file
397	9 580 869 873	Print f, α', T, ρ, N
398	7 661 398 400	HALT if SW 1 is ON
399	7 600 000 000	(Not used)
		START OF MAIN PROGRAM
400	6 062 441 555	Set integration Transfer Switch for 1st pass
401	0 000 857 754	Initialize α' to 0
402	0 000 816 757	Initialize $\Delta\alpha'$
403	4 000 841 787	$\Delta\alpha' \div 2$ → wkng storage
404	4 757 842 788	$\Delta\alpha' \div 3$ → wkng storage
405	3 808 808 776	$D_d \times D_{d1}$ → temp storage
406	3 000 856 772	$\times 4\sqrt{6} = k_{12}$ → wkng storage
407	1 805 810 000	$M_{wd} + M_{wi}$
408	4 000 810 000	$\div M_{wi}$
409	8 835 000 799	$\sqrt{(M_{wd} + M_{wi})/M_{wi}}$ → temp storage
410	3 804 776 797	$C_1 \times D_d^2$ → temp storage
411	3 812 812 000	$D_i \times D_i$
412	3 000 750 000	$\times (1 - C_1)$
413	1 000 797 000	$+ C_1 D_d^2$
414	3 000 799 000	$\times \sqrt{(M_{wd} + M_{wi})/M_{wi}}$
415	3 000 750 000	$\times (1 - C_1)$
416	3 000 858 773	$\times 2\sqrt{2} = k_{13}$ → wkng storage
417	7 600 000 000	No operation
418	0 000 797 785	Move $C_1 D_d^2$ into $(C_1 - \alpha') D_d^2$ location
419	3 760 761 799	$M_1^2 \times k_1$ → temp storage

420	2 000 762 798	$M_1^2 k_1 - k_2 = (P_o/P_1) \rightarrow$ temp storage
421	3 000 762 000	$\times k_2$
422	1 000 840 000	$+ 1$
423	4 000 799 000	$\div k_1 M_1^2$
424	3 000 798 000	$\times (P_o/P_1)$
425	3 000 802 755	$\times T_1 = T_o \rightarrow$ wkng storage
426	7 820 443 480	Call T Subroutine, return to 443
427	7 760 428 670	Sign test f. If neg, the calc is invalid; go to final integration. If pos, proceed.
428	8 874 775 799	Exp $(q_1) \rightarrow$ temp storage
429	8 835 871 000	$\sqrt{T}$
430	3 000 775 000	$\times q_1$
431	4 000 799 000	$\div e^{q_1} = q_2$
432	3 000 872 000	$\times \rho$
433	3 000 872 000	$\times \rho$
434	3 000 774 000	$\times (c_1 - \alpha')$
435	3 000 869 000	$\times f$
436	4 770 000 779	$k_{10} \div$ [above] $= q_5 \rightarrow$ wkng storage
437	3 870 772 784	$\alpha' \times k_{12} = q_{10} \rightarrow$ wkng storage
438	3 785 775 777	$[(c_1 - \alpha') D_d^2] \times q_1 = q_3 \rightarrow$ wkng storage
439	3 872 780 873	$\rho_1 \times q_6 = N \rightarrow$ answer file
440	7 661 440 441	HALT if SW 1 is ON
441	7 820 645 200	Call "Multiple Integration Sub-routine, then out to Integration. The B ads of this instruction is the "Integration Transfer Switch."
442	7 600 000 000	
443	0 000 479 000	Move K_e to acc
444	7 820 427 545	Call f Subroutine, return to 427
		K_e INTERPOLATION SUB-ROUTINE
445	6 063 464 000	Set sub-routine exit
446	2 000 985 000	$T - T_c$
447	4 000 986 998	$\div h = u \rightarrow$ temp storage
448	3 000 000 000	$u \times u = u^2$
449	2 000 840 997	$u^2 - 1 \rightarrow$ temp storage

450	2̄ 000 842 996	$(u^2-1)-3=(u^2-4)$ → temp storage
451	3̄ 998 993 000	$u \times c_6$
452	1̄ 000 992 000	$+ c_5$
453	3̄ 000 996 996	$\times (u^2-4) =$ "a" → temp storage
454	3̄ 998 991 000	$u \times c_4$
455	1̄ 000 990 000	$+ c_3$
456	1̄ 000 996 000	+ "a"
457	3̄ 000 997 996	$\times (u^2-1) =$ "b" → temp storage
458	3̄ 998 989 000	$u \times c_2$
459	1̄ 000 988 000	$+ c_1$
460	1̄ 000 996 000	+ "b" = "c"
461	3̄ 000 998 000	"c" × u
462	1̄ 000 987 000	$+ \gamma_c = \ln K_e(T)$
463	8̄ 874 000 479	Exp (ln K_e) = K_e → wkng storage
464	7̄ 700 000 [545̄]	Exit from sub-routine
465	7̄ 600 000 000	
466	7̄ 600 000 000	(Not used)
		"ESTIMATE T" SUB-ROUTINE
467	6̄ 063 475 000	Set sub-routine exit
468	0̄ 000 000 799	$\Delta\alpha'$ → temp storage
469	1̄ 844 870 798	$9 + \alpha_i'$ → temp storage
470	1̄ 759 871 000	$[2D_i/R] + T_i$
471	3̄ 000 799 000	$\times \Delta\alpha'$
472	4̄ 000 798 000	$\div (9+\alpha_i') = \Delta T$
473	2̄ 871 000 755	$T_i - \Delta T = T_{i+1}$ → wkng storage
474	1̄ 754 799 754	$\alpha_{i+1}' = \alpha_i' + \Delta\alpha_i'$ → wkng storage
475	7̄ 700 000 [426̄]	Exit from sub-routine
476	0̄ 000 000 000	
477	0̄ 000 000 000	(Not used)
478	0̄ 000 000 000	
479	[0̄ 000 000 000]	Working storage location, K_e

480	6 063 544 000	Set sub-routine exit
481	2 804 754 774	$c_1 - \alpha' \rightarrow$ wkng storage
482	1 840 754 799	$1 + \alpha' \rightarrow$ temp storage
483	4 766 799 783	$k_6 \div (1+\alpha') = g_9 \rightarrow$ wkng storage
484	3 807 754 000	$K_N \times \alpha'$
485	1 000 804 000	$+ c_1$
486	3 000 769 000	$\times k_9$
487	1 000 768 780	$+ k_8 = g_6 \rightarrow$ wkng storage
488	3 771 754 000	$k_{11} \times \alpha'$
489	3 000 754 000	$\times \alpha'$
490	4 000 774 778	$\div (c_1 - \alpha') = g_4 \rightarrow$ wkng storage
491	4 809 755 775	$(D_0/R) \div T = g_1 \rightarrow$ wkng storage
492	1 804 754 000	$c_1 + \alpha'$
493	4 804 000 781	$c_1 \div (c_1 + \alpha') = g_7 \rightarrow$ wkng storage
494	0 000 755 000	Move T to acc
495	9 000 730 720	Table Look Up: $\beta_{N_2}(T)$
496	2 755 002 799	$T - T_n \rightarrow$ temp storage
497	2 001 002 000	$T_{n+1} - T_n = \Delta T$
498	4 799 000 798	$(T - T_n) \div \Delta T \rightarrow$ temp storage
499	2 003 004 000	$\beta_{N_2}(T_{n+1}) - \beta_{N_2}(T_n) = \Delta\beta_{N_2}$
500	3 000 798 000	$\Delta\beta_{N_2} \times \left(\frac{T-T_n}{\Delta T}\right)$
501	1 000 004 000	$+ \beta_{N_2}(T_n) = \beta_{N_2}(T)$
502	3 000 774 782	$\beta_{N_2}(T) \times (c_1 - \alpha) = g_8 \rightarrow$ wkng storage
503	0 000 755 000	Move T to acc
504	9 000 740 720	Table Look Up: $\beta_N(T)$
505	2 003 004 000	$\beta_N(T_{n+1}) - \beta_N(T_n) = \Delta\beta_N$
506	3 000 798 000	$\Delta\beta_N \times \left(\frac{T-T_n}{\Delta T}\right)$
507	1 000 004 000	$+ \beta_N(T_n) = \beta_N(T)$
508	3 000 841 000	$\beta_N(T) \times 2$
509	1 000 775 000	$+ g_1$

510	3 000 754 000	$(2\beta_{N(T)} + g_1) \times \alpha'$
511	1 000 782 000	$+ g_8$
512	3 000 781 000	$\times g_7$
513	1 000 763 799	$+ k_3 = \bar{\beta} \rightarrow$ temp storage
514	3 000 841 000	$2 \times \bar{\beta}$
515	2 000 840 798	$-1 \rightarrow$ temp storage
516	3 000 765 797	$\times k_5 = g_{10} \rightarrow$ temp storage
517	3 764 799 799	$k_4 \times \bar{\beta}$ temp storage
518	3 000 000 000	$(k_4 \bar{\beta})^2$
519	2 000 797 000	$- g_{10}$
520	8 835 000 000	$\sqrt{(k_4 \bar{\beta})^2 - g_{10}}$
521	2 799 000 000	$(k_4 \bar{\beta}) - \sqrt{\ }$
522	4 000 798 874	$\div (2\bar{\beta} - 1) = \bar{M} \rightarrow$ answer file
523	4 767 000 872	$k_7 \div \bar{M} = \rho \rightarrow$ answer file
524	2 764 874 000	$k_4 - \bar{M}$
525	3 000 874 000	$\times \bar{M}$
526	3 000 783 871	$\times g_9 = T \rightarrow$ answer file
527	2 000 755 756	$T - T_{initial} = \Delta T \rightarrow$ wkng storage
528	4 809 871 775	$(p_0/R) \div T = g_1 \rightarrow$ wkng storage
529	7 733 533 532	Optional print T, ΔT if SW 3 is ON
530	7 600 000 000	(Not used)
531	7 600 000 000	
532	9 580 755 756	Print order (bypassed if SW 3 is OFF)
533	8 894 756 000	Set ΔT positive
534	2 000 815 000	$\lvert\Delta T\rvert - T_{error}$
535	7 661 535 536	HALT if SW 1 is ON
536	7 760 538 541	Sign test and transfer + : Not finished, repeat − : T calc finished, calculate f
537	7 600 000 000	
538	0 000 871 755	Move T to $T_{initial}$
539	7 700 000 495	Repeat

540	7 600 000 000	(Not used)
541	0 000 754 870	Here when T calc finished. Move α' to ans file
542	3 774 776 785	$(\alpha_1 - \alpha') \times D_d^2 \longrightarrow$ wkng storage
543	0 000 871 755	Move T to T_{init} and to acc
544	7 661 544 [000]	HALT if SW 1 is ON. Then exit from T Subroutine
545	6 063 549 [000]	**f SUBROUTINE** Set exit
546	4 872 479 000	$\rho \div K_e$
547	3 000 778 000	$\times g_4$
548	2 840 000 869	$1 - [(\rho/K_e) g_4] = f \longrightarrow$ answer file
549	7 661 549 [000]	HALT if SW 1 is ON. Then exit from f Subroutine
550	0 000 000 000	
551	0 000 000 000	(Not used)
552	0 000 000 000	
553	0 000 000 000	
554	0 000 000 000	**INTEGRATION, FIRST PASS**
555	6 062 441 575	Set Transfer Switch for Second Pass
556	9 580 870 874	Print α', T, ρ, N, M
557	6 062 561 886	Initialize Y_i address
558	6 063 563 889	Initialize Y_i "delay line" address
559	0 000 857 790	Move 0 into Δa_o location
560	0 000 000 791	Move 0 into a_o location
561	0 000 [911] 789	Move Y_{oi} from file to wkng location
562	9 580 789 791	Print Y_{oi}, a_{oi}, Δa_{oi}
563	0 000 789 [914]	Move Y_{oi} to delay line
564	6 012 561 005	Increment Y_{oi} file address
565	6 013 563 005	Increment delay line storage address
566	6 124 561 561	Repeat if Y_{oi} file ads $\leq$ IR 4 (which contains final address)
567	7 661 567 568	HALT if SW 1 is ON
568	0 000 757 000	Move $\Delta q'$ to acc
569	7 820 426 467	Call "Estimate T" subroutine, then return to main program at 426.

570	0 000 000 000	
571	0 000 000 000	
572	0 000 000 000	(Not used)
573	0 000 000 000	
574	0 000 000 000	INTEGRATION, SECOND PASS
575	6 062 441 590	Set Transfer Switch for Third Pass
576	0 005 870 880	Move (α', T, ρ, N, $\bar{M}$) to delay location
577	6 062 579 886	Initialize Y_i address
578	6 063 579 888	Initialize Y_i "delay line" address
579	0 000 [911] [913]	Move Y_i
580	6 012 579 005	Increment Y_i address
581	6 013 579 005	Increment Y_i "delay line" address
582	6 124 579 579	Repeat if Y_{1i} file ads $\leq$ IR 4 (contains final ads)
583	0 000 757 000	Move $\Delta\alpha'$ to acc
584	7 661 584 585	HALT if SW 1 is ON
585	7 820 426 467	Call "Estimate T" subroutine, then return to main program at 426.
586	0 000 000 000	
587	0 000 000 000	(Not used)
588	0 000 000 000	
589	0 000 000 000	INTEGRATION, THIRD PASS
590	6 062 441 605	Set Transfer Switch for Fourth Pass
591	0 005 870 875	Move (α', T, ρ, N, $\bar{M}$) to delay location
592	6 062 594 886	Initialize Y_{2i} address
593	6 063 594 887	Initialize Y_{2i} "delay line" address
594	0 000 [911] [912]	Move Y_{2i}
595	6 012 594 005	Increment Y_{2i} address
596	6 013 594 005	Increment Y_{2i} "delay line" address
597	6 124 594 594	Repeat if Y_{2i} file ads $\leq$ IR 4 (contains final ads)
598	7 661 598 599	HALT if SW 1 is ON
599	0 000 757 000	Move $\Delta\alpha'$ to acc

600	7 820 426 467	Call "Estimate T" subroutine, then return to main program at 426.
601	0 000 000 000	
602	0 000 000 000	(Not used)
603	0 000 000 000	
604	0 000 000 000	INTEGRATION, FOURTH PASS
605	6 062 441 645	Set Transfer Switch for Nth Pass
606	6 062 609 886	Initialize Y_{3i} address in delay line
607	6 063 624 885	Initialize new "delay line" address
608	9 580 880 884	Print (α', T, ρ, N, M) corresponding to Y_1
609	0 004 [911] 791	Move Y_{3i}, ... , Y_{0i} from delay line to wkng loc
610	3 843 793 000	$4 \times Y_1$
611	1 000 794 000	$+ Y_0$
612	1 000 792 000	$+ Y_2$
613	3 000 788 789	$\times (\Delta\alpha'/3) = a_2$
614	1 794 791 799	$Y_0 + Y_3 \rightarrow$ temp storage
615	1 793 792 798	$Y_1 + Y_2 \rightarrow$ temp storage
616	2 000 799 000	$- (Y_0 + Y_3)$
617	4 000 845 000	$\div 12$
618	1 000 798 000	$+ (Y_1 + Y_2)$
619	3 000 787 790	$\times (\Delta\alpha'/2) = \Delta a_2$
620	2 789 790 798	$a_2 - \Delta a_2 = a_1 = \Delta a_1$
621	0 000 000 799	Move Δa_{1i} to print position
622	0 000 793 797	Move Y_{1i} to print position
623	9 580 797 799	Print Y_{1i}, a_{1i}, Δa_{1i}
624	0 005 789 [910]	Move $(\Delta a_{1i}+\Delta a_{2i})$, Δa_{2i}, Y_{3i}, Y_{2i}, Y_{1i} to delay
625	6 012 609 005	Increment old delay line address
626	6 013 624 005	Increment new delay line address
627	6 124 609 609	Repeat if old delay line ads $\leq$ IR 4 (final ads)
628	7 661 628 630	HALT if SW 1 is ON
629	7 600 000 000	(Not used)

630	6 062 632 885	Initialize delay line ads
631	9 580 875 879	Print (α', T, ρ, N, $\bar{M}$) corresponding to Y_2
632	0 004 [910] 790	Move $(a_{1i}+\Delta a_{2i})$, Δa_{2i}, Y_{3i}, Y_{2i} from delay
633	0 000 793 789	Move Y_{2i} to print position
634	9 580 789 791	Print Y_{2i}, a_{2i}, Δa_{2i}
635	6 012 632 005	Increment delay line ads
636	6 124 632 632	Repeat if delay line ads $\leq$ IR 4
637	0 005 870 875	Move (α', ... , $\bar{M}$) for Y_3
638	7 661 638 639	HALT if SW 1 is ON
639	0 000 757 000	Move $\Delta\alpha'$ to acc
640	7 820 426 467	Call "Estimate T" subroutine, return to main program at 426.
641	7 600 000 000	
642	7 600 000 000	(Not used)
643	7 600 000 000	
644	7 600 000 000	INTEGRATION, N^{th} PASS
645	6 062 648 885	Initialize old delay line address
646	6 063 659 885	Initialize new delay line address
647	9 580 875 879	Print (α', T, ρ, N, $\bar{M}$) corresponding to Y_{N-1}
648	0 005 [910] 792	Move a_{n-1}, Y_n, ... , Y_{n-3} to wkng loc
649	1 796 793 799	$Y_{n-3} + Y_n \rightarrow$ temp storage
650	1 795 794 798	$Y_{n-2} + Y_{n-1} \rightarrow$ temp storage
651	2 000 799 000	$(Y_{n-2} + Y_{n-1}) - (Y_{n-3} + Y_n)$
652	4 000 845 000	$\div 12$
653	1 000 798 000	$+ (Y_{n-2} + Y_{n-1})$
654	3 000 787 799	$\times (\Delta\alpha'/2) = \Delta a_{n-1} \rightarrow$ temp storage
655	1 792 000 791	$a_{n-2} + \Delta a_{n-1} = a_{n-1} \rightarrow$ print position
656	0 000 799 792	Move Δa_{n-1} to print position
657	0 000 794 790	Move Y_{n-1} to print position
658	9 580 790 792	Print $Y_{n-1,i}$, $a_{n-1,i}$, $\Delta a_{n-1,i}$
659	0 005 791 [910]	Move $a_{n-1,i}$, $\Delta a_{n-1,i}$, Y_{ni}, $Y_{n-1,i}$, $Y_{n-2,i}$ to delay

660	6 012 648 005	Increment old delay ads
661	6 013 659 005	Increment new delay ads
662	6 124 648 648	Repeat if delay line ads ≤ IR 4
663	0 005 870 875	Move (α', T, ρ, N, $\bar{M}$) to delay storage
664	7 661 664 665	HALT if SW 1 is ON
665	0 000 757 000	Move $\Delta\alpha'$ to acc
666	7 820 426 467	Call "Estimate T" subroutine, return to main program at 426.
667	0 000 000 000	
668	0 000 000 000	(Not used)
669	0 000 000 000	INTEGRATION, FINAL LINE
670	6 062 672 885	Initialize delay line ads
671	9 580 875 879	Print (α', T, ρ, N, $\bar{M}$)
672	0 005 [930] 790	Move a_{n-1}, Δa_{n-1}, Y_n, Y_{n-1}, Y_{n-2} to wkng
673	3 843 793 000	$4 \times y_{n-1}$
674	1 000 794 000	$+ y_{n-2}$
675	1 000 792 000	$+ y_n$
676	3 000 788 000	$\times (\Delta\alpha'/3) = \Delta a_{n-1} + \Delta a_n$
677	2 000 791 791	$(\Delta a_{n-1} + \Delta a_n) - \Delta a_{n-1} = \Delta a_n$
678	1 000 790 790	$a_{n-1} + \Delta a_n = a_n$
679	0 000 792 789	Move Y_n to print position
680	9 580 789 791	Print $Y_{n,i}$, $a_{n,i}$, $\Delta a_{n,i}$
681	6 012 672 005	Increment delay line ads
682	6 124 672 672	Repeat if delay line ads ≤ IR 4
683	7 662 683 100	HALT if SW 2 is ON. Then go to "Bootstrap" for new data.

T, β_{N_2}, β_N, TABLE

Location	T°K	Location	β_{N_2}	Location	β_N
720	5,000	730	4.249	740	2.557
721	6,000	731	4.306	741	2.622
722	7,000	732	4.353	742	2.703
723	8,000	733	4.397	743	2.786
724	9,000	734	4.445	744	2.875
725	10,000	735	4.503	745	2.951
726	11,000	736	4.576	746	3.017
727	12,000	737	4.666	747	3.072

CONSTANTS USED BY THE PROGRAM

Location	Quantity
840	1.0
841	2.0
842	3.0
843	4.0
844	9.0
845	12.0
846	1.50
847	2.50
848	$\gamma_i = 1.6666667$
849	$\gamma_d = 1.40$
850	$\gamma_k = 1.2857143$
851	10^6
852	$No \left[\pi R_u\right]^{1/2} = 9.73393 \times 10^{27}$
853	$\Delta\alpha_e' = 0.01$
854	10.0
855	-1
856	$4\sqrt{6} = 9.797960$
857	0
858	$2\sqrt{2} = 2.828427$

WORKING STORAGE ASSIGNMENTS

Location	Quantity
750	$(1 - c)$
751	$\gamma_1' = c\,\gamma_d + (1 - c)\,\gamma_i$
752	$\gamma_k' = c\,\gamma_k + (1 - c)\,\gamma_i$
753	$M_{w_{mix}}$
754	α' (working value)
755	$T_{initial}$, T (working value)
756	$(T - T_{initial})$
757	$\Delta\alpha'$ (working value)
758	$\delta\alpha'$ (from Equilibrium Calculation)
759	$2(D_o/R)$
760	M_1^2
761	$k_1 = 2\gamma_1 / (\gamma_k' + 1)$
762	$k_2 = (\gamma_k' - 1) / (\gamma_k' + 1)$
763	$k_3 = 2.5\,(1 - c)$
764	$k_4 = (1 + \gamma_1' M_1^2)\,\gamma_1' M_1$

Location	Quantity
765	$k_5 = M_1^2 + 2 / (\gamma_1' - 1)$
766	$k_6 = T_1 \gamma_1'$
767	$k_7 = \rho_1 M_1$
768	$k_8 = 10^6 Mw_i (1 - c) K_i / Mw_{mix}$
769	$k_9 = 10^6 Mw_d K_d / Mw_{mix}$
770	$k_{10} = Mw_{mix} \rho_1 U_s (Mw_d)^{1/2} / \left[N_o (\pi R_u)^{1/2}\right]$
771	$k_{11} = 4 / Mw_{mix}$
772	$k_{12} = 4 \sqrt{6} D_d^2$
773	$k_{13} = (1 - c) 2 \sqrt{6} D_{ave}^2 \left[(M_{w_d} M_{w_i})/M_{w_i}\right]^{1/2}$
774	$(c - \alpha')$
775	$q_1 = (D_o/R) / T$
776	D_d^2
777	$q_3 = (c - \alpha') q_1 D_d^2$
778	$q_4 = k_{11} \alpha'^2 / (c - \alpha)$
779	$q_5 = k_{10} / \left[q_2 \rho'^2 (c - \alpha') f\right]$

Location	Quantity
780	$q_6 = k_8 + k_9 (c + K_N \alpha')$
781	$q_7 = c / (c + \alpha')$
782	$q_8 = (c - \alpha') \beta_{N_2}$
783	$q_9 = k_6 / (1 + \alpha')$
784	$q_{10} = \alpha' k_{12}$
785	$(c - \alpha') D_d^2$
786	—
787	$\Delta\alpha' / 2$
788	$\Delta\alpha' / 3$

GENERAL ELECTRIC

SPACE SCIENCES LABORATORY
MISSILE AND SPACE VEHICLE DEPARTMENT

TECHNICAL INFORMATION SERIES

AUTHOR	SUBJECT CLASSIFICATION	NO.
I. S. Scala and L. Talbot II. B. Cary	Shock Waves Non-equilibrium Gas Dynam	R62SD032
		DATE March 30, 1962

TITLE

HIGH ALTITUDE SHOCK WAVE STRUCTURE, Parts I and II

ABSTRACT

I. A theoretical model is developed for the structure of a shock wave in a diatomic gas including rotational and vibrational relaxation phenomena.

II. Experiments are carried out in a combustion driven shock tube. Experimental data for vibrational relaxation times and dissociation rates are obtained for nitrogen.

G. E. CLASS	REPRODUCIBLE COPY FILED AT	NO. PAGES
I	G. E. TECHNICAL INFORMATION CENTER 3100 CHESTNUT STREET PHILADELPHIA, PENNA.	129
GOV. CLASS None		

Summary:

I. 1. More realistic estimates are provided for the distribution of translational temperature through a normal shock wave than would have been obtained with the neglect of relaxation phenomena.

2. More realistic values of the thickness of the shock transition have been obtained.

3. The extent of the coupling between the internal degrees of freedom has been investigated.

II. 1. It has been demonstrated that combustion generated shocks may be used for shock structure studies.

2. The relative efficiency of nitrogen atoms and molecules in producing dissociation was determined.

3. Up to temperatures of 6000°K in pure nitrogen, the data indicate that vibrational relaxation and dissociation may be treated in an uncoupled manner.

4. The new experimental data have been compared with the data obtained by earlier investigators and the differences noted.

By cutting out this rectangle and folding on the center line the above information can be fitted into a standard card file.

AUTHOR By: B Cary I. S. Scala L. Talbot

COUNTERSIGNED J. L. Talbot Manager

DIVISION Defense Electronics

LOCATION Valley Forge Space Technology Center, King of Prussia, Pa.